Studies on the Mechanism of Photocurrent Multiplication Phenomena at Organic/Metal Interface

2000

KEN-ICHI NAKAYAMA

Material and Life Science
Faculty of Engineering
Osaka University

Studies on the Mechanism of Photocurrent Multiplication Phenomena at Organic/Metal Interface

（有機／金属接合界面における光電流増倍機構に関する研究）

2000

Ken-ichi Nakayama

Matrial & Life Science
Faculty of Engineering
Osaka University

Preface

The studies of this thesis were performed under the guidance of Professor Masaaki Yokoyama at Matrial and Life Science, Faculty of Engineering, Osaka University.

The objects of this studies are to elucidate the mechanism of photocurrent multiplication phenomena at organic/metal interface, which were first discovered at Yokoyama's laboratory. The author sincerely hopes these studies done here prorovide some insights not only in photocurrent multiplication phenomena but also in the physics at organic/metal interface more generally.

Ken-ichi Nakayama

Ken-ichi Nakayama

Material and Life Science,
Faculty of Engineering,
Osaka University
Yamadaoka 2-1. Suita. Osaka 565
Japan

January 2000

Contents

Chapter 1	General Introduction	1
Chapter 2	Direct Tracing of Photocurrent Multiplication Process in Organic Pigment Film	9
Chapter 3	Field-activated Structural Traps at Organic/Melta Interface Causing Photocurrent Multiplication Phenomena	17
Chapter 4	Photocurrent Multipication at Organic/Metal Interface and Morphology of Organic Film and Metal Electrode	25
Chpater 5	Numerical Simulations of Photocurrent Multiplication Process at Organic/Metal Interface	44
Chapter 6	High-speed Photocurrent Multiplication Device Based on an Organic Double-layered Structure	76
Chapter 7	Summary	87
References		90
List of Publications		91
Acknowledgment		93

Chapter 1

General Introduction

1-1. Photocurrent multiplication phenomena in organic pigment films

Photoconduction is the phenomenon that the electric current takes place in a materail upon irradiation of light. Charge carriers generated by absorption of photons are observed as a photocurrent. Such most basic process in the photon-electron conversion is observed in a wide variety of semiconducting materials including organic semiconductors, and has been applied to many kinds of devices such as photosensor, solar cell[1] and electrophotography[2].

In the photoconduction phenomena observed commonly in there, the quantum efficiency of photocurrent, i.e., photon-electron conversion ratio never exceeds unity because not more than one pair of carriers is generated from one photon at most. However, there exists the case that the quanum efficiency of photocurrent can exceed unity by some amplification in a material, which is called "photocurrent multiplication phenomenon". As such a phenomenon, Avalanche effect in inorganic materials such as silicon crystal and amorphous selenium[3] is well-known, while no reports have appeared in organic materials so far.

Recently, however, a similar phenomenon of the large photocurrent multiplication was discovered even in organic materials quite accidentally during the investigation of photo-electrical properties in organic pigments. The first observation of photocurrent multiplication phenomena was performed in a vacuum deposited organic film of a perylene pigment, simply sandwiched with two metal electrodes[4] (see Fig. 1-1). Figure 1-2 shows a typical voltage dependence of quantum

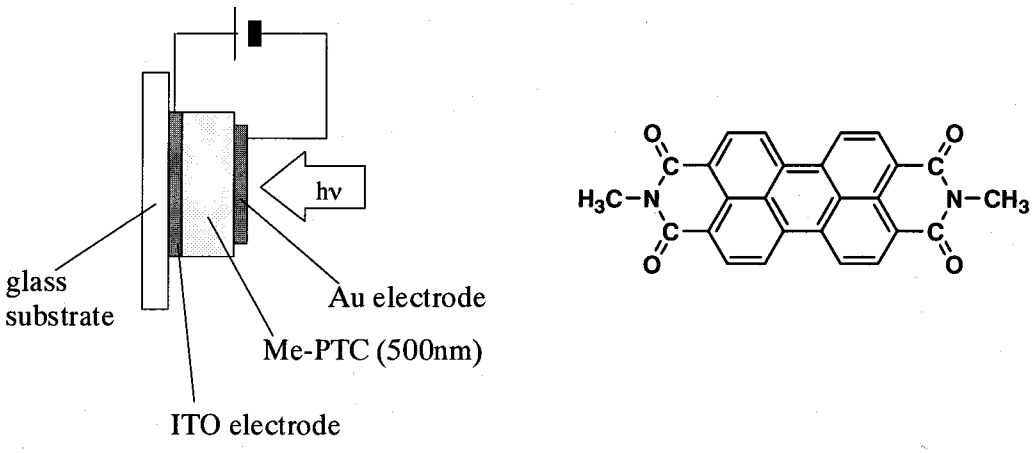

Fig. 1-1 Device structure of photocurrent multiplication device and chemical structure of Me-PTC.

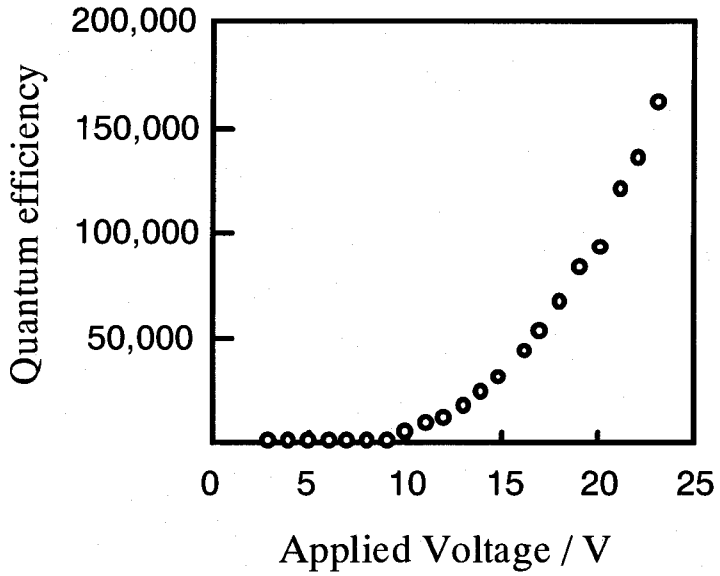

Fig. 1-2 Typical dependence of multiplication rate on applied voltage for ITO/Me-PTC(500 nm)/Au(20 nm) cells. Au electrode was negatively biased with respect to ITO electrode. Monochromatic light of 600 nm was irradiated on Au electrode. Measurements were performed at 223 K.

efficiency of the photocurrent. The quantum efficiency exceeded unity in a few volts applied and finally reaches 10^5 at 20V. This means that more than 10^5 electrons flowed across the device for one input photon. The value of 10^5 seems to be comparable to the mulitiplication rate of the photo-multiplier tubes which are widely used as a highly sensitive photon detector.

1-2. Organic materials showing photocurrent multiplication

Thereafter, many kinds of organic semiconductors have been revealed to show such photocurrent multiplication phenomena.[4-6] Figure 1-3 summarizes these compounds. The typical organic semiconducting pigments such as perylene[4], phthalocyanine and quinacridone[5] are included. Thus, the photocurrent multiplication is considerably common in organic semiconducting compounds. This fact indicates that this phenomenon is attributed to the some essential nature of organic materials rather than the characteristics of individual molecules.

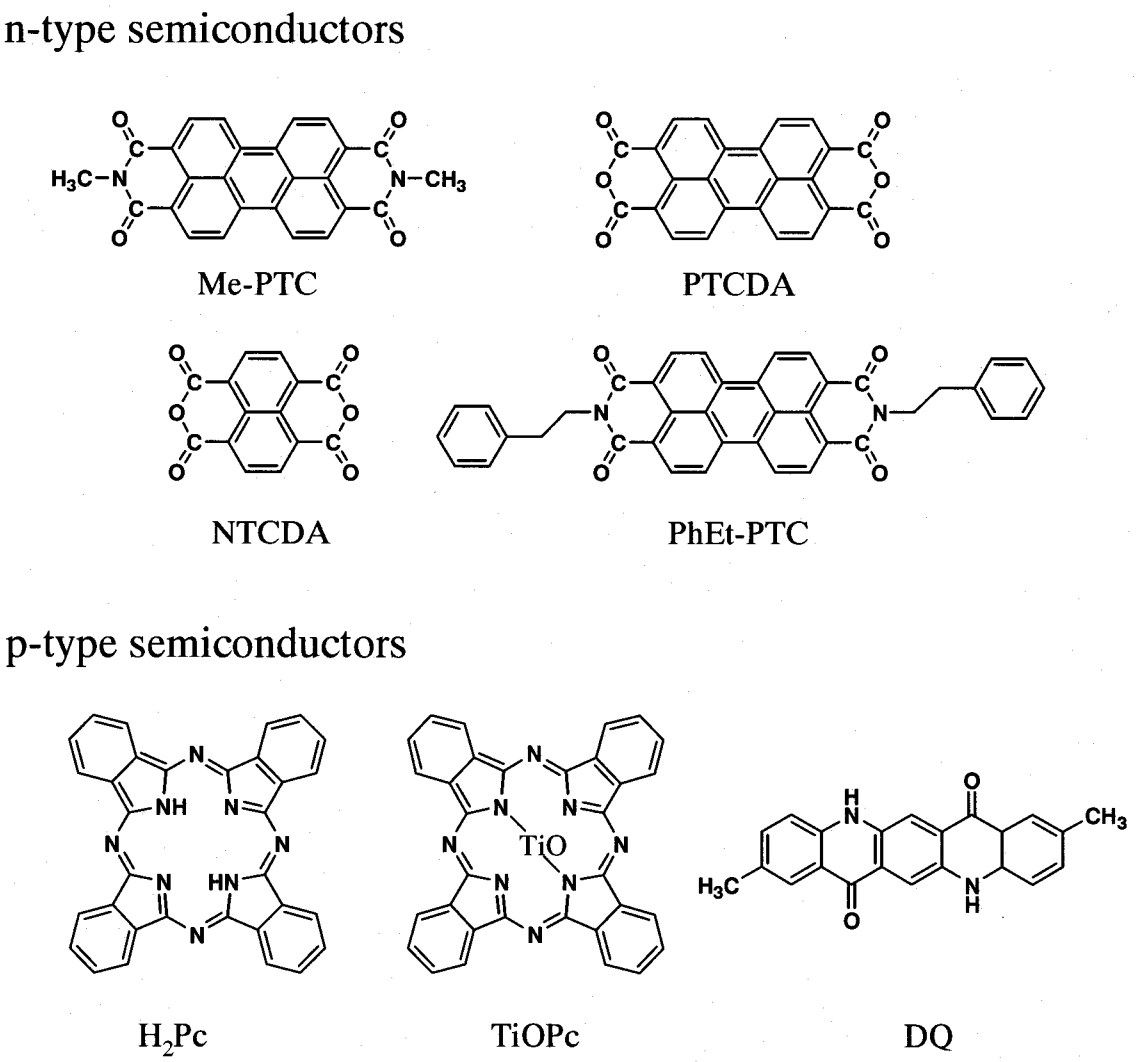

Fig. 1-3 Organic semiconducting molecules showing the photocurrent multiplication phenomenon.

1-3. Application of photocurrent multiplication

The exremely high photo-electrical conversion efficiency is expected to be applied to various opto-electronic devices. In fact, several examples of application have been already achieved.[7-9] Figure 1-4 shows, for instance, a light amplification device, which was fablicated by combining a photocurrent multiplication device with organic electroluminescent device in a layered strucure[7]. This device can amplify the input light 25 times at most with keeping the spatial pattern of input light. Thus, the photocurrent multipilcation in organic films has a great potential as a key process of photon-electron conversion in various organic opto-electronic devices.

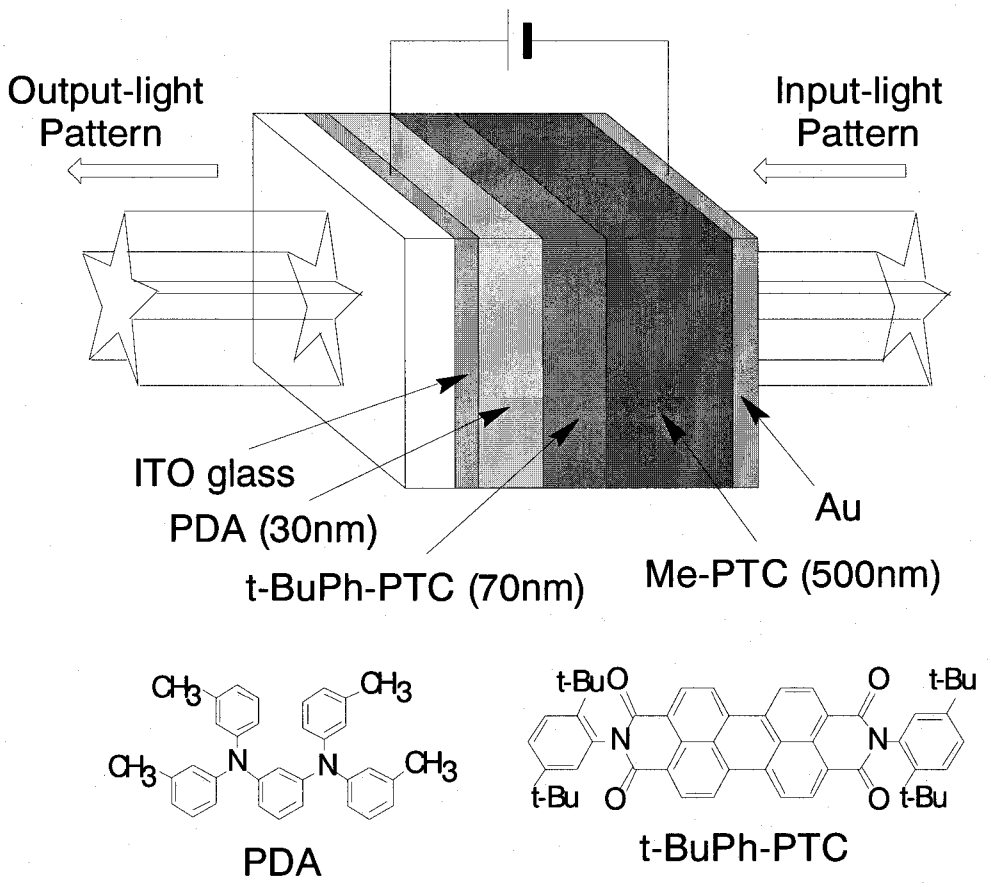

Fig. 1-4 Light amplification device composed of organic deposited films. This device is composed of photon-electron convesrsion part by photocurrent multiplication (Me-PTC) and electron-photon-conversion part by electroluminescent diode (PDA/t-BuPh-PTC).

1-4. Origin of the multiplied photocurrent

Before the present work was started, a mechanism for the photocurrent multiplication in organic films has been presumed based on the following experimental facts.

(1) The action spectrum of multipled photocurent depends strongly on the absorption spectrum of the pigment films. That is, a large multiplication rate is observed when the irradiated light is of the wavelength to excite organic film at near the metal/organic interface.

(2) The multipled photocurrent also depends on the kinds of metal electrodes negatively biased and irradiated by light.

These results suggest that the multiplication phenomenon occurs at the metal/organic interface of the negatively biased metal electrode side.

(3) The multiplied photocurrent always exhibits very slow transient response on the order of several ten seconds to reach a constant value for switching light on and off, inspite of typical electronic conduction. This characterstic implies that the multiplication process has to involve some trapping events of photogenerated carriers.

(4) The current-voltage characteristics observed in the multiplication devices obey Fowler-Nordheim equation describing tunneling injection current from metal electrode. This result indicates that multiplied photocurrent originates from tunneling inejction process, which requires high electric field at organic/metal interface.

From the above-mentioned experimental facts, it is unlikely to consider that this phenomenon is caused by Avalanche effect, especially because the mobility of organic materials is too low for electrons to obtain enough kinetic energy leading to

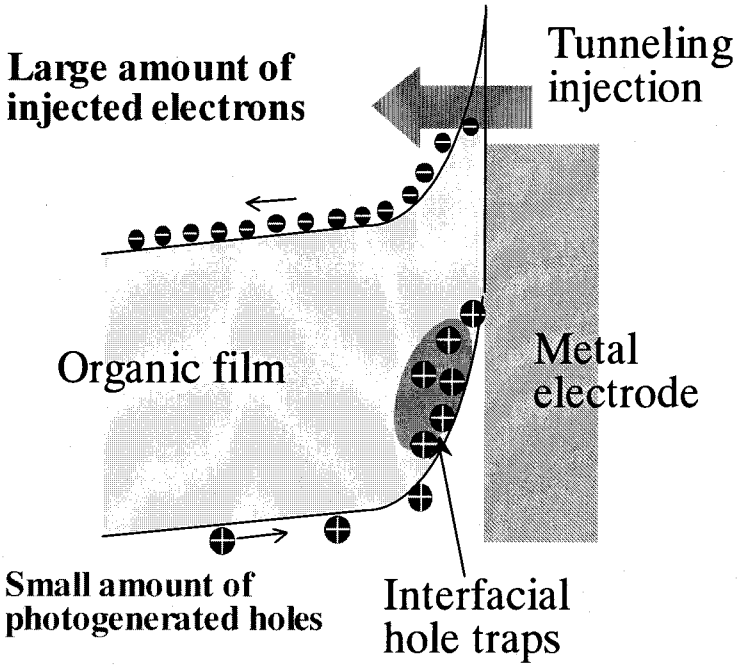

Fig. 1-5 Energy diagram of organic/metal interface during multiplication. Photogenerated holes accumulate to some interfacial traps near the metal electrode and cause high electric field. As a result, a large amount of leectrons are injected from metal electrode.

avalanche, and it is rather reasonable to interpret that the photocurrent multiplication phenomena in organic pigment films is the interfacial phenomenon between organic films and metal electrode. Thus, the following mechanism as shown in Figure 1-5 had been presumed.[4] Some of the photogenerated carriers (i.e., holes for the case in the figure) are trapped to some interfacial traps existing near organic/ metal interface. The accumulation of photogenerated carriers causes high electric field concentration at organic/metal interface. As a resut, a large number of electrons are injected from the metal electrode by tunneling injection process. In this way, the quantum efficiency, which is defined as the ratio of the number of carriers flowing through the device to the number of photons absorbed in organic film, exceeds unity.

1-5. Purpose of the present study

The purpose of this study is to elucidate the proposed mechanism of the photocurrent multiplication phenomenon at organic/metal interface in detail. As mentioned above, the photocurrent multiplication in organic films seems to have a great potential for its application to fabricate the novel organic opto-electronic devices. At the starting point of this work, however, we did have only a vague concept of the photo-induced tunneling injection mechasnim as mentioned above, and did not have any definite answers for the questions what kinds of materials do show the large multiplication or why the organic materials shows so large multiplication rate, for instance. Furthermore, it must be also solved how to control the multiplication charcteristics in order to apply this phenomenon to practical devices.

The mechanism of photucrrent multiplication based on electron injection also stimulate us from the standpoint of a basic problem of charge injection process at organic/metal interface more widely. Recently, the organic materials realized high current density up to 100mAcm^{-2} in organic electroluminescent devices.[10] Thus, the charge injection from the electrodes also becomes a great concern in that field. The basic understanding of charge injection process at organic/metal interface through clarifying the mechanism of photocurrent multiplication, would provide more general insight to the charge injection in the organic materials.

This thesis consists of the following chapters.

In Chapter 1, the background and outlines of photocurrent multiplication phenomena in organic pigment films were described.

In Chapter 2, in order to verify the previously proposed mechanism for the photocurrent multiplication in organic materails, the transient response of multipled

photocurrent were measured in multiplication devices. The observed transient photocurrent faithfully traced the mechanism of photocurrent multiplication proposed previously and some guiding principles for improving the photoresponse time was also discussed.

In Chapter 3, the nature of interfacial traps, which plays an essential role in the multiplication process, was investigated by introducing thermally stimulated current measurement. Based on the results on the interfacial traps, the field-activated structural trap model is proposed as a candidate for the interfacial traps causing photocurrent multiplication.

In Chapter 4, the relationship between the morphological structure at organic/metal interface and multiplication behaviors was investigated in order to verify the proposed field-activated structural trap model.

In Chapter 5, in order to obtain the more microscopical mechanism of the photocurrent multiplication, the charge accumulation process at organic/metal interface was simulated and analyzed by numerical calculation based on electromagnetism.

In Chapter 6, based on the guidance obtained through this work, new type multiplication device showing a high-speed response with large multiplication rate was developed.

In Chapter 7, the obtained results in this study were summarized.

Chapter 2

Direct Tracing of Photocurrent Multiplication Process in Organic Pigment Film

2-1. Introduction

Photocurrent multiplication phenomena in organic pigment film show a large quantum efficiency reaching 10^5. However, the multiplied photocurrent observed always exhibits a slow transient response on the order of several tens of seconds until current saturation is attained. Based on our proposed model that the accumulation of trapped holes causes the multiplication[4,6], slow response seems to be associated with the accumulation process of trapped holes at the interface. From this point of view, it is very important to investigate the charge accumulation process of photogenerated holes by measuring the initial stage of the transient photocurrent. This may offer guiding principle for accomplishing high-speed photocurrent multiplication for organic films, which would be applicable to practical photo-sensing devices. There have been a few reports on photocurrent multiplication for amorphous silicon-based materials,[12,13] but no reports of the transient response measurement, especially for the newly observed organic photocurrent multiplication.

In this chapter, we report the transient response of the photocurrent multiplication, which was observed for the first time for the organic/metal junction between a perylene pigment and gold. Observed photocurrent transients were found to follow the proposed photocurrent multiplication process faithfully. Based on the results obtained, a guiding principle for constructing high-speed organic multiplication devices is proposed.

2-2. Experimental Section

Figure 2-1 shows a block diagram for the transient photocurrent measurements together with the cell structure. The perylene pigment (3,4,9,10-perylenetetracarboxylic 3,4:9,10-bis(methylimide), Me-PTC) was purified twice by the train sublimation technique[14]. The thin film cell on an indium tin oxide (ITO) substrate was prepared by vacuum evaporation under 10^{-3} Pa. The deposition rates were 0.2 nm s^{-1} for Me-PTC and 0.05 nm s^{-1} for Au, respectively. Under continuous light irradiation (600 nm, 40 mW cm^{-2}), this cell showed a multiplication rate of 1.5 x 10^4–fold when Au was negatively biased at 14 V with respect to the ITO electrode. The cell was set in an optical cryostat (Janis Research Co. Inc., VPF-475) evacuated to 10^{-1} Pa. Measurements were carried out at 203 K. A light emitting diode (LED), which emits orange light of 620 nm having FWHM of 20 nm, was used as a light source. This was driven by the step voltage from a function generator (Iwatsu Electric Co. Ltd., FG-330) in order to obtain a light source having a sharp rise within 10

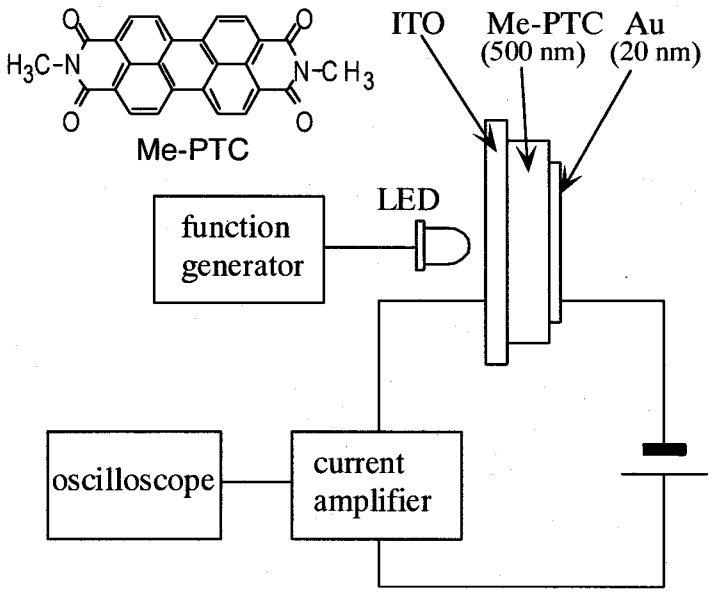

Fig.2-1 Block diagram for the transient photocurrent measurements. The structure of the photocurrent multiplication device and the chemical formula of perylene pigment (Me-PTC) are also shown.

μs. LED light was irradiated on an ITO electrode biased positively. Light intensity was measured by a silicon photodiode (Hamamatsu Photonics, S1337-66BQ) calibrated before use. The transient response of the photocurrent was measured by a high speed current amplifier (Keithley Instruments, Inc., 428) connected to a digital oscilloscope (Nicolet 3091). The photocurrent quantum efficiency, that is, multiplication rate, was calculated as the ratio of the number of collected photoinduced carriers to the number of photons absorbed by the Me-PTC film.

2-3. Results and Discussion

Figure 2-2 shows the typical initial transient response of the photocurrent observed at 203 K. Interestingly, the transient photocurrent apparently consists of two components. The first component rises within 10 μs and reaches a plateau. This rise time is due to the limitation of the response of the LED light source and the current amplifier used. The second component rises drastically after an onset time of 43 ms in the case of a light intensity of 0.19 mW cm^{-2}. The onset time of the second component is defined simply as the inflection point of the transient curve in which the second component rises.

The photocurrent quantum efficiency of the first component in the plateau region was found to be 0.6 % at 15 V. The photocurrent density of the first component was proportional both to the applied voltage (Figure 2-3(a)). In contrast, the photocurrent quantum efficiency of the second component increased drastically after the onset time, exceeded unity at 130 ms and reached 180-fold at 1 s. Moreover, the photocurrent density of the second component drastically increased with applied voltage and obeyed the Fowler-Nordheim relation describing tunneling injection (Figure 2-3(b)).

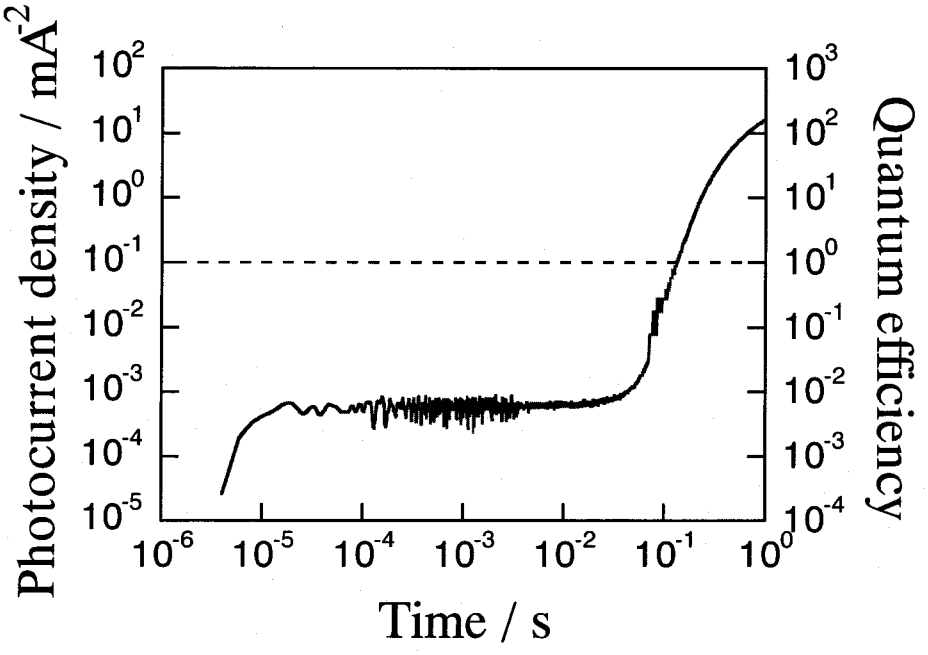

Fig.2-2 Typical transient response of photocurrent in mutiplication device. The Au electrode was negatively biased 15 V with respect to the ITO electrode. The measurement was performed at 203 K.

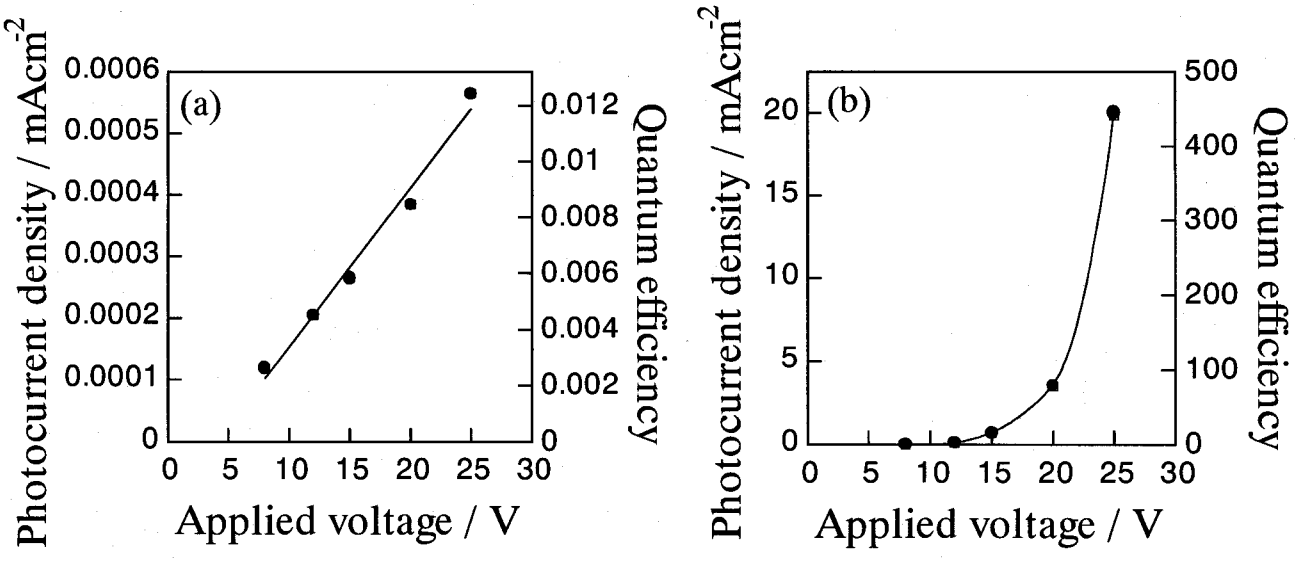

Fig.2-3 Voltage dependence of photocurrent density and quantum efficiency. (a) 1st component before onset time. (b) 2nd component after onset time.

Since the photocurrent observed before the onset time was constant for a given voltage and light intensity and showed a quantum efficiency far smaller than unity, this can be regarded as the primary photocurrent due to the photogeneration of carriers in the Me-PTC film. On the other hand, since the photocurrent observed after the onset time showed a remarkably large photocurrent quantum efficiency greater than unity and obeyed the Fowler-Nordheim relation, it can be regarded as the multiplied photocurrent due to electron tunneling from the Au electrode. In other words, the observed transient response clearly traces the multiplication process including the accumulation of trapped holes near the organic/metal interface during the primary photocurrent flow before onset (Fig. 2-4(a)) and the subsequent tunneling injection of electrons under the concentrated electric field due to hole accumulation (Fig. 2-4(b)). Thus, the observed transient photocurrent behavior successfully supports the proposed photo-induced electron tunneling mechanism for photocurrent multiplication as mentioned in Chapter 1 (Fig. 1-5).

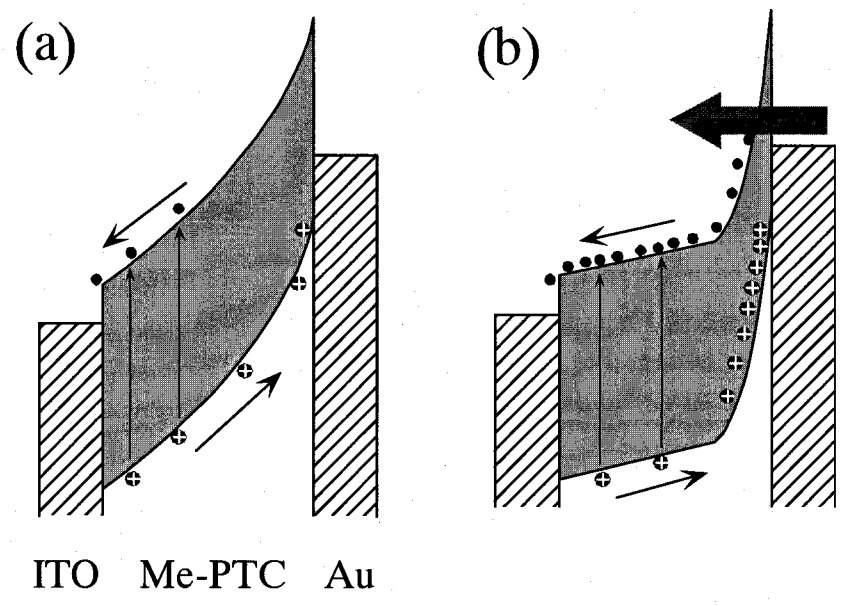

Fig.2-4 Energy structures of the photocurrent multiplication device under light irradiation. The Au electrode was negatively biased with respect to the ITO electrode. (a) Before the onset time. (b) After the onset time.

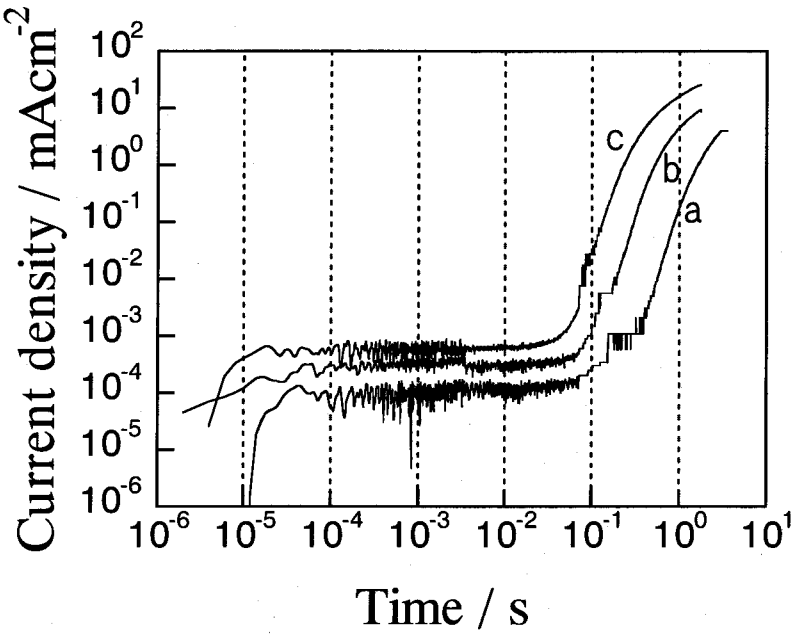

Fig. 2-5 Initial stage of the transient photocurrent curves for light intensities of (a) 36, (b) 95 and (c) 190 mW cm-2. Both axes have a logarithmic scale. Measurements were performed at 203 K. The Au electrode was negatively biased 15 V with respect to the ITO electrode.

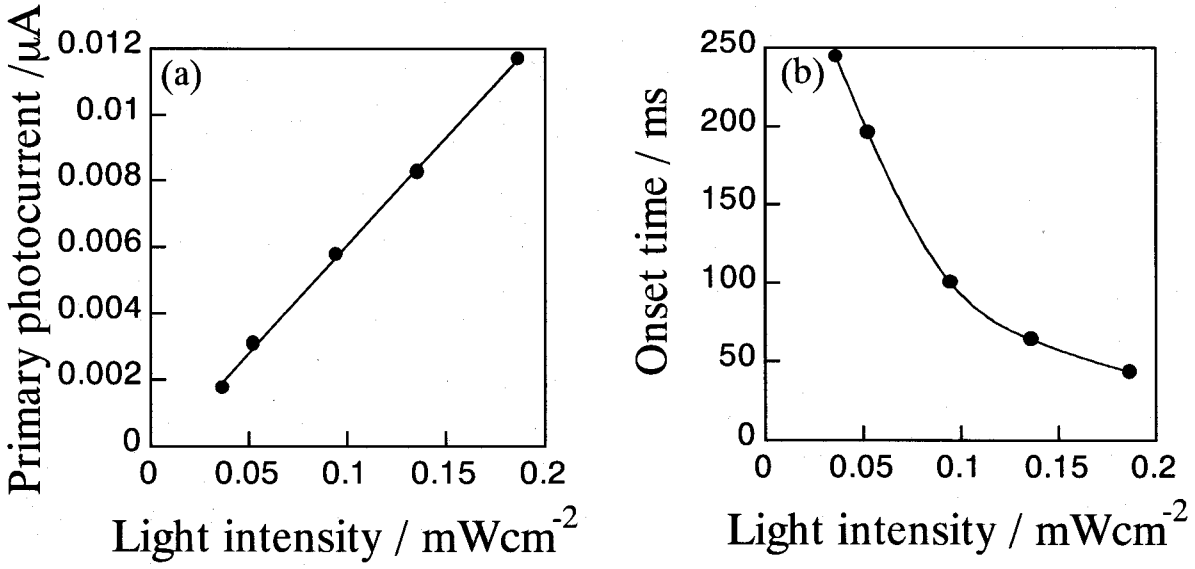

Fig. 2-6 Light intensity dependence of the primary photocurrent (a), and the onset time of the multiplied photocurrent (b).

Based on the above considerations, the onset time can be regarded as the beginning of tunneling injection of electrons, that is, the beginning of multiplication. In other words, the trapped hole accumulation at the interface is required for attaining a field concentration sufficient for multiplied current. Therefore, we measured the transient response when the supply of photogenerated holes was controled by the light intensity (Figure 2-5). It is clearly seen that the onset time becomes shorter with increasing light intensity (curves a, b and c). The light intensity dependence of the primary photocurrent and the onset time of the second photocurrent is shown in Fig. 2-6. When the light intensity increased from 36 to 190 $\mu W\ cm^{-2}$, the onset time was remarkably shortened from 250 to 43 ms, and the primary photocurrent density increased proportionally with light intensity.

Here we evaluated the integration of the primary photocurrent until the onset time. It gives the total amount of charge flowing through the cell before the onset

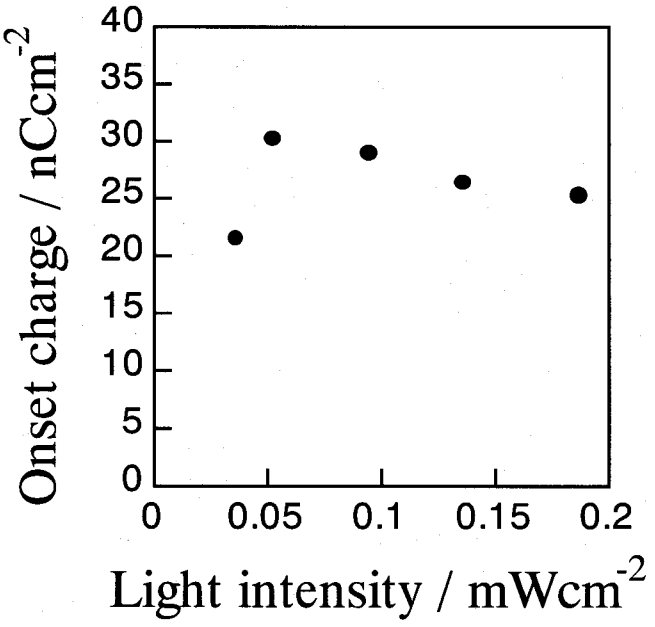

Fig. 2-7 Dependence of the amount of onset charge on light intensity. The onset charge is calculated by multiplying the onset time by the primary photocurrent density.

time (onset charge), which relates to the total number of holes passed through the Me-PTC/Au interface. Figure 2-7 shows the light intensity dependence of such onset charges. Very interestingly, the onset charge was found to be independent of the light intensity and was estimated to be 30 nC cm^{-2}. This means that the required number of holes supplied to the organic/metal interface for inducing electron tunneling seems to have a specific value. Therefore, effective supply of a given number of holes to the organic/metal interface could bring about a decrease in the onset time. Since the photocurrent quantum efficiency of the primary photocurrent in the present device is only 0.6 %, the improvement of carrier photogeneration efficiency would increase the hole supply and then, provide a high-speed multiplication device.

2-4. Conclusion

In conclusion, the transient response of photocurent in multiplication devices was investigated. The responses were revealed to have two components of the primary and the subsequent multiplied photocurrents. This results indicate that our previously proposed model that the electron tunneling injection is caused by the accumulation of photogenerated holes to the interfacial traps was directly verified. The amount of charge required for multiplication onset was found to have a specific value, implying that an increase of the carrier generation efficiency of the primary photocurrent is expected to be effective at achieving high speed multiplication.

Chapter 3

Field-activated Structural Traps at Organic Pigment/Metal Interfaces Causing Photocurrent Multiplication Phenomena

3-1. Introduction

In a previous chapter, the transient response of photocurrent in multiplication devices proved our previously proposed model that the electron tunneling injection is caused by the accumulation of photogenerated holes to the interfacial traps. In this chapter, we focus on the nature of the interfacial traps. Taking into consideration the essential role of hole traps in the multiplication process, the origin of carrier traps should be identified to attain high performance of the multiplication, such as fast photoresponse and high current density. Thus, we have investigated the properties of hole traps in Me-PTC films responsible for the multiplication phenomenon by using thermally stimulated current (TSC) measurements. We have also estimated the density of the interfacial traps from analyzing current-voltage characterstics in multiplication device. Based on the results, we propose a model of field-activated structural traps located at the organic/metal interface, which would be the basis of the photocurrent multiplication phenomenon.

3-2. Experimental Section

Me-PTC (Dainichiseika Color & Chemicals Manufacturing Co. Ltd., Figure 3-1) was purified twice by the train sublimation technique.[14] A 500 nm thick Me-PTC film was sandwiched between indium tin oxide (ITO) and Au electrodes (see Fig. 3-1). Me-PTC and Au were deposited on an ITO glass substrate by vacuum evaporation under 1×10^{-3} Pa at deposition rates of 0.2 and 0.05 nm/s, respectively. The cells were set in an optical cryostat evacuated to 10^{-1} Pa. Photocurrent measurements were carried out using an electrometer (Keithley, model 485) with an applied voltage negative to the Au electrode. To measure the thermally stimulated current, monochromatic light of 600 nm was shone onto the sample at -80 °C to capture and freeze carriers, then the sample was heated at the rate of β °C/min in the dark by

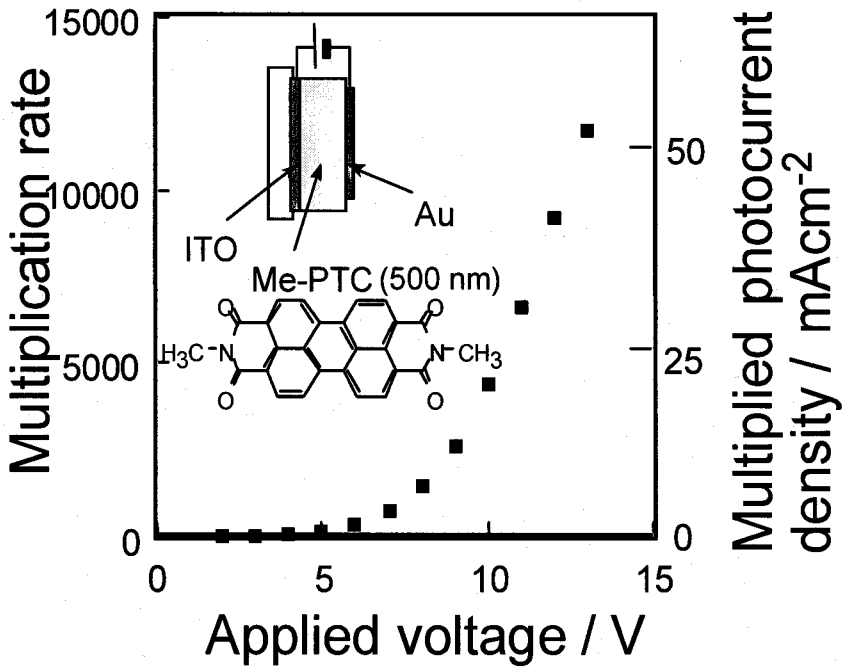

Fig.3-1 Dependence of multiplication rate and multiplied photocurrent density on applied voltage for the cell composed of ITO/Me-PTC(500nm)/Au. Monochromatic light of 600 nm (0.04 mW/cm^2) was shone onto the Au electrode. Cell structure and chemical formula of Me-PTC are also shown.

applying a carrier collection field of Vc to measure the current due to the release of trapped carriers.

Figure 3-1 shows the dependence of the multiplication rate and the multiplied photocurrent density on the applied voltage. The Au electrode was biased negatively with respect to the ITO electrode. The multiplication rate is defined as the ratio of the number of photogenerated carriers collected to the number of photons absorbed by the Me-PTC film. When the Au electrode was biased negatively, the multiplication rate and photocurrent density reached 1.2×10^4-fold and 55 $mAcm^{-2}$ at 13 V, respectively.

3-3. Results and Discussion

First, we estimated the density of the interfacial traps. The multiplied photocurrent-voltage characteristics can be analyzed by the Fowler-Nordheim equation describing the tunneling process.[15] In the region of a high electric field during multiplication, the Fowler-Nordheim relation of $\ln(JE^{-2})$ vs. E^{-1} (J: photocurrent density, E: electric field) gave a straight line as shown in Fig. 3-2. When the applied field was assumed to be uniformly distributed throughout the Me-PTC bulk, however, the injection barrier height obtained from the slope was only 0.07 eV, which is far smaller than the value of 1.5 eV estimated from atmospheric photoelectron emission analysis.[16] In order to resolve this discrepancy, according to the multiplication mechanism, we assumed that the applied electric field is concentrated at the interfacial region as shown in the inset of Fig. 3-2. As a result, a barrier height of 1.5 eV was obtained from the slope for a field concentration width of 4 nm.

The field concentration width of 4 nm means that a field strength of 10^7 V/cm is built up at the interface when the voltage is only 4 V. The required number of

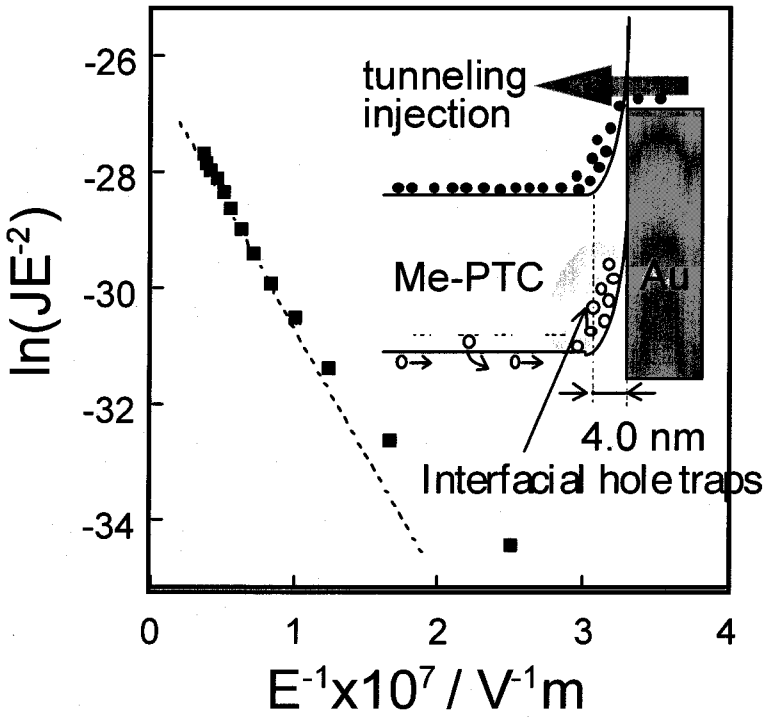

Fig.3-2 Fowler-Nordheim plot obtained from the multiplied photocurrent-voltage characteristics in Fig.3-1. Inset is the energy structure of the Me-PTC/Au interface during multiplication. The Au electrode is biased negatively. Filled and open circles indicate electrons and holes, respectively.

trapped holes for such an intense field concentration can be estimated as 5×10^{12} cm^{-2} when the relative dielectric constant for Me-PTC is assumed to be 4.0. This means that five holes are trapped in the area of 10 nm^2. Taking the molecular size of about 1 nm into consideration, this surprisingly high areal charge density implies that a hole trap at the interface must be some peculiar type.

To clarify the nature of such a trap, thermally stimulated current measurements were performed. Figure 3-3(a) shows the TSC curves for a collection field (V_c) of 0.9 V. The Au electrode was biased negatively with respect to the ITO electrode. The TSC peak (T_m) shifted to higher temperature when the heating rate, β was increased. If this TSC came merely from the release of trapped holes, the trap depth

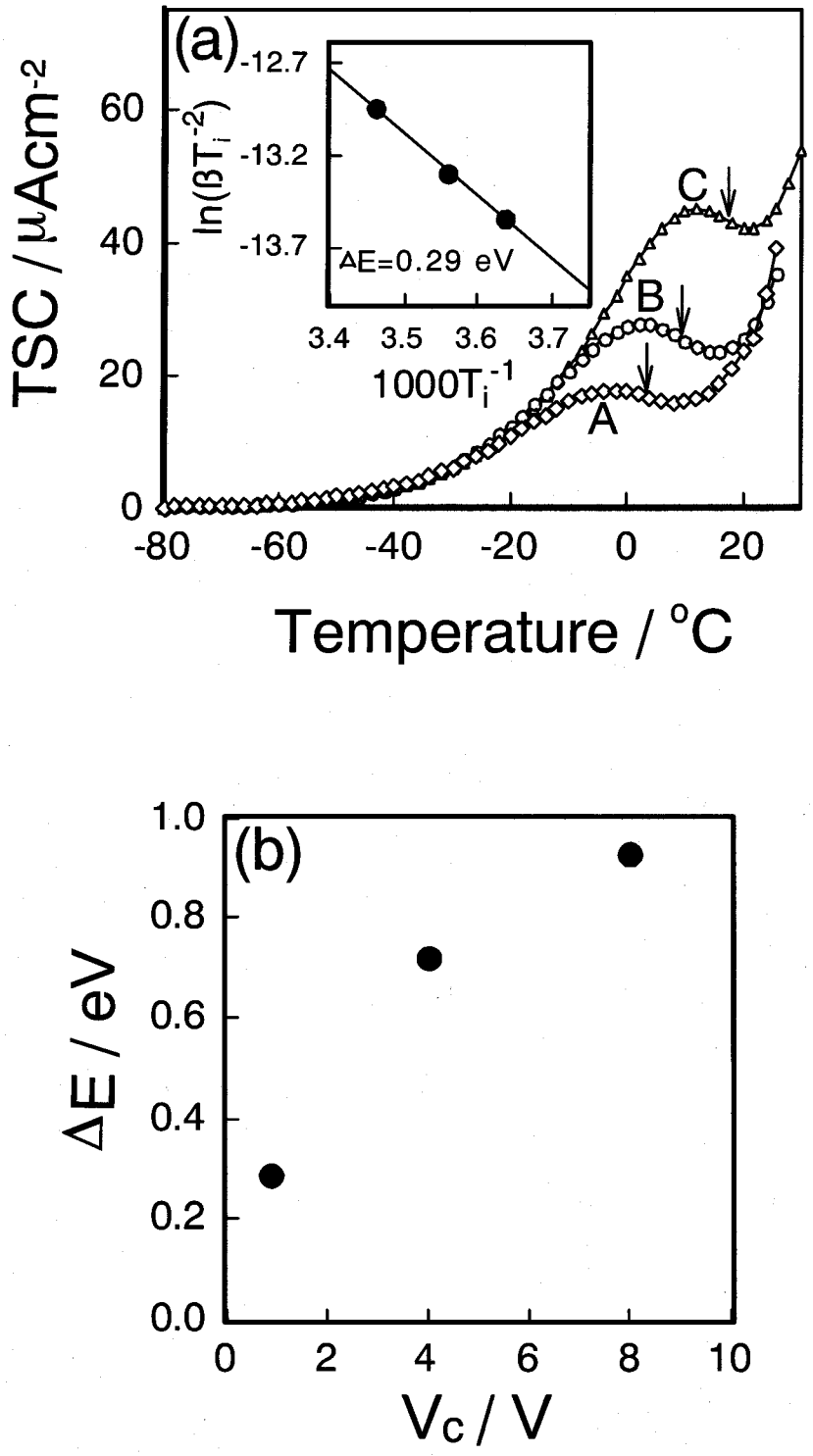

Fig. 3-3 (a) TSC curves of interfacial hole trap observed when applying a V_c of 0.9 V. The Au electrode was biased negatively with respect to the ITO electrode. Heating rates are 6 (curve A), 8 (curve B), and 12 °C/min (curve C). Arrows indicate Ti. Inset is $\ln(\beta T_i^{-2})$ vs. Ti^{-1}. (b) Dependence of ΔE on V_c.

(ΔE) could be directly determined from the slope of the plot of $\ln(\beta T_m^{-2})$ vs. T_m^{-1} as a widely used analytic procedure. The slope gives the value of $-\Delta Ek$ (k: Boltzmann constant).[17] However, the very large magnitude of the thermally stimulated current observed (>10 $\mu A/cm^2$) implied that the current cannot be explained simply to occur by released holes. Thus, we concluded that the TSC observed in the present study was the multiplied current due to electron tunneling from the Au electrode resulted from hole accumulation at interfacial traps. Actually, such a multiplication effect was scarcely suppressed during the TSC measurements. In this case, however, the decay of TSC beyon the maximum can be considered to reflect the process of holes releasing from interfacial traps, because the reduction of trapped holes results in a smaller number of injected electrons. Moreover, the point of inflection of decay (T_i), which coincides with the peak of the differentiated TSC curves, can be regarded as the peak temperature for hole release. Based on the above consideration, $\ln(\beta T_i^{-2})$ was plotted against T_i^{-1} (inset) and then, a straight line relation was obtained, which is much more precise than in the case of T_m. Consequently, ΔE of 0.29 eV was obtained from this slope.

Figure 3-3(b) shows the dependence of ΔE on V_c. Interestingly, ΔE increased with applied field and approached to 1 eV at 8.0 V. Generally, in the case of a normal electronic trap-like impurity, ΔE should decrease with increasing field strength due to the Poole-Frenkel effect. Moreover, it is hard to imagine hole accumulation at such traps under so intense field concentration. Therefore, another type of trap should be considered.

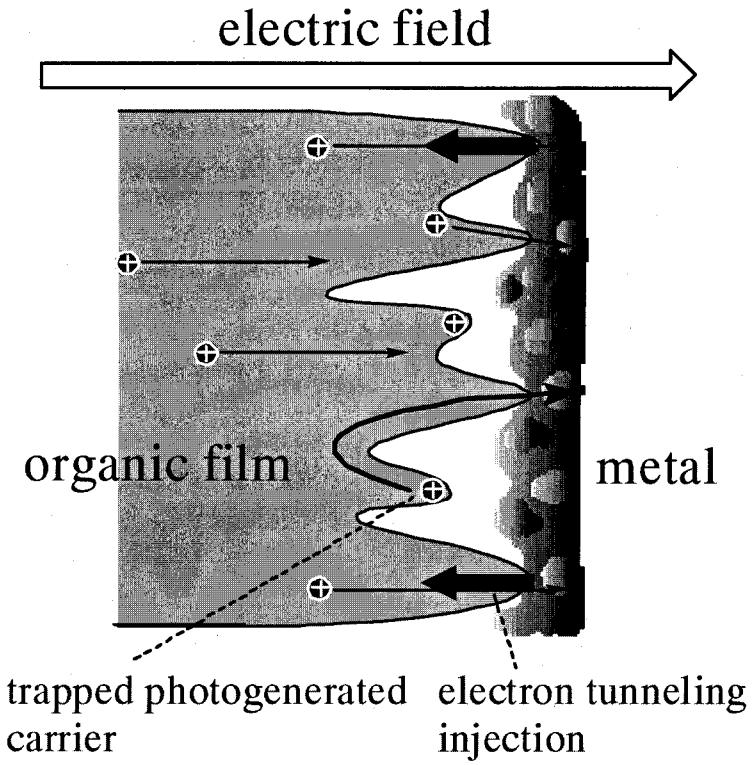

Fig. 3-4 Schematic view of pigment/metal interface. Holes are trapped by dead ends (structural trap) when the electric field is towards the metal.

From above mentioned consideration, we proposed the field-activated structural trap model. Figure 3-4 shows a schematic image of the structural trap at the pigment/metal interface. The pigment film usually has a microscopically rough surface, so the metal does not have uniform contact and there must be a large number of sites forming dead ends. Such sites could act as hole traps when the field is towards the metal. Assuming a dead end of 1 nm long, for instance, under the concentrated electric field of 10^7 Vcm^{-1}, the energy needed to release holes against the field, namely, the energy depth of the trap (ΔE) reaches 1 eV. Since holes become harder to release, that is, ΔE becomes larger under a stronger electric field, the result of TSC measurements can be reasonably explained by this model.

The origin of the structural traps has not been fully clarified yet. However,

high areal density reaching 5 per 10 nm^2 and dead ends about 1 nm deep imply that it is related to the molecular-sized roughness. This suggests that the multiplication behavior is greatly affected by the organic film morphology. Thus, the multiplied photocurrent should be sensitive to the film preparation conditions. The dependence of the multplied photocurrent on the surface morphology of the organic pigment film will be discussed in the following chapter.

3-4. Conclusion

In conclusion, the origin of the hole traps at organic/metal interface playing a key role in photocurrent multiplication was investigated by TSC measurement and analysys of current-voltage characteristics. As a result, it was found that the trap depth showed anomalous dependence on applied field, and the trap density was estimated to be surprisingly high value. In order to explain these results, we proposed a field-activated structural trap model that photogenerated carriers are trapped at blind alleys resulting from imperfect contacts between organic film and metal electrode. It should be pointed out that charge injection in various organic films, which is crucially important for their optoelectronic application, such as organic electroluminescence,[11] is greatly influenced by imperfect contact at the organic/metal interface.

Chapter 4

Photocurrent Multiplication at Organic/Metal Interface and Surface Morphology of Organic Films and Metal Electrode

4-1. Introduction

In Chapter 3, we introduced the field-activated structural trap model for the traps playing crucial roll on the photocurrent multiplication phenomena occuring at the organic/metal interface. This model insists that the charge accumulation is caused by the surface roughness of vacuum deposited organic film. The proposed model implies that the multiplication characteristics should be sensitive to the surface morphology of organic films and metal electrode composing the organic/metal interface. Therefore, the detailed inspection of the relationship between the morphological structure of organic/metal interface and multiplication characteristics would provide a strong evidence for the existence of blind alleys acting as structural trap as well as an approach for the intentional control of multiplication characteristics. From this standpoint of view, we have fabricated the organic films and metal electrode layers under the various preparation conditions and investigated the relation with the multiplication behavior.

In this chapter, we would like to demonstrate that the photocurrent multiplication characteristics in various kinds of perylene pigments (PTC, Fig. 4-1) are affected by the morphological structure of organic/metal interface.

4-2. Experimental Section

Three derivatives of perylene pigments, Me-PTC(N,N'-dimethyl-perylene-3,4:9,10-bis(dicarboximide)), n-Bu-PTC (N,N'-dibutyl-perylene-3,4:9,10-bis(dicarboximide)) and PhEt-PTC (N,N'-bis(phenylethyl)-perylene-3,4:9,10-bis(dicarboximide)) were used. These were supplied from Dainichiseika Color & Chemicals Manufacturing Co. Ltd., and purified twice by the train sublimation technique at least.[14] Sandwich-type cells (Fig. 4-1) were fabricated by the vacuum evaporation technique. PTCs and Au were deposited on an indium tin oxide (ITO) glass substrate under 1 x 10^{-3} Pa at room temperature. Deposition rate was monitored by an oscillating quartz crystal thickness monitor (ULVAC, CRTM-1000). Deposition rate of Au was maintained constant at 0.04 nms^{-1}. Typical deposition rate of PTCs was 0.2 nms^{-1}. Some of the PhEt-PTC films deposited on ITO glass substrates were exposed to tetrahydrofuran (THF) vapor in the glass vessel for 12 hours before the deposition of Au electrode.

Cells were set in an optical cryostat evacuated to 10^{-1} Pa. Photocurrent mea-

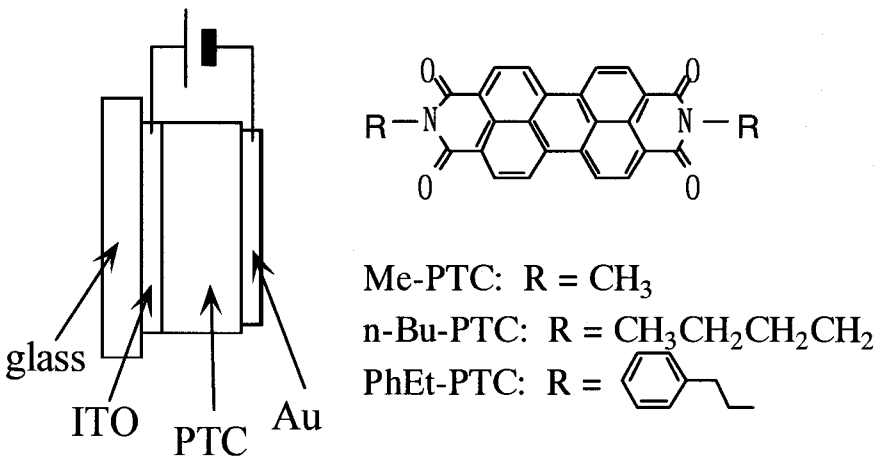

Fig. 4-1 Cell structure and chemical formulas of perylene pigments used.

surements were carried out using an electrometer (Keithley, model 617). Monochromatic light of 600 nm (0.04 $mWcm^{-2}$) from Xe-lamp through monochromator (Shimadzu, SPG-100ST) was irradiated onto transparent Au electrode. Au electrode was biased negatively with respect to ITO electrode. Multiplication rate is defined as the ratio of the number of photocurrent carriers collected to the number of photons absorbed by the PTC film.

Morphology of organic films was observed by using scanning electron microscope (SEM, Hitachi S-800). Crystallinity of organic films was evaluated by using X-ray diffractmeter (Rigaku, RINT-2000). Ionization potential of PTC films and work function of Au film were evaluated by an atmospheric photoelectron emission analyzer (Riken-Keiki, AC-1M).

4-3. Results and Discussion

4-3-1. Correlation between the surface morphology of organic films and multiplication behavior

Figure 4-2 shows the applied voltage dependence of multiplication rate observed for various perylen pigments having different substiruents, Me-PTC (curve a), n-Bu-PTC (curve b) and PhEt-PTC (curve c). Au electrode was biased negatively with respect to ITO electrode. Obviously, multiplication behavior was strongly dependent on the kinds of PTC pigments. At 20 V, both Me-PTC and n-Bu-PTC showed the large multiplication rate exceeding 2×10^4, and 5×10^3, respectively, but very interestingly, PhEt-PTC hardly showed the multiplication, i.e., multiplication rate was only 1.9 even at 20 V.

SEM pictures for as-deposited films of Me-PTC (a), n-Bu-PTC (b) and PhEt-PTC (c) are shown in Figure 4-3. In the cases of Me-PTC and n-Bu-PTC having

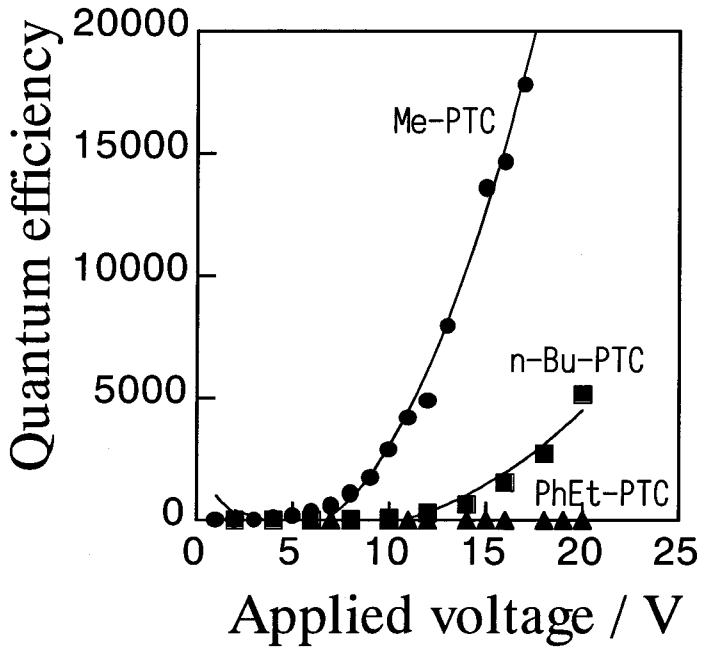

Fig. 4-2 Dependence of multiplication rate on applied voltage for ITO/PTC(500 nm)/Au(20 nm) cells. Me-PTC (a), n-Bu-PTC (b) and PhEt-PTC (c) were used as organic films. Au electrode was negatively biased with respect to ITO electrode. Monochromatic light of 600 nm (0.04 mWcm-2) was irradiated on Au electrode. Measurements were performed at room temperature.

relatively small substituents, the deposited films was found to be consisted of a gathering of microcrystals and to have the rough surface, since molecules tend to form aggregates easily due to the strong intermolecular interaction. On the other hand, in the case of PhEt-PTC having bulky substituent of phenylethyl, the deposited film had considerably flat and smooth surface. In the X-ray diffraction measurements, the Me-PTC film (a) showed intense diffraction peaks, but PhEt-PTC film (b) showed no diffraction peaks as shown in Figure 4-4. Thus, we concluded that the Me-PTC and n-Bu-PTC films which showed large multiplication are polycrystalline and PhEt-PTC film which hardly showed multiplication is amorphous.

In Chapter 2, it was suggested that the structural traps are related to the molecular-sized roughness of the organic film surface. Then, we tried to observe more

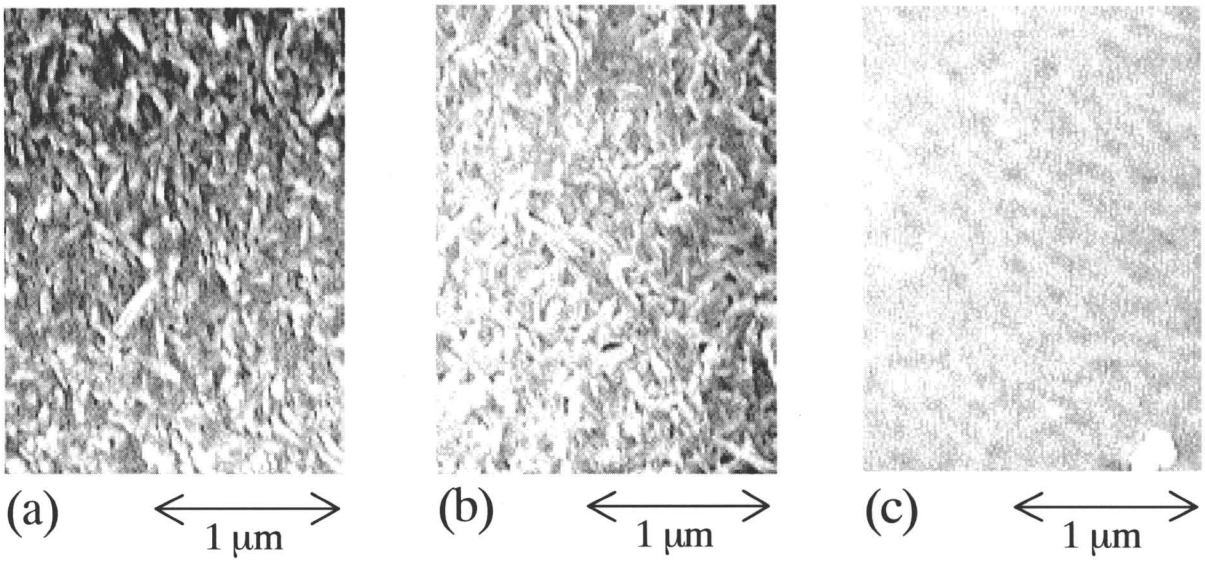

Fig. 4-3 SEM pictures for as-deposited films of Me-PTC (a), n-Bu-PTC (b), PhEt-PTC(c), and for THF-exposed film of PhEt-PTC (d). Thickness of all films were 500 nm.

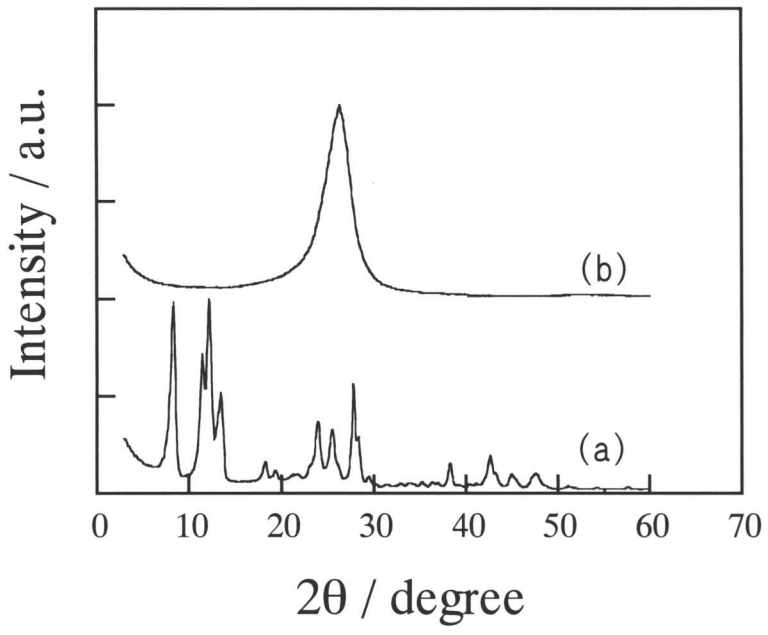

Fig. 4-4 X-ray diffraction patterns for as-deposited PTC films (500 nm). (a) Me-PTC. (b) PhEt-PTC

(a)

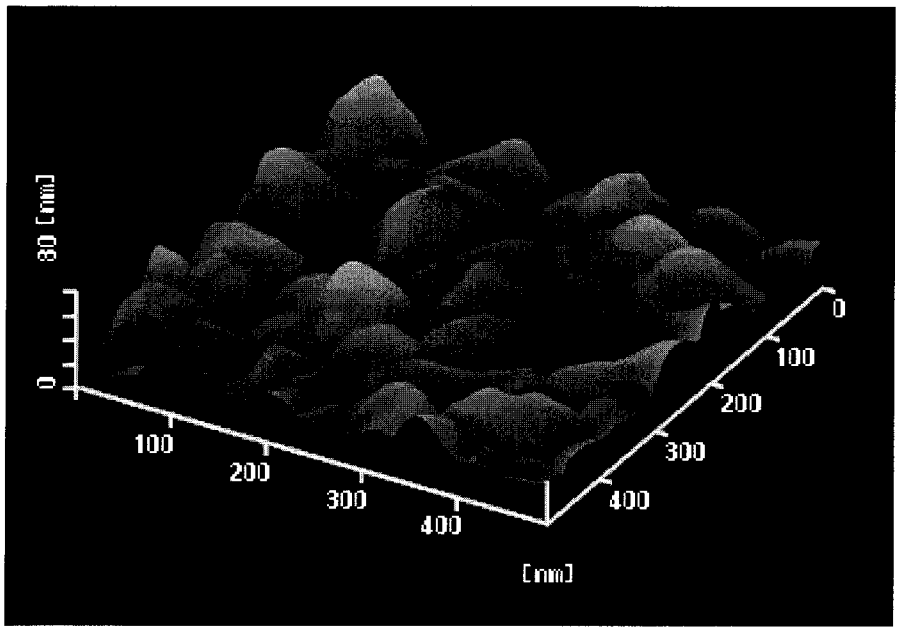

(b)

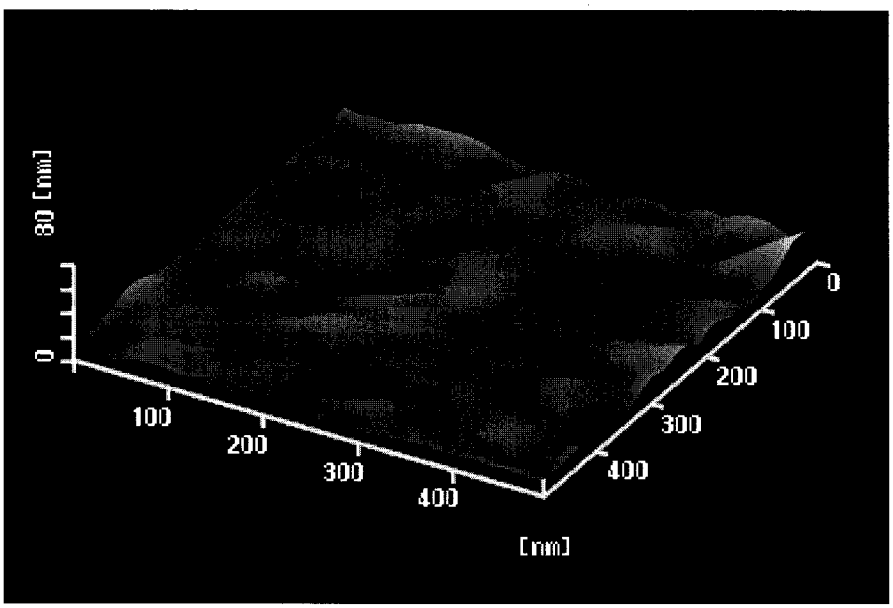

Fig. 4-5 AFM images of the vacuum deposited organic film. (a) Me-PTC. (b) PhEt-PTC.

microscopic surfce morphology of the organic film by using AFM. The AFM images of Me-PTC and PhEt-PTC are shown in Figure 4-5. The Me-PTC film was composed of many grains and showed a rough surface, while the surface of PhEt-PTC film was relatively flat and smooth. This result is consistent with the SEM images in Fig. 4-3, however unfortunately, moleular-size roughness can not be observed in our measurement.

The multiplication mechanism of photo-induced electron tunneling injection from metal electrode implies that the multiplication behavior should depend on the barrier height for electron injection from Au to the conduction state of PTC films. Figure 4-6 shows the energy levels of Me-PTC, n-BuPTC and PhEt-PTC. Work function of Au film is also shown in the figure. The work function of the Au electrode (4.9 eV) and the energy value of the upper edges of the valence band of PhEt-PTC films from the vacuum level (Me-PTC: 5.44 eV, n-Bu-PTC: 5.69 eV, PhEt-PTC: 5.55 eV) were measured by atmospheric photoelectron emission analysis. The

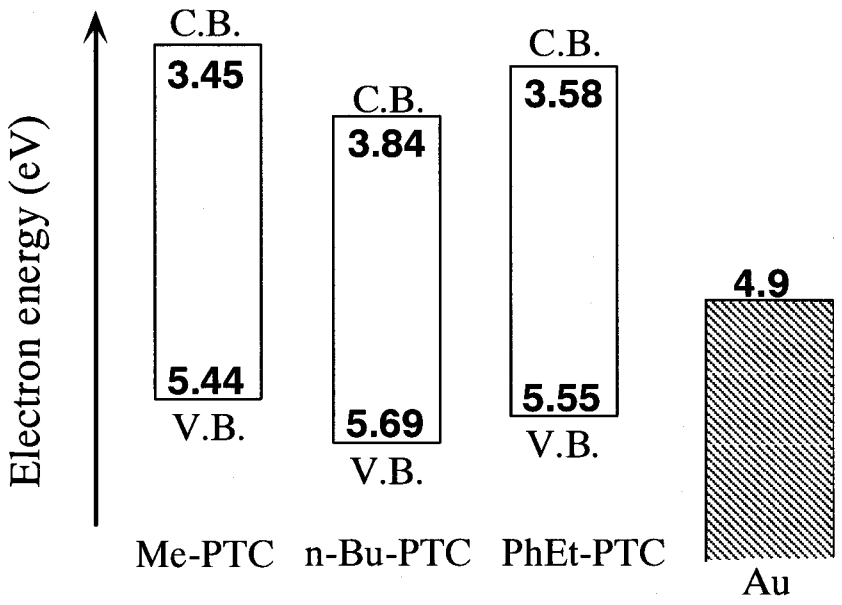

Fig. 4-6 Energy diagram of Me-PTC, n-Bu-PTC and PhEt-PTC films and Au film. V.B. and C.B. denote the valence band and the conduction band, respectively.

optical band gaps of Me-PTC (1.99 eV), n-Bu-PTC (1.85 eV) and PhEt-PTC (1.97 eV) were estimated from the edge of the absorption spectra. From these values, the lower edges of the conduction band (3.45, 3.84 and 3.58 eV) and the barrier heights (1.45, 1.06 and 1.32 eV) were obtained. Obviously, the barrier heights do not range in the order of multiplication rate, and moreover, Me-PTC showing the largest multiplication rate has the highest barrier. This result indicates that the energetic difference of the perylene pigments can hardly explain the large difference in the multiplication rate from unity to 2 x 10^4-fold.

As-deposited film of PhEt-PTC is known to undergo the phase change easily from amorphous to crystalline by exposing THF vapor.[18] In Figs. 4-7(a) and 4-7(b) are compared the SEM pictures of as-deposited and THF-exposed films of PhEt-PTC, respectively. As mentioned before, the surface of as-deposited film seems to be smooth and flat. On the contrary, the surface of THF-exposed film becomes rough and looks a gathering of bamboo leaf-like crystals of several micrometer-long. The X-ray diffraction analysis for both films clearly indicates that as-deposited and THF-exposed films are like amorphous and crystalline, respectively (Figure 4-8). After THF treatment, a sharp diffraction peak was observed at 6°. Further details of the solvent treatment effects for diffraction patterns of PhEt-PTC films were reported.[19] Figure 4-9 shows the dependence of multiplication rate on applied voltage for ITO/PhEt-PTC/Au cells. When the as-deposited film was used (curve a), multiplication rate was 1.2 under applying the bias of 16 V. Very interestingly, however, when the film exposed to THF vapor was incorporated in the cell (curve b), multiplication rate reached 360-fold at 18 V. The present result clearly indicated that the photocurrent multiplication phenomenon can be induced by changing the organic film morphology from amorphous to polycrystalline at least. From the re-

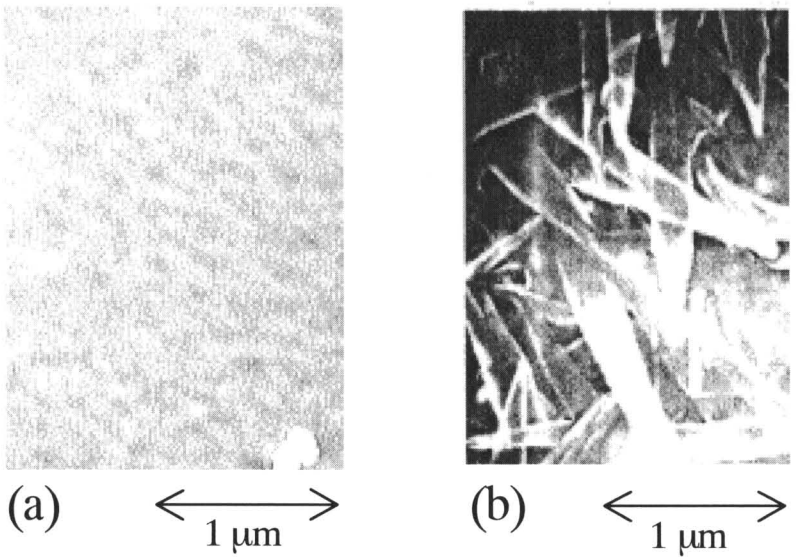

Fig. 4-7 SEM images of PhEt-PTC deposited film. (a) as-deposited. (b) exposed to THF vapor.

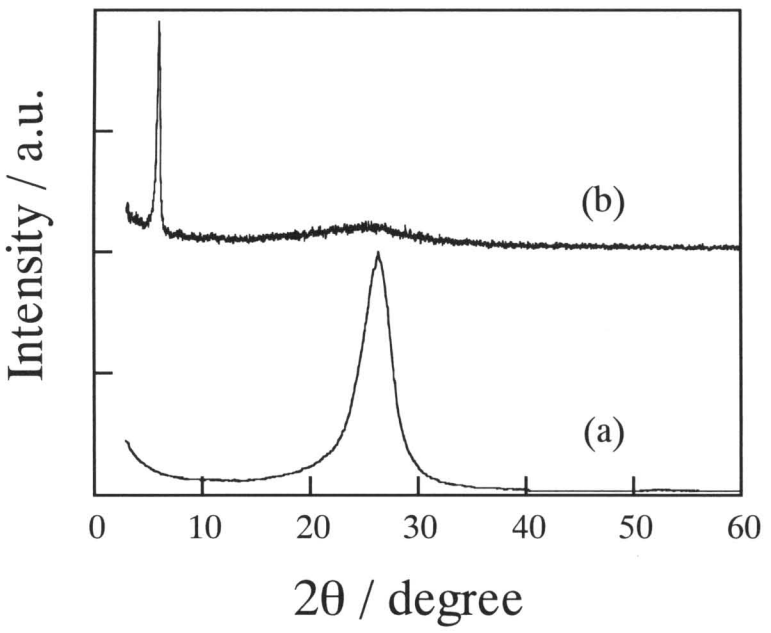

Fig. 4-8 X-ray diffraction patterns for deposited PhEt-PTC films. (a) as-deposited. (b) exposed to THF vapor.

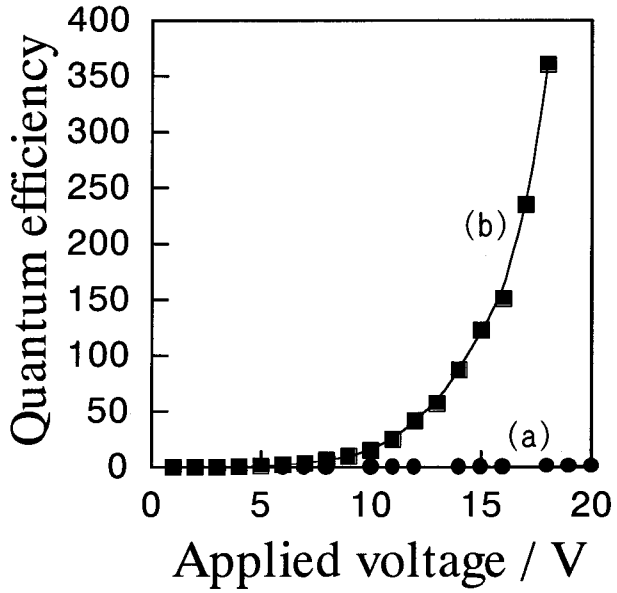

Fig. 4-9 Dependence of multiplication rate on applied voltage for ITO/ PhEt-PTC(500 nm)/Au(20 nm) cells. As-deposited (curve a) and THF-exposed (curve b) PhEt-PTC films were used. Au electrode was biased negatively with respect to ITO electrode. Measurements were performed at 233 K. Monochromatic light of 600 nm (0.04 mWcm-2) was irradiated on Au electrode.

sults mentioned above, we concluded that the multiplication characteristics are dominated not by the energetic structure but by the spatial structure of organic/metal interface, i.e., surface morphology of the organic film.

As a candidate of interfacial traps causing multiplication, we have proposed the field-activated structural trap model in Chapter 3. Organic pigment films having microscopically rough surface and metal do not form uniform contact and there exists a large number of sites forming blind alleys, which may act as hole traps when there is the electric field toward metal. This model reasonably explains the present results. Surface of polycrystalline PTC films such as Me-PTC, n-Bu-PTC, THF-exposed PhEt-PTC can be assumed to be microscopically rough and, on the contrary, that of amorphous state such as the as-deposited PhEt-PTC film to be micro-

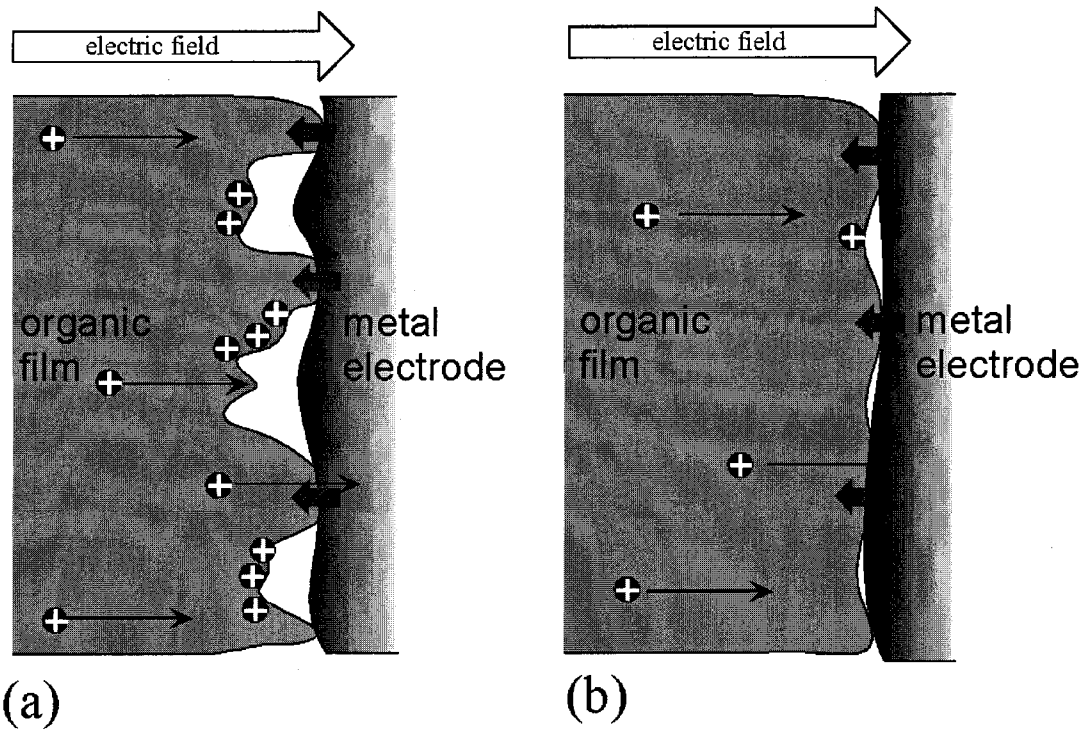

Fig. 4-10 Schematic illustrations of pigment/metal interfaces. (a) Crystalline PTC films having the rough surface. Holes are trapped to blind alleys at pigment/metal interface when the electric field toward metal exists. (b) Amorphous PTC films having the smooth surface. Holes are passed through the pigment/metal interface easily.

scopically smooth. In the case of crystalline films, therefore, there may exist a large number of blind alleys at which holes can not pass through the organic/metal interface due to uneven contact. The trapped carriers thus captured at organic/metal interface cause effective field concentration leading to a large multiplication (Figure 4-10(a)). On the other hand, in the case of amorphous films, there are little number of blind alleys and consequently multiplication hardly occurs (Figure 4-10(b)). Thus, substituent effects and THF exposing effect can be considered to affect the multiplication characteristics through changing the surface morphology of the organic films. The present observations suggest the close relation between the molecular stacking and the formation of blind alleys at organic/metal interface and support the proposed structural trap model.

It should be noted that the whole PhEt-PTC film including the bulk was crystallized by the THF treatment. Similarly, in the cases of the as-deposited films of Me-PTC, n-Bu-PTC and PhEt-PTC, crystallinity of the whole films including the bulk was different depending on the kinds of substituents. According to the structural trap model, however, only the molecular stacking near the organic/metal interface should affect the multiplication behavior. In order to confirm this, we have tried to disturb the molecular stacking only neighboring part to the organic/metal interface by means of the high-rate evaporation. Figure 4-11 shows the dependence of multiplication rate on applied voltage for ITO/n-Bu-PTC(500 nm)/Au cells. Cell structures are also shown in the figure. When the organic film was deposited at the slow

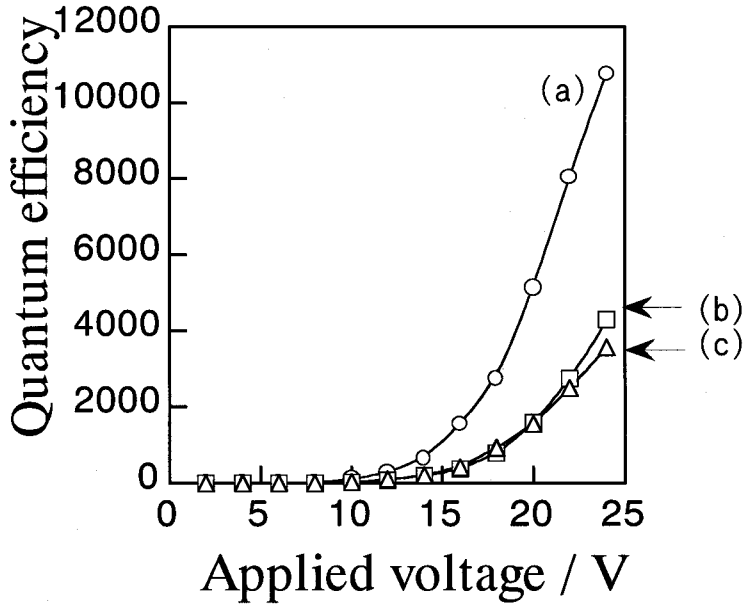

Fig. 4-11 Dependence of multiplication rate on applied voltage for ITO/n-Bu-PTC(500 nm)/Au cells. (a) n-Bu-PTC was deposited at the rate of 0.2 nms-1. (b) n-Bu-PTC was deposited at the rate of 3.0 nms-1. (c) 450 nm-thick n-Bu-PTC film was deposited at the rate of 0.2 nms-1 and then the residual 50 nm-thick n-Bu-PTC film was deposited at the rate of 3.0 nms-1. Au electrode was negatively biased with respect to ITO electrode. Monochromatic light of 600 nm (0.04 mWcm-2) was irradiated on Au electrode. Measurements were performed at room temperature.

deposition rate of 0.2 nms^{-1}, large multiplication was observed (curve a). When the whole organic film was deposited at the very high-rate of 3.0 nms^{-1}, multiplication was effectively suppressed (curve b). Interestingly, when only very thin organic layer of the thickness of 50 nm neighboring to Au electrode was evaporated at very high deposition rate of 3.0 nms^{-1}, suppressed multiplication rate similar to the curve b was observed (curve c). Fundamentally, the same result was obtained also in the case of Me-PTC film. These results clearly show that the multiplication was suppressed only by disturbing the molecular stacking near the pigment/metal interface, as was expected from the structural trap model.

4-3-2. Correlation between the morphology of metal electrodes and multiplication behavior

The structural trap model predicts that multiplication behaviors should be affected by not only organic film structure but also metal electrode structure. Therefore, we also investigated the multiplication devices in the case where the structure of metal electrode was varied.

Figure 4-12 shows the dependence of multiplication rate on the applied voltage observed for two kinds of ITO/Me-PTC/Au cells prepared using different Au deposition techniques. When Au film was deposited only by vacuum evaporation, the multiplication rate exceeded 2 x 10^4-fold at 16 V (curve A). However, when Me-PTC film was covered by Au film deposited by ion sputtering prior to Au vacuum deposition, a small multiplication rate of 2 x 10^3-fold was observed even when a higher voltage of 24 V (curve B) was applied. Figure 4-13 shows the dependence of the multiplication rate on Au deposition rate in case of Au film deposition by vacuum evaporation. The multiplication rate increased by 30 times from 6 x 10^2 to 1.8 x 10^4-fold by decreasing the deposition rate from 0.7 to 0.008 nms^{-1}.

Figures 4-12 and 4-13 clearly indicate that the multiplication characteristics are also quite sensitive to the preparation conditions of Au films. This result verifies again that the observed multiplication is a phenomenon that occurs at the organic/metal interface. As mentioned previously, the multiplication is caused by the photocarriers accumulation to the interfacial traps depending on the structure of organic/metal interface. In this mechanism, the nature of the traps near the organic/metal interface determines the multiplication characteristics. Thus, we interpreted from the present results that the trap concentration at the Me-PTC/Au interface varies depending on preparation conditions of Au films.

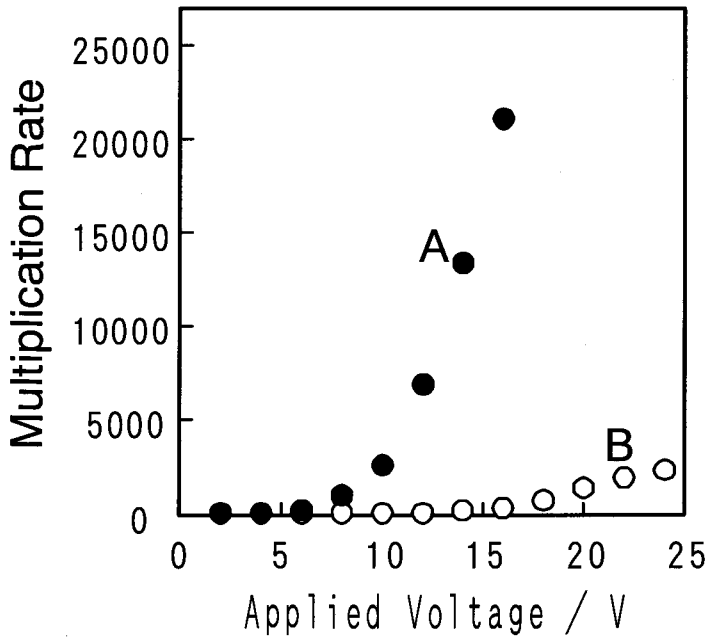

Fig. 4-12 Dependence of multiplication rate on the applied voltage observed for ITO/Me-PTC/Au cells deposited by means of two techniques: (A) Au film (20 nm) was deposited by vacuum evaporation. (B) Au film (2 nm) was deposited by ion sputtering technique, and then, residual Au (18 nm) was deposited by vacuum evaporation. The Au electrode was negatively biased with respect to ITO electrode. Monochromatic light of 600 nm (0.04 mWcm-2) was irradiated onto the Au electrode.

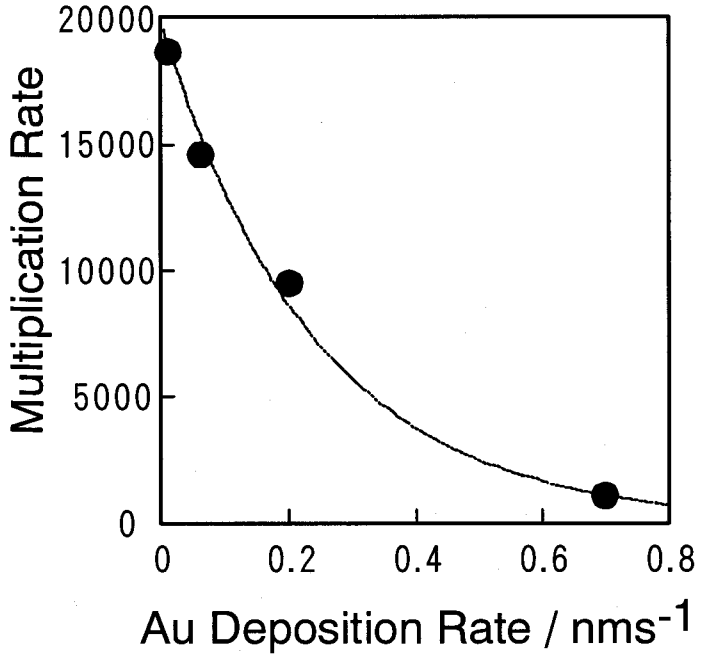

Fig. 4-13 Multiplication rate dependence on the Au deposition rate during vacuum evaporation. Multiplication rates were compared with the values at an applied voltage of 17 V. Monochromatic light of 600 nm (0.04 mWcm-2) was irradiated onto the Au electrode.

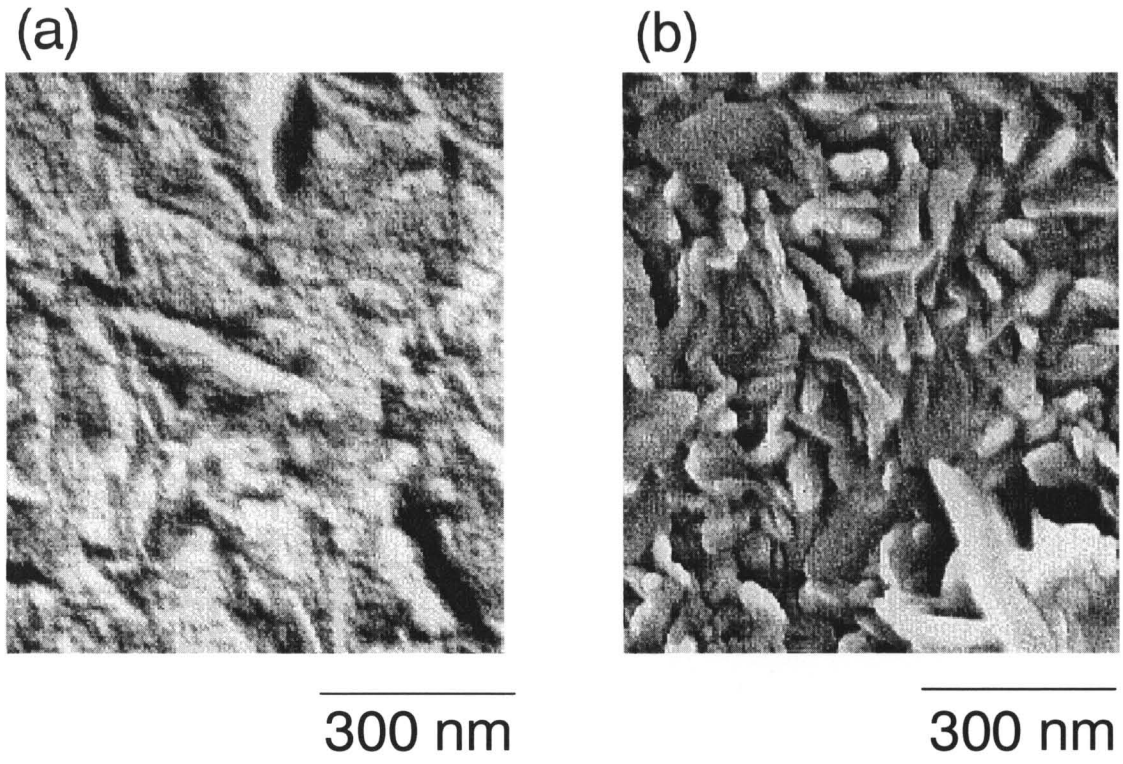

Fig. 4-14 SEM micrographs of Me-PTC films covered with Au films (thickness: 2 nm) deposited by the low-rate vacuum evaporation of 0.008 nms-1 (a) and by the ion sputtering technique (b).

Figure 4-14 shows the SEM micrographs for Me-PTC films covered with 2-nm-thick Au film by means of different deposition methods. When Au was deposited by the ion sputtering technique, the unique rough surface consisting of a cluster of 100-nm-long nanoscale crystals was clearly observed (Fig. 4-14(b)). The SEM micrograph of Me-PTC film without Au revealed a nearly identical morphology. Thus, we concluded that the morphology in Fig. 4-14(b) is that of the Me-PTC surface and the Au film deposited on this Me-PTC surface seems to adhere fairly uniformly to the microscopically rough surface of Me-PTC film. On the other hand, when Au was deposited by vacuum evaporation at the low rate of 0.008 nms-1, only the flat morphology of the deposited Au film seems to cover the entire polycrystal-

line surface structure of Me-PTC film (Fig. 4-14(a)). In this case, we therefore concluded that the Au film having an almost flat morphology hides the rough Me-PTC surface. In the case of vacuum evaporation at the high-rate of 0.7 nms-1, however, a morphology similar to that in Fig. 4-14(b) was observed.

The present results also can be explained based on the structural trap model as well as in the case of organic film structure. The Me-PTC/Au interface formed by Au film that aggregates itself flatly shows the large photocurrent multiplication and that formed by Au film that clings to the Me-PTC surface shows a small photocurrent multiplication. Figure 4-15 shows the schematic illustrations of these two types of organic/metal interfaces. When the deposited Au film aggregates itself flatly (Fig. 4-14(a)), it does not uniformly cover the microscopically rough surface of Me-

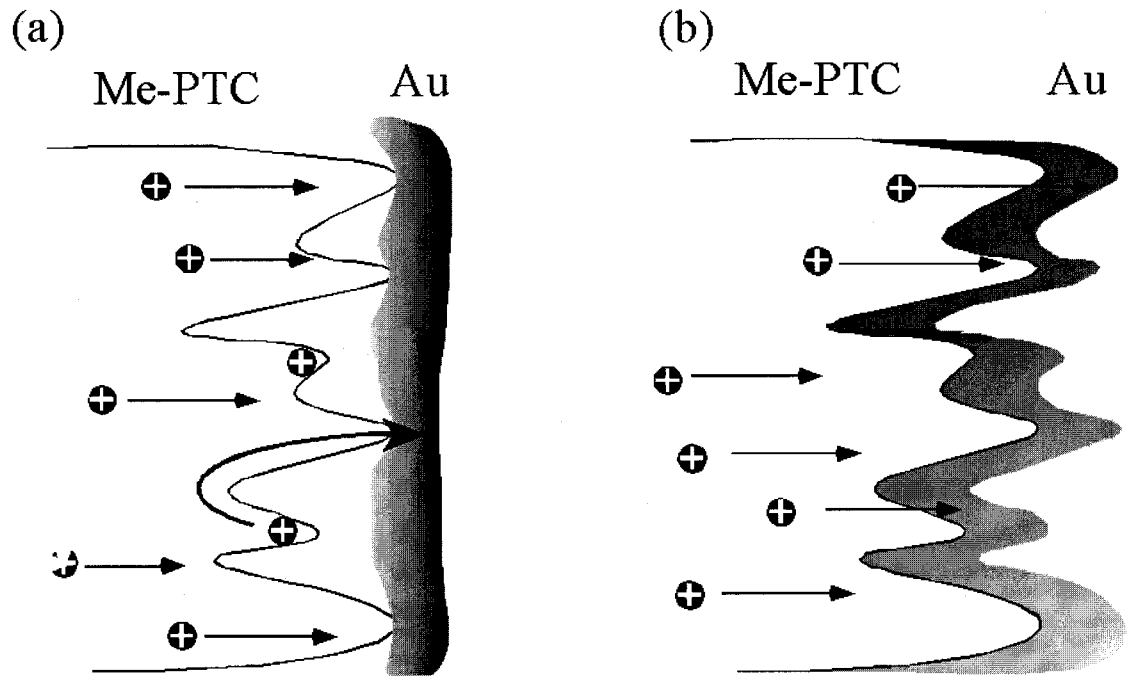

Fig. 4-15 Schematic illustration of the pigment/metal interfaces: (a) Au film aggregates itself flatly and is partly separated from the Me-PTC surface. Holes are trapped by blind alleys (structural traps) when there is an electric field toward the metal surface. (b) Au film clings to Me-PTC surface and uniformly covers the entire rough surface of Me-PTC film.

PTC film and is partly separated from the Me-PTC surface. In this type of organic/ metal interface shown in Fig. 4-15(a), a large number of blind alleys exist, acting as the sites preventing the holes to pass through to the metal electrode (structural trap). This accumulation of the photogenerated holes results in a large multiplication. In contrast, when the deposited Au clings to the Me-PTC surface (Fig. 4-14(b)), Au film uniformly covers the entire rough surface of Me-PTC film. In the organic/ metal interface shown in Fig. 4-15(b), there are few blind alleys, holes easily pass through the interface to the Au electrode and multiplication hardly occurs.

By decreasing the deposition rate during vacuum evaporation, a more closely packed film of better quality is known to be formed. On the other hand, the curve shown in Fig. 4-3 implies that an imperfect Me-PTC/Au contact with a large number of blind alleys, which shows large multiplication rate, tends to be formed by decreasing the deposition rate. Though these two facts seem to contradict each other, they can be consistently explained by microscopically considering the Me-PTC/Au interface formation process. Since the interaction among Au atoms can be assumed to be stronger than that between Me-PTC and Au, Au atoms have a fundamental tendency to aggregate themselves apart from Me-PTC film during the deposition process. This tendency is enhanced by decreasing the deposition rate because a more closely packed Au film is formed by slow deposition as mentioned above. As a result, an imperfect contact between Me-PTC and Au with a large number of separated sites occurs (see Fig. 4-15(a)).

4-4. Conclusion

In conclusion, photocurrent multiplication phenomenon at organic/metal interface was confirmed to be strongly dependent on the both structures of organic film and metal electrode. In the case of crystalline organic film having microscopically surface roughness or aggregated electrode prepared by slow deposition rate, the organic/metal interface has many microvacancies and the photogenerated carriers are efficiently trapped, resulting in large multiplication rate. On the other hand, in the case of amourphous-like organic film or smooth electrode prepared by high deposition rate or ion sputtering, the interface is formed more perfectly and the photogenerated carriers pass through the interface, resulting in small multiplication rate.

In the case of PhEt-PTC film, multiplication phenomenon reaching several hundred fold was intentionally induced by the solvent treatment. This result can be regarded as the first step toward the intentional control of multiplication characteristics based on the molecular level design of the organic film morphology.

All the present results strongly support the existence of structural trap at organic/metal interface. Thus, we cocluded that photocurrent multiplication is caused by photocarriers accumulation to the structrual traps, namely, blind alleys resulting from imperfect contact between organic film and metal electrode.

Chapter 5

Numerical Simulations of Photocurrent Multiplication Process at Organic/Metal Interface

5-1. Introduction

In a previous chapter, we have obtained a lot of strong supports for the field-activated structural trap model. That is, the photocurrent multiplication due to the electron tunneling injection caused by photocarrier accumlation has been revealed to be governed by the structural traps of blind alleys having imperfect contacts at the organic/metal interface. However, the distribution of accumulated charges at organic/metal interface can hardly be detected directly. In order to understand the whole mechanism more microscopically, we proceed to elucidate the field distribution in the interface formed by the accumulated charges and the charge accumulation process itself, namely, where and how much photogenerated carriers accumulate at the organic/metal interface.

In this chapter, therefore, we have tried to calculate the electric field distribution formed by accumulated space charges at such an imperfectly contacting organic/metal interface. The organic/metal interface was modeled based on the AFM images observed for photocurrent multiplication devices. In the first section, the electric field distribution was calculated by assuming the charge distribution based on the structural trap model. By comparing the tunneling current density based on various calculated field distribution and the experimental results, we examined the validity of the proposed structural trap model again. In the second section, we extended the calculation to simulating charge flow at organic/metal interface by tracing the time-development of space charge distribution. From the obtained results, we approached to the most essential mechanism of the photocurrent multiplication.

5-2. Calculation Method

Photocurrent multiplication phenomenon is observed in the simple device composed of an organic pigment film sandwiched between two metal electrodes prepared by vacuum evaporation. Figure 5-1 shows the AFM images of NTCDA (naphthalene tetracarboxylic dianhydride) film and Au electrode on it. NTCDA is a typical material showing a large multiplication rate at room temperature. In the NTCDA film, many grains of more than 100 nm size are grown and the surface seems to be rather smooth. On the other hand, the Au electrode deposited on the NTCDA film is composed of the gathering of spherical fine particles having a diameter of about 20 nm. Based on these observed AFM images, we have modeled the structure of the organic/metal interface as shown in Fig. 5-2. The imperfect contact at the organic/

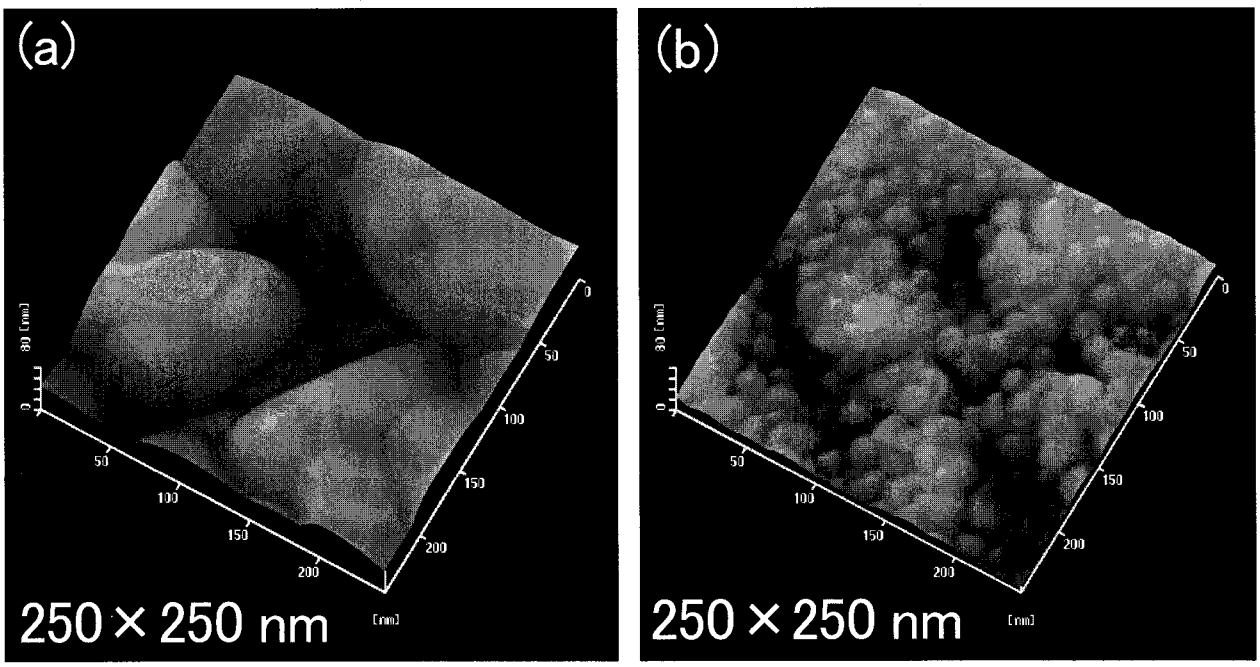

Fig.5-1 AFM images of deposited film surface and modeled organic/metal interface. (a) NTCDA film. (b) Au electrode deposited on NTCDA film.

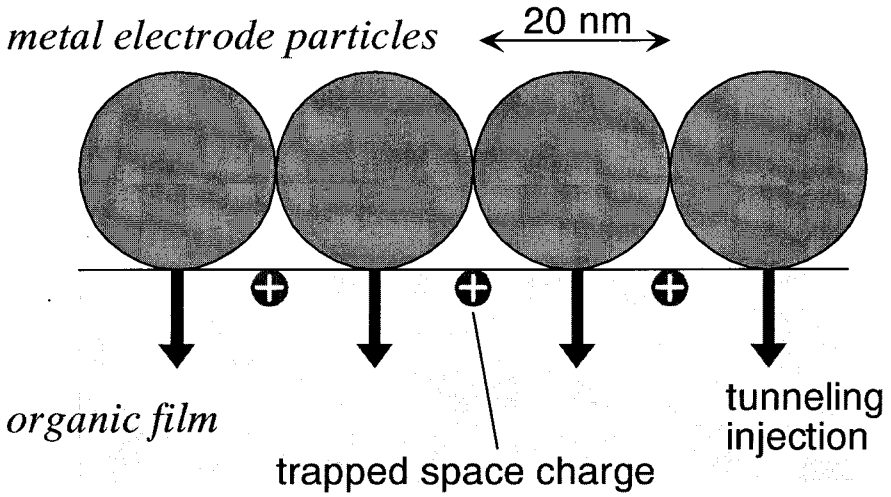

Fig.5-2 AFM images of deposited film surface and modeled organic/metal interface. (a) NTCDA film. (b) Au electrode deposited on NTCDA film.

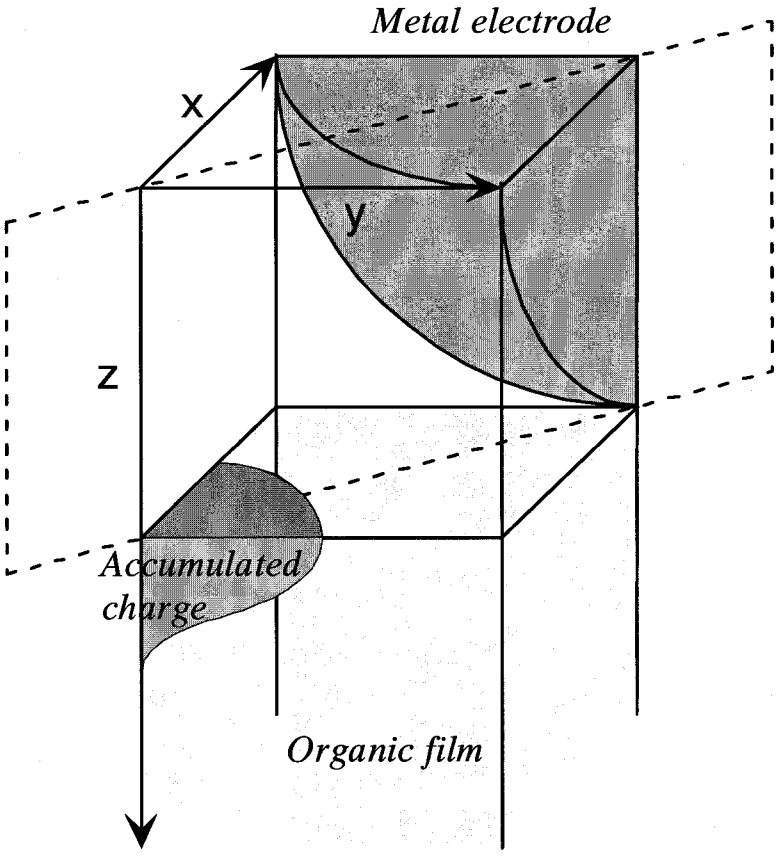

Fig.5-3 Schematic illustration of the boundry conditions for electrostatic potential calculation. The dashed line represents cross sention for evaluating field distribution.

metal interface in structural trap model is replaced with the even surface of organic film and spherical particle electrode covering the surface periodically and closely for simple and easy calculations.

The boundary conditions are shown in Fig. 5-3. The calculation was carried for one electrode particle under the periodic boundary condition. The size of the

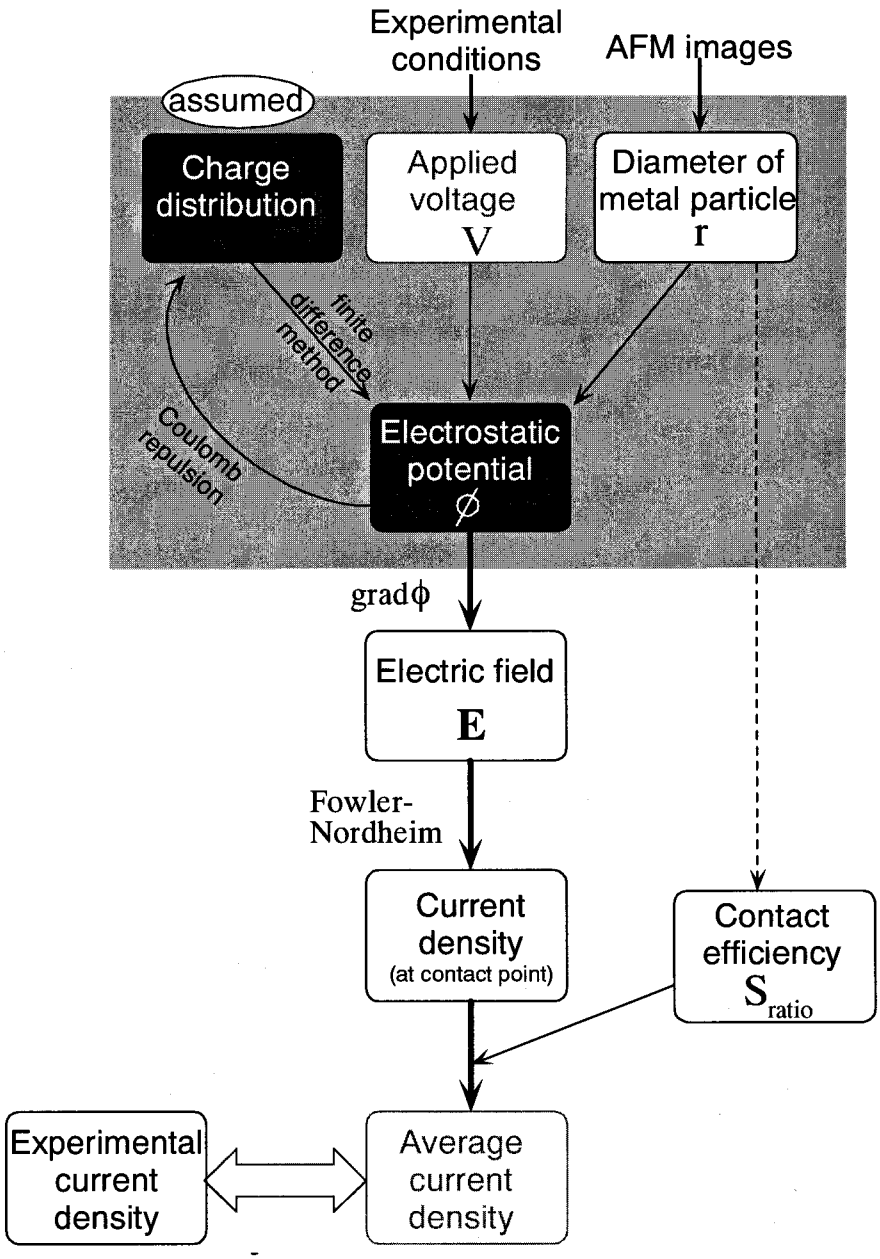

Fig.5-4 Sequence of calculation and analysis for the electric field formed by assumed space charges. Average current density obtained in the last result can be compared with the experimental current density.

calculating system in the z direction, namely, the film thickness was 50 nm. The potential of the metal electrode was assumed to be zero and that of the opposite side of the organic film was kept at the applied voltage.

For these modeled interface, an appropriate amount of space charge density, i.e., the accumulated charge distribution, was assumed to be located at the non-contact position between two electrode particles with Gaussian distribution. The parameter of d is the depth of the distribution center from the surface. The parameter of cx and cz represent the extent of distribution in the parallel and perpendicular direction to the surface, respectively. The amount of the accumulated charges was assumed to be the maximum amount of charges within the limit of Coulombic repulsion.

The sequence of calculation and analysis is shown in Figure 5-4. The electrostatic potential was obtained from the assumed charge distribution and the boundary condition by solving Poisson's equation by applying differential finite method to the system divided into 1 angstrom mesh. From the calculated potential, the local injection current density was obtained from the local electric field at the contact point between organic film and electrode fine particle by means of Fowler-Nordheim equation describing tunneling injection. Finally, we can obtain a mean current density that can be compared with the current density observed experimentally.

Next, the calculation was extended to simulating time-developing charge distribution at the organic/metal interface and the dynamic flow of the photogenerated carriers as shown in Figure 5-5 and 5-6. The photogenerated carriers were supplied from film bulk in each time step. For each time step, each charge within the pigment film was moved along the calculated electric field at a given time step. For the charge movement, field drift and diffusion drift were taken into account. Thus, the

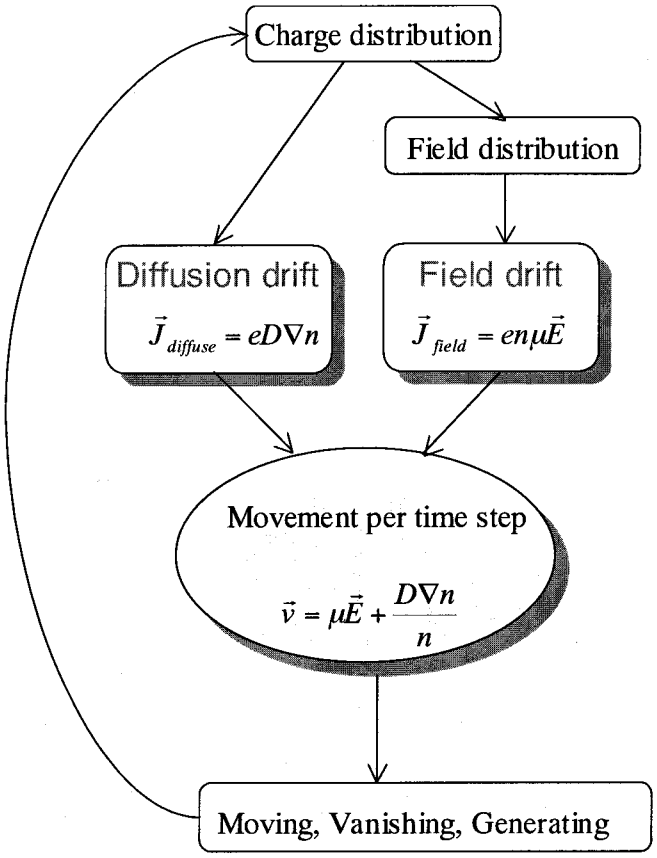

Fig.5-5 Calculation sequence for simulating the dynamic flow of photogenerated carriers.

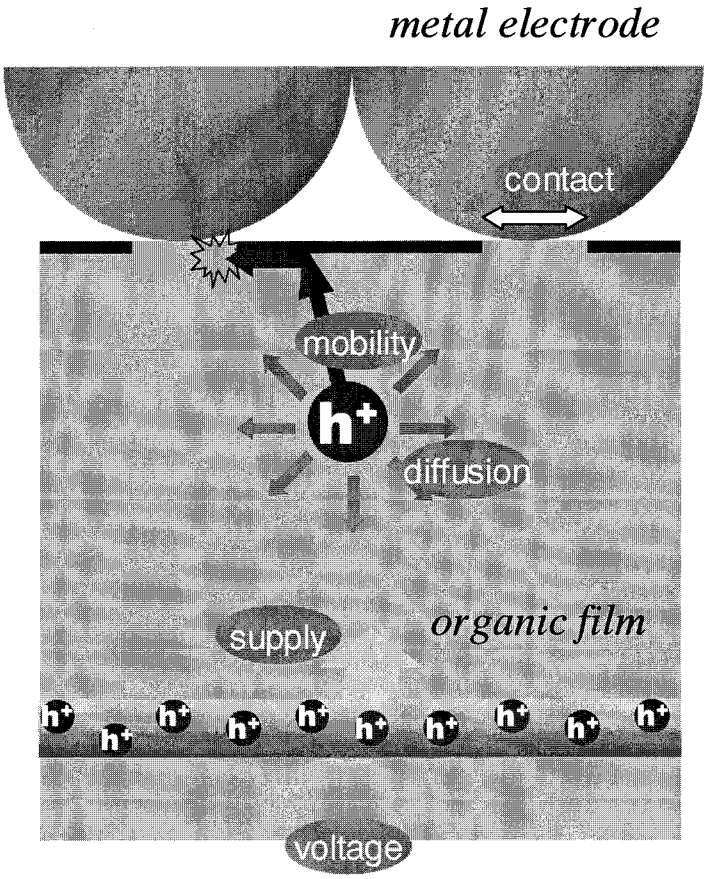

Fig.5-6 Schematic illustration of organic/ metal interface for simulating the dynamic flow of photogenerated carriers.

dynamic charge flow at organic/metal interface was simulated by calculating the time development of charge distribution one after another. For expressing the imperfect contact of organic/metal interface, the photogenerated carriers were assumed to be able to vanish only at the contact point of organic/metal interface.

5-3. Results and Discussion

5-3-1. Electric field distribution formed by assumed space charges

In this section, we have calculated the static distribution of electric field at the modeled oragnic/metal interface. By performing the calculation for various distribution of assumed space charges, we examined the validity of the proposed structural trap model.

The injection field is determined by the applied voltage and film thickness in a simple capacitor. However, at the moedeld interface, the injection field for electrons at organic/metal interface is determined by further two factors, namely, interfacial structure and space charges. In order to investrigate the structural effect, we firstly calculated the electric field at the modeled interface without space charge. Figure 5-7(a) shows a typical result of electrostatic potential calculation without space charge. The flat half circle part of left below side represents the metal electrode at that potential is kept at zero. In the absence of space charges, the voltage is applied to the whole organic film almost uniformly and the potential changes almost straight like a simple capacitor. However, it was found that the spherical shape of electrode particles slightly modulated the field distribution near the organic/metal interface. From now on, we will evaluate the field distribution at organic/metal interface by two parametric values, i.e., the field (E_c) at contact point between organic film and metal electrode and the field (E_{nc}) at non-contact point (see Figure 5-8). The E_c represents the injection field

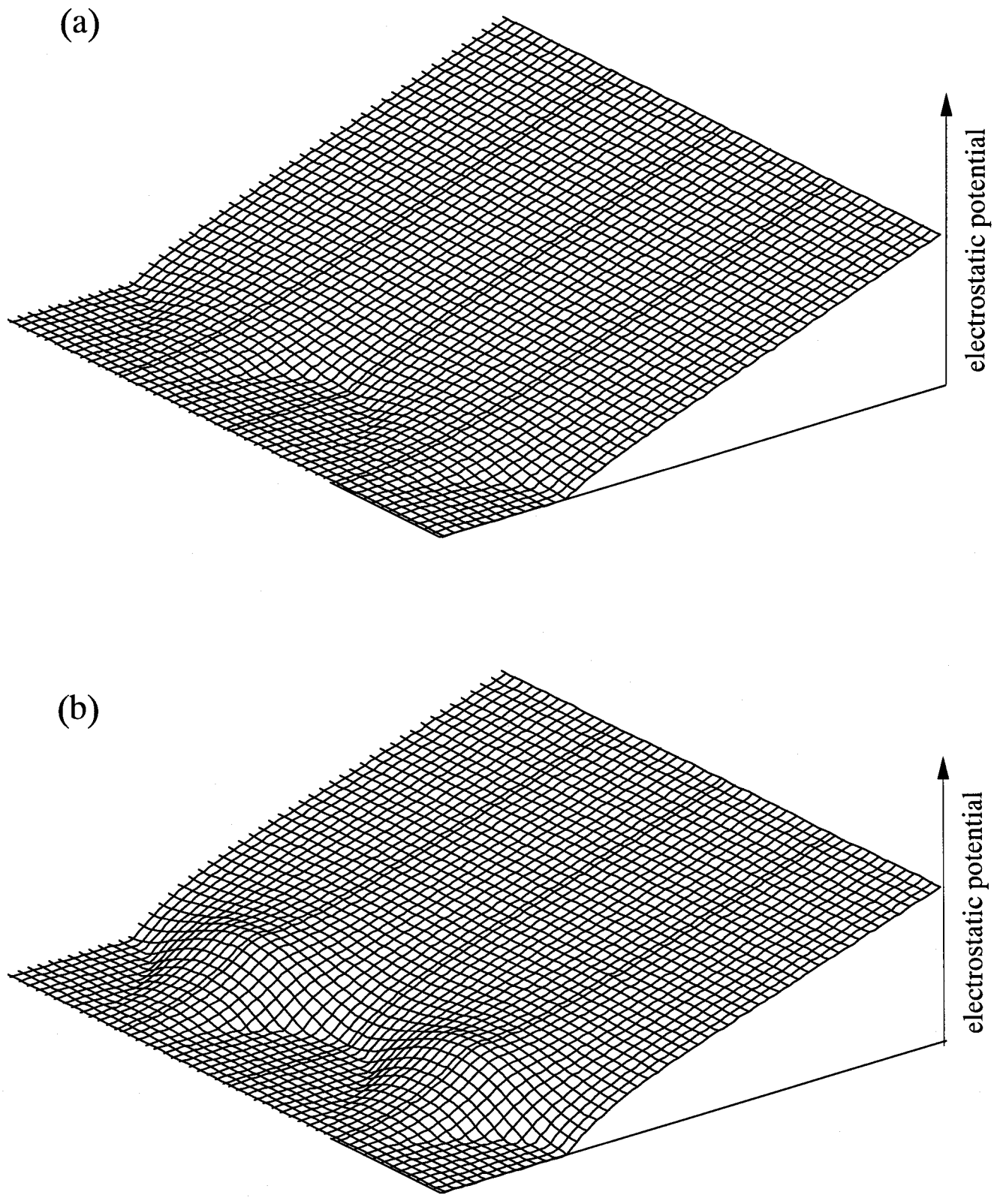

Fig.5-7 Typical result for electrostatic potential calculations at modeled organic/metal inteface. (a) without space charge. (b) with space charges.

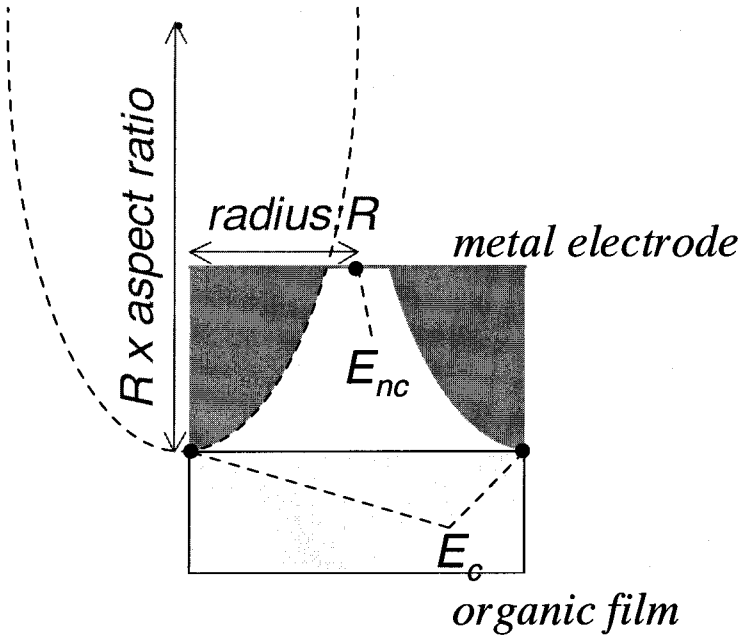

Fig.5-8 Geometric configurations of the parameters, E_c, E_{nc}, radius and aspect ratio of metal electrode particles.

perpendicular to the organic film at contact point of the organic/metal interface, while the E_{nc} represents the field on metal electrode surface between two metal electrodes, namely, the injection field from metal to vacuum.

Figure 5-9(a) shows the dependence of each electric field of E_c and E_{nc} on radius of electrode particles. The E_c is much larger than E_{nc}, and becomes larger with increasing radius of electrode particles, reaching 4.2×10^6 Vcm^{-1} for radius of 5 nm. If the electrode is a flat plate like a simple capacitor, the injection field has a constant value of 2.0×10^{-6} Vcm^{-1}. Therefore, it is found that the injection field was found to be enhanced about 2 times at the contact point by the spherical shape of electrode particles in comparison with the case where the voltage was applied to the organic film uniformly. On the other hand, the injection field at non-contact point was weakened to 2.1×10^5 Vcm^{-1}.

Not only the radius but also the shape of electrode particles affect the electric field distribution. The electric fields were calculated for various aspect ratio, i.e.,

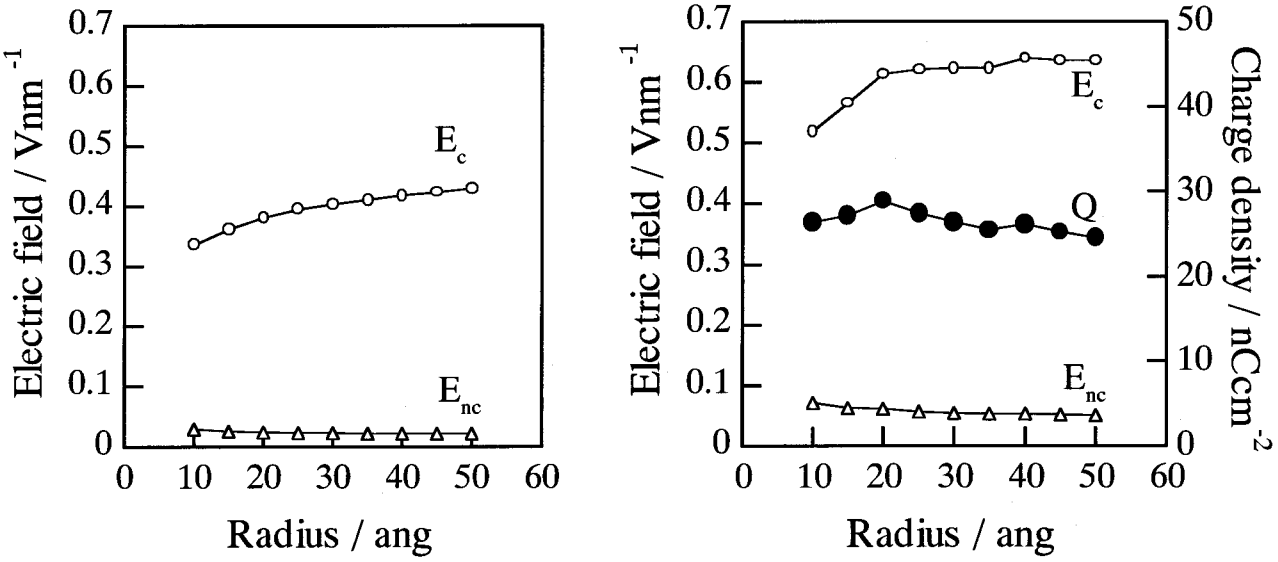

Fig.5-9 Dependence of electric field and charge density on the radius of metal electrode particles. (a) without charge. (b) with charge.

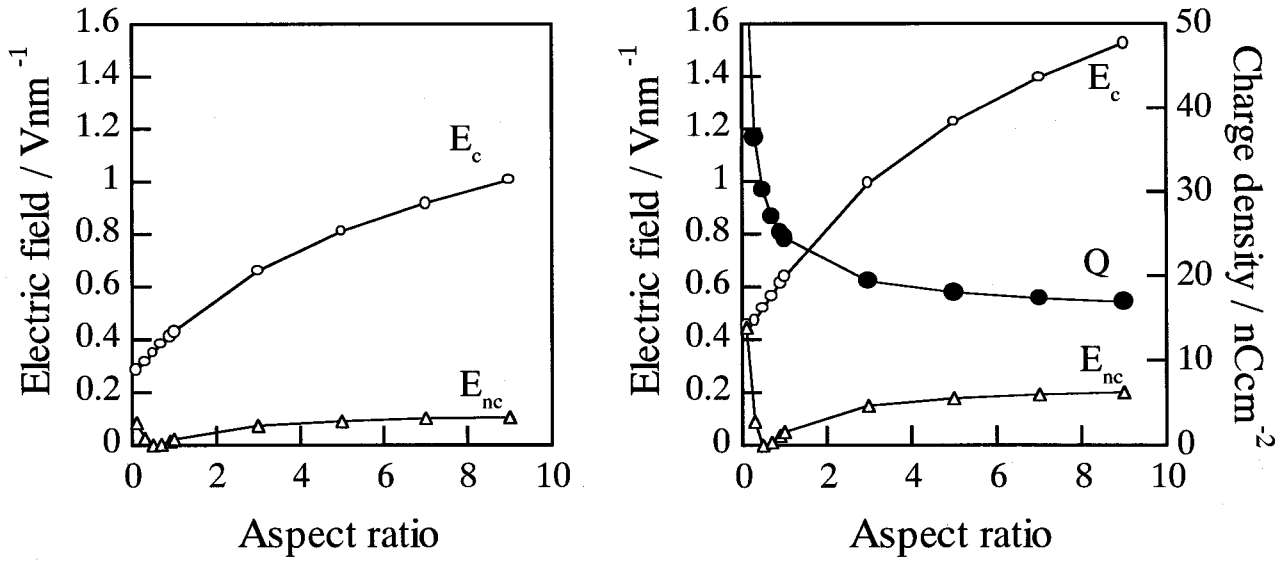

Fig.5-10 Dependence of electric field and charge density on the aspect ratio of metal electrode particles. (a) without charge. (b) with charge.

sharpness of electrode particles. For the calculation, the elliptical metal particles with various aspect ratios were replaced at the same center of gravity. The limiting aspect ratio of zero corresponds to the case of a simple capacitor, where E_c and E_{nc} have the same value of 2.0×10^6 Vcm^{-1}. As show in Figure 5-10(a), only E_c becomes larger with an increase of aspect ratio and reaches 1.0×10^7 Vcm^{-1} at aspect ratio of 9, whereas the E_{nc} remained at a small values of near 1.0×10^6 Vcm^{-1}. This result clearly shows that the shape of electrode particles seriously affects the injection field, and sharper electrode causes electric field concentration at the contact point of the organic/metal interface, even when space charges do not exist.

These results come from that electric force lines easily concentrate at the tip of the metal electrodes when the electrode has a definite curvature radius. Thus, it is conluded that the specific structure of the organic/metal interface in multiplication device can enhance the injection field even in dark condition, and consequently, assist the concentration of high electric field leading to tunneling injection when photogenerated carriers are supplied to the interface.

Electric field distribution formed by the assumed space charges

Next, we investigated the electric field distribution formed by the assumed space charges placed between electrode particles. Figure 5-7(b) shows a typical result of calculation. Compared with the previous case without space charge, it is clear from Fig. 5-7(a) that the accumulated charges in the middle of two electrode particles enhances the gradient of potential at the contact point, i.e., injection field. When the parameters were chosen so that the calculated current density is consistent with the experimentally observed current density, the injected field of 7×10^6 Vcm^{-1} and the charge density of 90 nC/cm^2 were obtained.

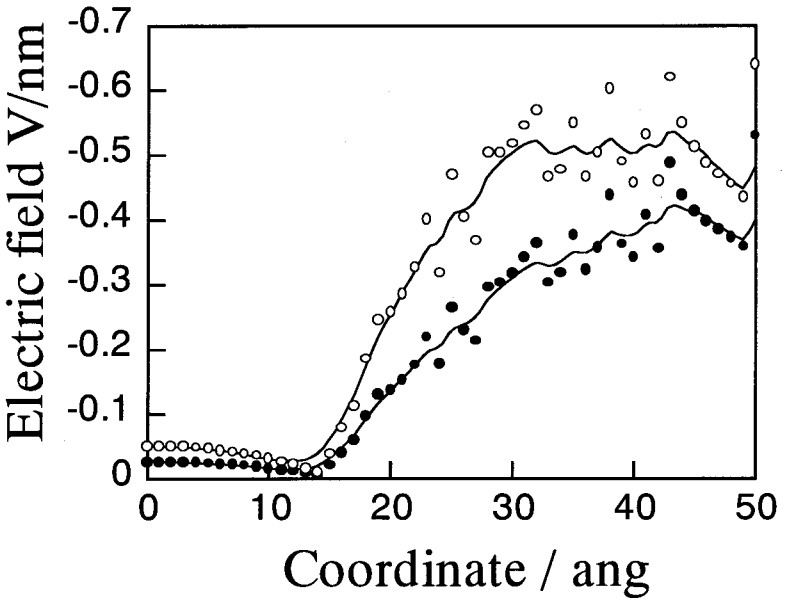

Fig.5-11 Distribution of electric field at the surface of metal electrode.

Figure 5-11 shows the potential distribution of the electric field at the surface of metal electrode in the both cases that space charges exist and not. This corresponds to the field intensity for tunneling injection because electron injection occurs at the electrode surface. The coordinate of 50 corresponds to the contact point and that of zero corresponds to non-contact point between electrode particles. In the both cases, the electric field at the contact point is enhanced by the spherical structure of electrode. It should be noted that the injection field at the contact point is also enhanced by the space charges placed between electrode particles. One of the questions for the structural trap model was whether the accumulated charge carriers could enhance the field intensity in the direction normal to the film or not, at the contact point where no accumulated charges exist. From the above-mentioned results, it is concluded that the electric field at the contact point can be enhanced sufficiently by the accumulated space charges between two electrode particles, and

is still much larger than the electric field between metal particles. The present result strongly supports the validity of the structural trap model which insists that the place where photogenerated holes accumulate differs from the place where electrons are injected.

From the present results, it is clear that the energy diagram of organic/metal interface varies from place to place because of the structure of organic/metal interface and the distribution of space charges. At the contact point of the organic/metal interface, where no accumulated charges exist, the conduction band of the organic pigment may bend gently and connects with the metal electrode directly. On the other hand, at the charge accumulating point, the conduction band bends sharply by the accumulated charges, and furthermore, the vacuum level was inserted between the organic film and metal electrode. It should be noted that these two different kinds of energy diagram emerge periodically. We can depict this distribution of energy diagram by using three-dimensional view as shown in Figure 5-12. The photogenerated holes accumulate in between the electrode particles and the electrons are injected through the contact point. Except for the contact point, tunneling injection of electrons is virtually impossible due to the high barrier of vacuum level. Since the place where the hole accumulates differs from the place where the electron flows by tunneling injection, the recombination of injected electrons and accumulated holes is prevented, resulting in retaining the injection field during multiplication. These results tell us that similar behavior may occur not only in multiplication device but also in usual organic/metal interface if there exists imperfect contacts. In such a system, we should carefully estimate the relation between applied voltage and injection field for analysys of current-voltage characteristics.

We will now discuss the structural effect of the organic/metal interface on field

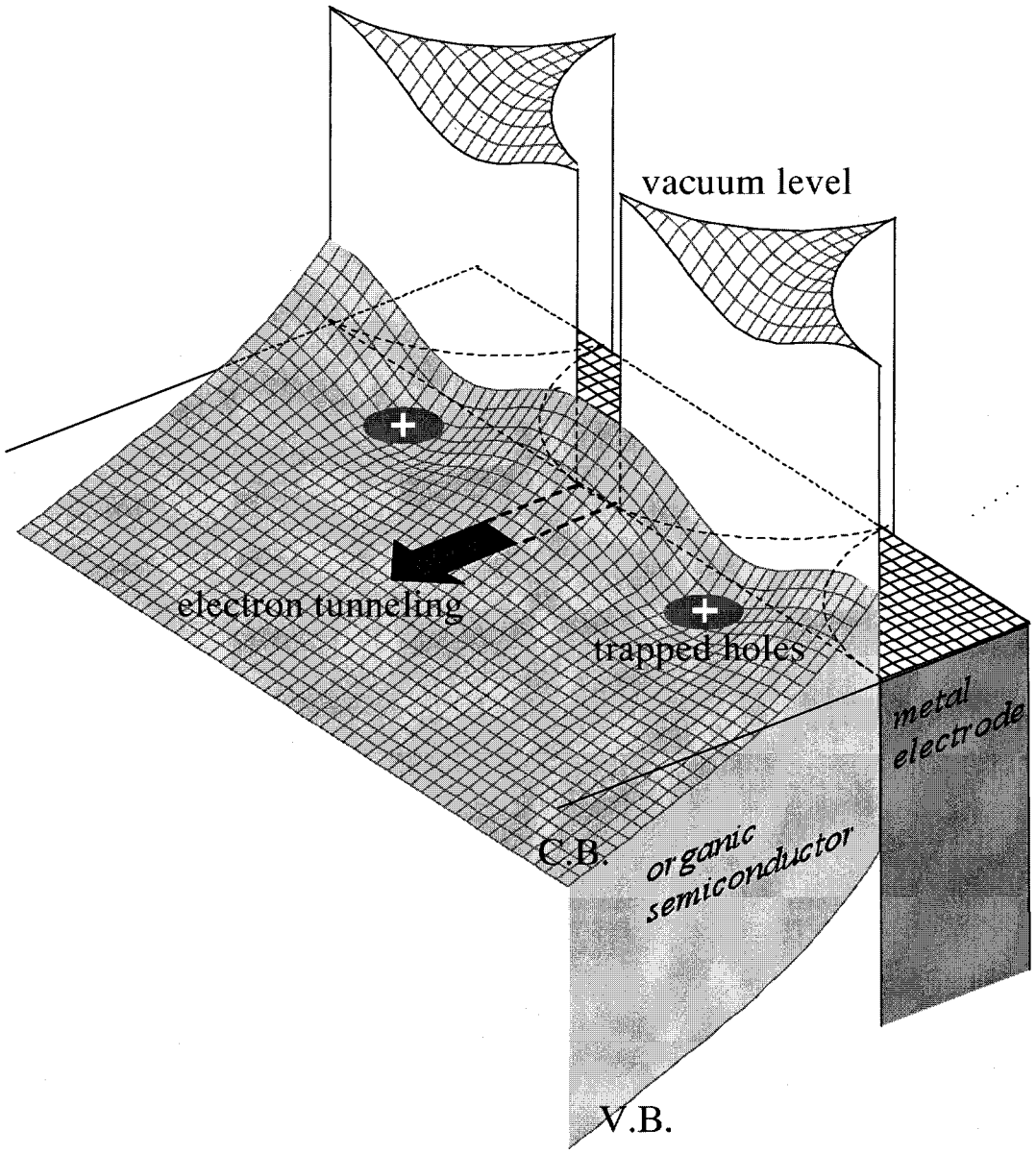

Fig.5-12 3-dimensional view of energy diagram at organic/metal interface based on the calculation resuts. The z axis corresponds electron energy.

distribution when space charges exist. We added the parametric value of Q, which represents the mean space charge density obatained from the maximum amount of space charges within the limit of Coulombic repulsion. As shown in Fig. 5-9(b), the electric field and amount of charges depends on the radius of electrode particles. The injection field becomes larger with increasing radius of the metal. This tendency is similar to the case without charges, but apparently the space charges enhance the injection field about 1.5 times compared with the case when no space charges exist. The maximum amount of accumulated charges seems to be not so affected by the radius of electrode particles.

Figure 5-10(b) shows the dependence on the aspect ratio of metal electrode. Again, the injection field becomes larger with an increase of aspect ratio by the structural effect, and the space charges enhance the injection field at contact point about 1.5 times for all aspect ratio. In this case, however, the allowed space charge accumulation decreases with an increase of aspect ratio. For lower aspect ratio, which means capacitor-like electrode, the larger amount of space charges can be accumulated at non-contact point and enhances E_{nc}. On the other hand, for high aspect ratio, which means sharp-edged electrode, the amount of space charges decreases owing to Coulombic repulsion, but they efficiently enhance E_c. This result predicts that the large multiplication can be obtained with small amount of photogenerated carriers if point-contact electrode particles can be formed on the organic film. Decrease of photogenerated carriers required for multiplication may also give a high-speed response of multiplied photocurrent.

The problem which we have to consider next is the distribution effect of the charges, namely, how the Gaussian distribution shape and location of space charges influence the electric field. The dependence on the depth of accumulated charges

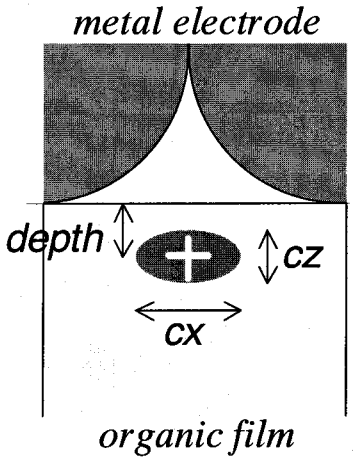

Fig.5-13 Geometric configurations of the parameters for Gaussian charge distribution.

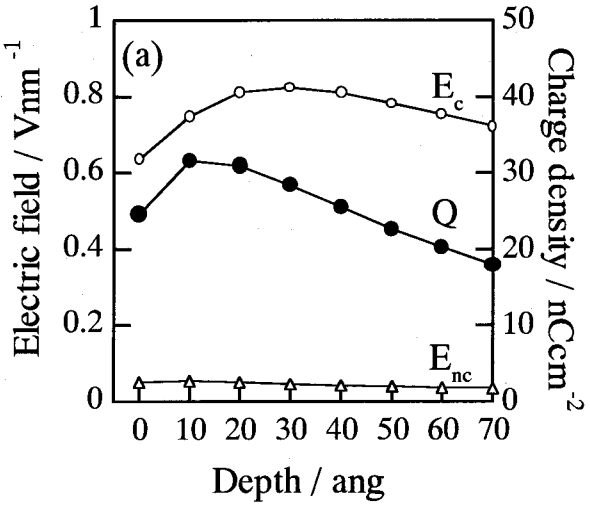

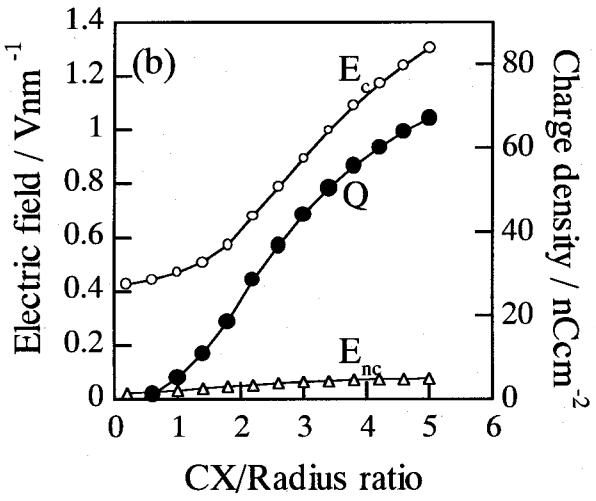

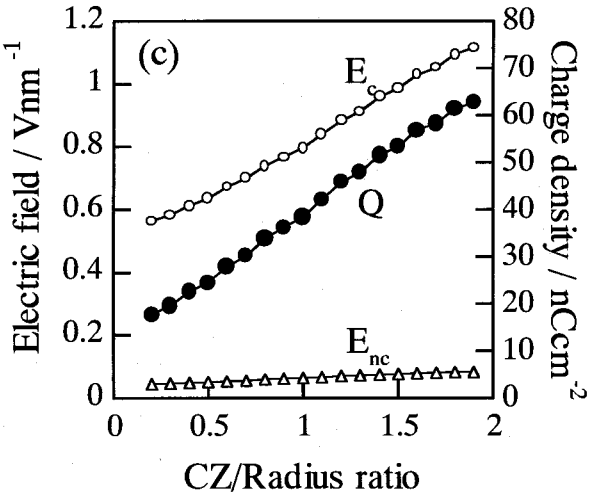

Fig.5-14 Dependence of electric field and charge density on the charge distribution. (a) depth (b) cz/R (c) cx/R.

from the surface is shown in Figure 5-14(a). The intersting thing is that there is the appropriate depth which makes the injection field maximum and it is found to be 3 nm. At the depth deeper than 3 nm, the injection field is weakened due to an increase of distance from the accumulated charges to the electrode. On the other hand, at the depth shallower than 3 nm, the injected field is also weakened because the charge distribution is limited by Coulombic repulsion and the vertical component at

the contact point decreases. Here, it should be noted that the value of 3nm quite agreed with the value of 4nm obtained from Fowler-Nordheim analysis of the multiplied photocurrent in Chapter 3.

The parameter of cx represents the extent of Gaussian charge distribution parallel to the surface (see Figure 5-13). The large cx represents the sheet-like charge distribution and the small cx represents the mesh-like charge distribution. The dependence of E_c on the width of charge distribution cx is shown in Figure 5-14(b). The injected field E_c at the contact point rapidly increases with an increase of cx. It was found that cx is the most influent parameter for the injection field. For efficient field concentration at the interface, larger cx, i.e., sheet-like charge accumulation is effective. The large multiplication observed in usual multiplication device may be due to such sheet-like charge accumulation in the insufficient contact of the organic/metal interface. In the same way, E_c, E_{nc} and Q increase monotonously with increasing the parameter of cz, which represents the extent of distribution perpendicular to the surface (Figure 5-14(c)).

From the results thus obtained, the charge effect by accumulation of photogenerated carriers seems to be smaller than the structural effect, which works even in dark condition. This result can be interpreted as follows. The multiplied photocurrent by tunneling injection obeys Fowler-Nordheim equation, which is extremely sensitive to the applied field. Figure 5-15 shows current-voltage curve of Fowler-Nordheim equation using parameters of Me-PTC/Au interface. The injection current drastically rises above the threshold of 4×10^6 Vcm^{-1}. Therefore, this fact tells us that if the electric field concentration below the threshold occured by the structural effect prior to the photo-illumination, even small enhancement by the charge effect of photocarriers accumulation can cause large multiplied photocurrent. This

presumption is supported by the fact that the multiplication device showing large multiplication rate tends to show large dark current. From another point of view, if we can tune the prior field concentration by the structural effect, much higher sensitivity or high-speed response of photocurrent multiplication can be attainable.

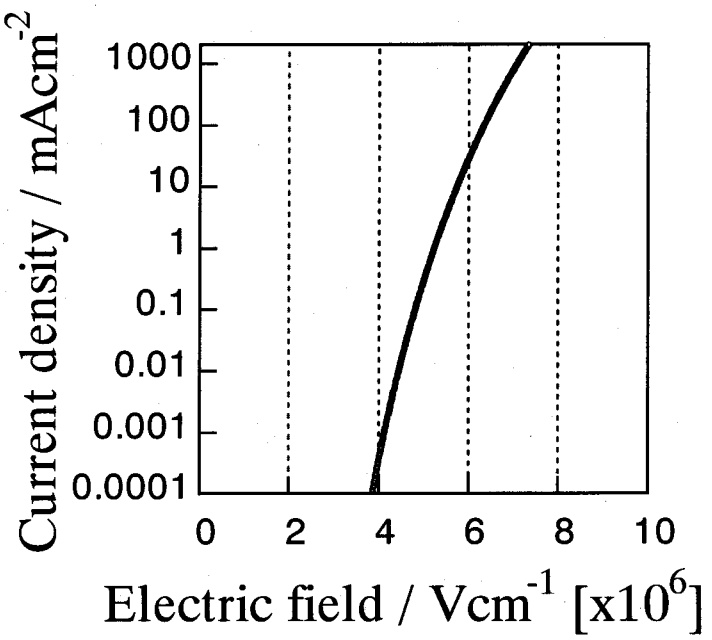

Fig.5-15 Current-voltage curve calculated by Fowler-Nordheim equation with experimental parameters.

Simulation of current-voltage characteristics

Finally, we will discuss the current-voltage characteristic which is directly related to the device performance. Since the present calculation contains the parameter of applied voltage, the injected electron current density for each voltage can be predicted. However, when applied voltage is simply swept with fixing other parameters, the calculated current rises up abruptly at some threshold and cannot reproduce the experimental result, because there is some proportional relation between the applied voltage and the injection field when other parameters are fixed. The multiplied photocurrent observed experimentally (Figure 5-16(a)) increases very slowly with increasing applied voltage in spite of tunneling injection described by Fowler-Nordheim equation (see Figure 5-15). This fact indicates that the parameter determining charge distribution should be dependent on applied voltage and some mechanisms which suppress the increase of injection field for an increasing voltage is needed. Therefore, we introduce the model that the parameter of cx decreased with increasing voltage V as follows.

$$cx(V) = cx(0) - aV$$

where $cx(0)$ is cx at zero volt, and a is a proportionality factor for applied voltage. In low voltage region, cx is large, which means sheet-like charge accumulation and efficient concentration of electric field. With an increase of applied voltage, cx becomes smaller, which means approach to mesh-like charge accumulation and suppression of field concentration. As a result, the injection field reached the ceiling for

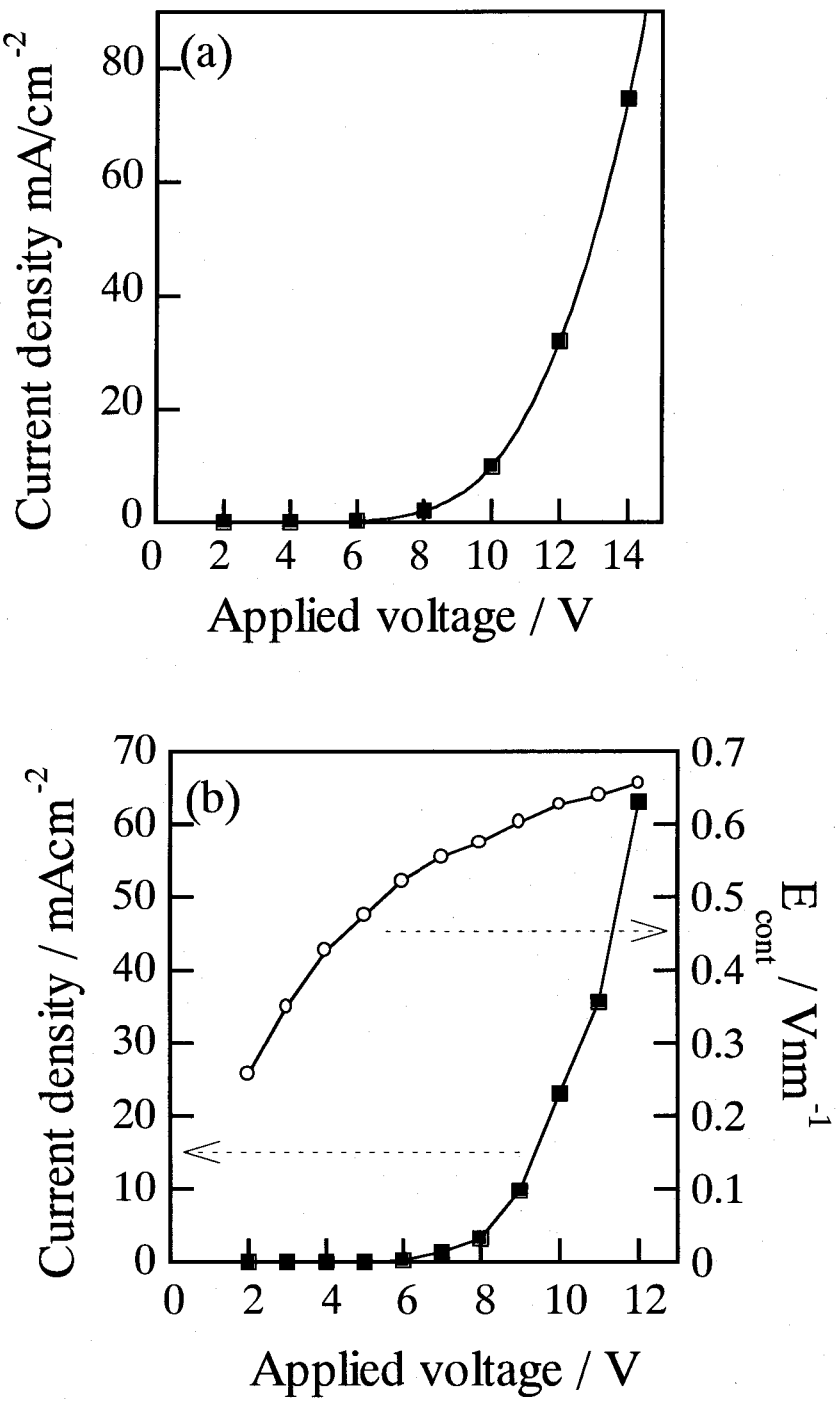

Fig.5-16 Current-voltage characteristics in multiplication device. (a) experimentally observed in ITO/NTCDA/Au device. (b) simulated by introducing recombination model.

an increase of applied voltage.

Figure 5-16(b) shows the current-voltage curve in this model. The injected current density increases gently for increasing applied voltage and is consistent with the experimental curve qualitatively. This consistence suggests that the decrease of charge distribution width with increasing voltage occurs in real device.

This model is interpreted by partial recombination between accumulated holes and injected electrons. That is to say, in low voltage region, since the number of injected electron is small, the photogenerated holes can accumulate even near the contact point, resulting in forming sheet-like accumulation (Figure 5-17(a)). On the other hand, in high voltage region, since a large number of electrons are injected into organic film, trapped holes near the contact point recombine with injected electrons and vanish (Figure 5-17(b)). Consequently, the distribution of trapped holes becomes mesh-like and the injected field is suppressed. Thus, the current-voltage characteristic was well reproduced by considering partial recombination of trapped holes and injected electrons.

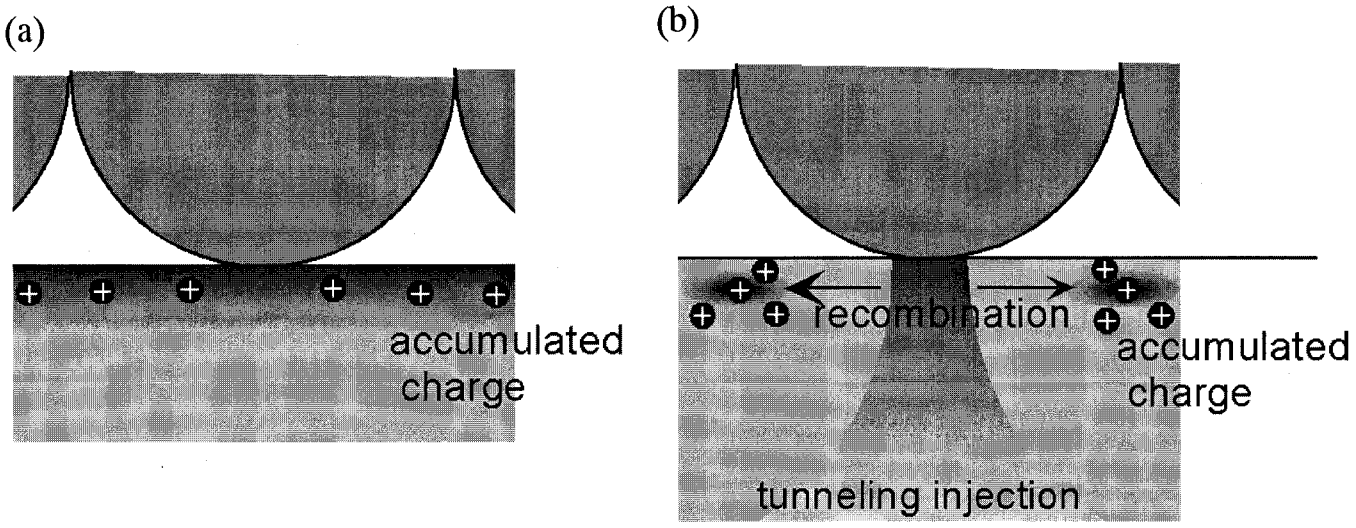

Fig.5-17 Recombination model for current-voltage characteristics. (a) in low voltage region. (b) in high voltage region.

5-3-2. Simulation for the dynamic flow of photogenerted charges at organic/ metal interface

In the previous section, we calculated electric field distribution at the modeled organic/metal interface by placing space charges as trapped holes on the pigment surface. In this section, we have tried to simulate the dynamic flow of photogenerated carriers at the imperfect organic/metal interface and anlyze the charge accumulation process itself. The simulation model was illustrated in Fig. 5-5 and Fig. 5-6. The dynamic flow was simulated by tracing the time development of charge distribution step by step. Figure 5-18 shows a typical result of numerical simulation for time development of charge distribution when the photogenerated carriers are supplied from the bulk of organic film continuously. The photogenerated carriers supplied in the film bulk (right up side in the figure) move toward the organic film surface in accordance with applied electric field. The carriers reaching the organic film surface apparently piles up at the non-contact point between two electrode particles as the high density of surface charges until the charges vanish at the contact point. Finally, the charge distribution reaches a steady state where the charge accumulation at the surface is balanced between the supply of photogenerated carriers from the bulk and the extinction at contact point to the metal electrode. Thus, it was shown that the high density of space charges emerges at the surface layer of organic film when photogenerated carriers are supplied continuously. It should be noted that an imperfect contact in the organic/metal interface inevitably brings about such a dynamic charge accumulation. Consequently, this result tells us that the interfacial charges accumulated at the imperfect organic/metal interface during the dynamic flow of charges may cause the photocurrent multiplication. Therefore, the charge accumulation to give electric field concentration may occur in every inter-

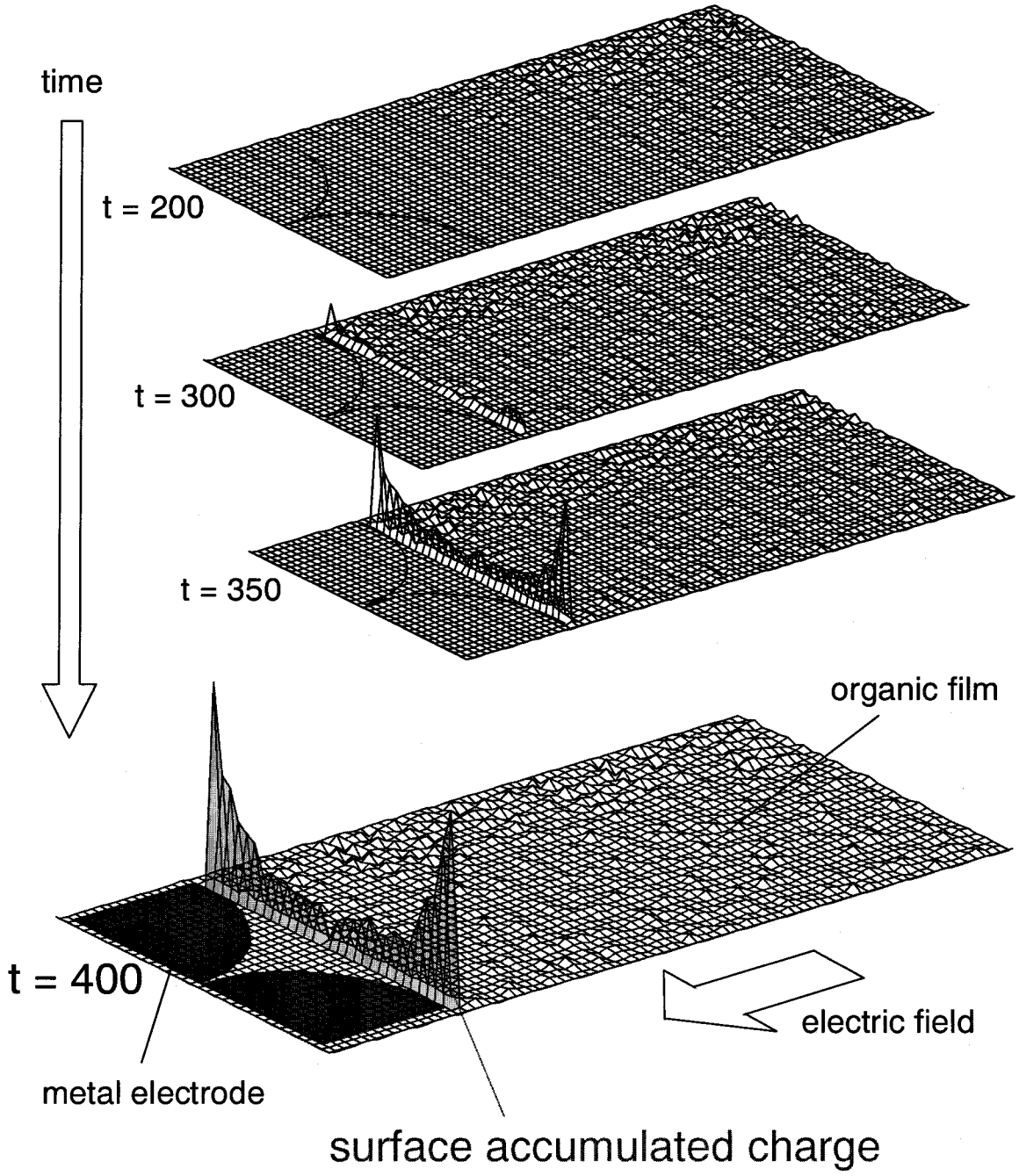

Fig.5-18 Simulation for time development of charge distribution at the modeled organic/metal interface in the case where the photogerated carriers are supplied from the film bulk continuously. The time step was also shown in the figure.

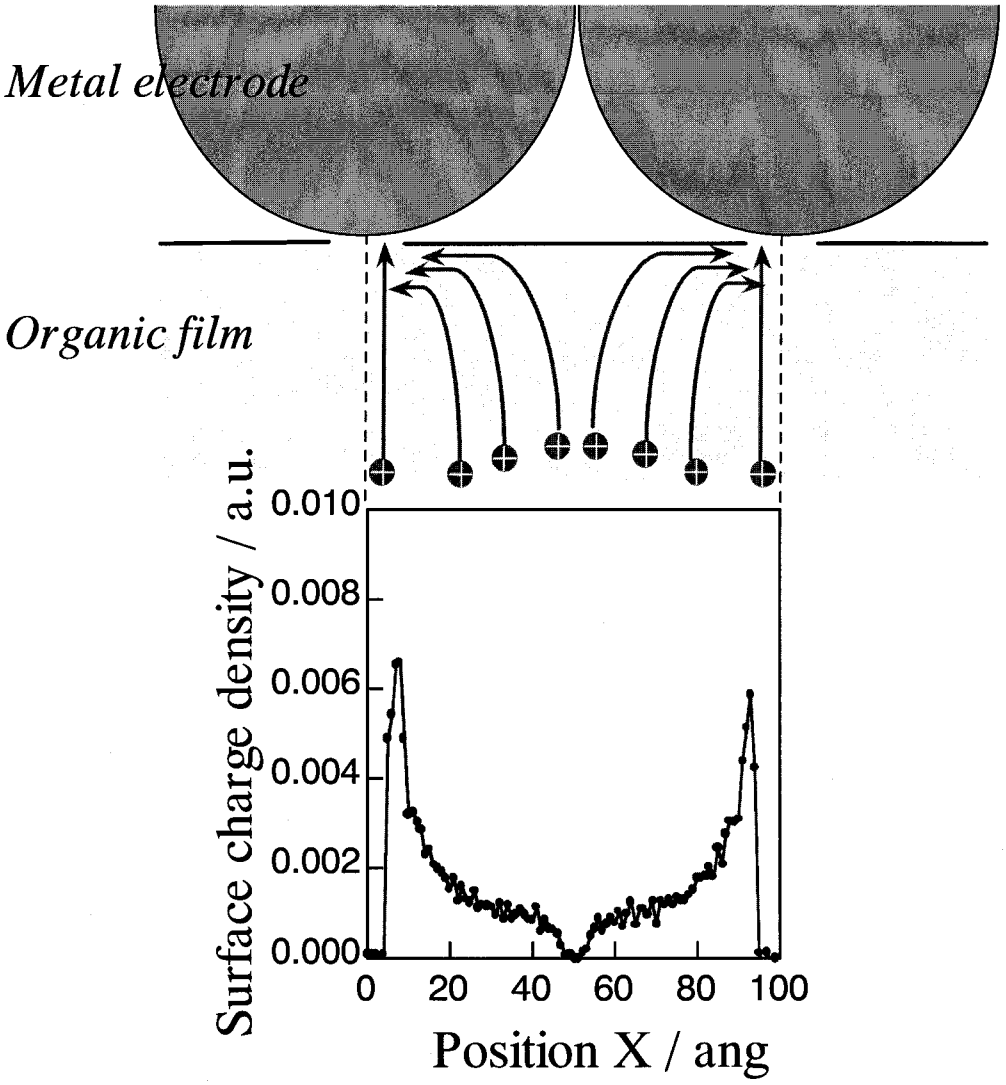

Fig.5-19 Charge distribution at the surface layer of organic film in the steady state.

face between deposited organic film and metal electrode if an imperfect contact in there. This conclusion supports the fact that photocurrent multiplication is observed commonly in a wide variety of organic semiconductors.

Figure 5-19 shows the charge distribution at the organic film surface in the steady state. It can be found that the accumulated charges are localized near the contact point rather than between the electrode particles. Since the photogenerated carriers tend to gravitate toward the tip of electrode particles before reaching the top surface of organic film, the charge density between electrode particles becomes lower. On the other hand, the charge density near the contact point becomes higher. Namely, the photogenerated carriers reaching at non-contact point, which should vanish in the case of perfect contact, keeps staying at the organic film surface until reaching the metal electrode at the contact point. This is the reason why the high density of space charges is accumulated at the surface layer of organic film. Therefore, it is said that the sojourn time of the photogenerated carriers in the organic film surface determines the amount of accumulated charges in the steady state.

Figure 5-20 shows mobility dependence of time development of injection field and surface charge density in the steady state. The larger mobility gives the more quick saturation of injection field, but simultaneously the weaker field and the less amount of accumulated charges. Namely, the high mobility flushes away the supplied photogenerated carriers and shortens the sojourn time in the surface layer, resulting in decrease of charge accumulation. This result indicates that the balance between in-flow and outflow of photogenerated carriers at organic/metal interface governs the charge accumulation . This result may explain why the remarkably large multiplication rate reaching 10^5 has been observed only in the organic film. Compared organic and inorganic materials, the photogeneration efiiciency in organic film is not infe-

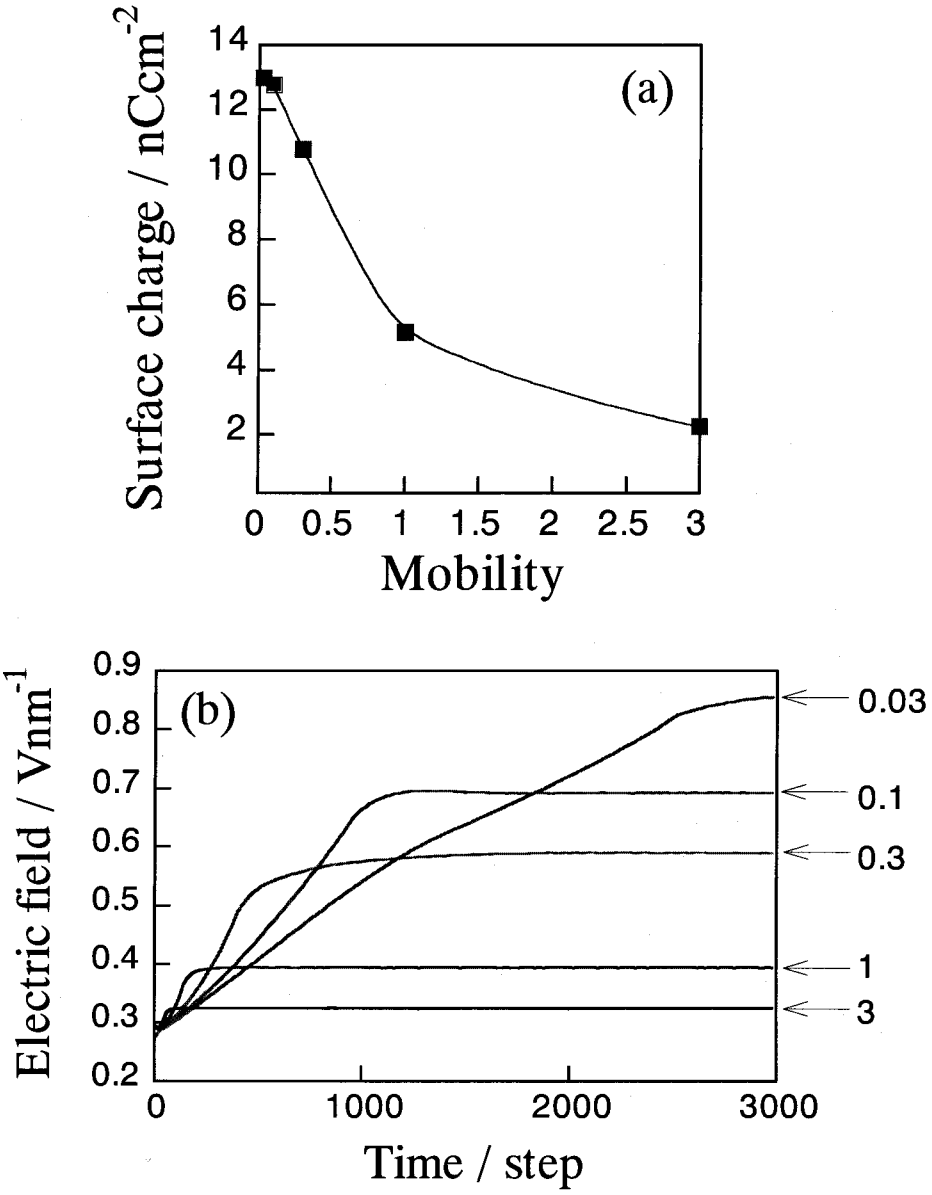

Fig.5-20 Dependence on the mobility. (a) surface charge density in the steady state. (b) transient electric field. The assumed mobility is shown for each transient curve in the figure (b).

rior to inorganic materials. On the other hand, the mobility is much smaller. Therefore, the sojourn time in the surface layer is much longer than that in inorganic materials. Thus, it is quite likely that the lower mobility of organic film results in such a large multiplication rate.

Thus, we succeeded in simulating the charge accumulation process at the imperfect organic/metal interface, and providing the microscopic mechanism of photo-

current multiplication phenomenon. However, it is difficult to simulate the multiplied photocurrent quantitatively in this calculation system. Because, the steady state emerges so quickly on the contrary to the fact that the multiplied photocurrent usually exhibits very slow response. If the charges at the surface layer can move as high as in the film bulk, the surface charge distribution reaches the steady state immediately after photogenerated carriers arrived at the interface. In other words, the transit time in the film bulk and the resopnse time for steady state became comparable. On the other hand, in real multiplication devices, the response time of multiplied photocurrnet takes several tens of seconds, while the transit time in the bulk is on the order of nano seconds at most (assuming moblity of 10^{-6}, film thickness of 500 nm and applied voltage of 20 V). Since the slow response time of photocurrent multiplication is attributed to the charge accumulation process, further consideration is required to explain the slow and large response of multiplied photocurrent.

To solve the above inconsistency, here, we introduce the surface mobility model as shown in Figure 5-21. It is not unreasonable that in the surface of organic film, the charge is hardly to move owing to the surface roughness and/or molecular stacking. Thus, the lower mobility than that in the bulk is assumed when the photogenerated carriers reaching the surface layer move to metal electrode at the contact point. We defined the surface mobility as a ratio of mobility in the surface layer to that in the bulk.

Figure 5-22 shows the surface mobility dependence for time development of injection field and surface charge density in the steady state. The initial rise of electric field is almost the same for various surface mobilities because the supply of photogenerated charges to the interface has no relation to the surface mobility. In

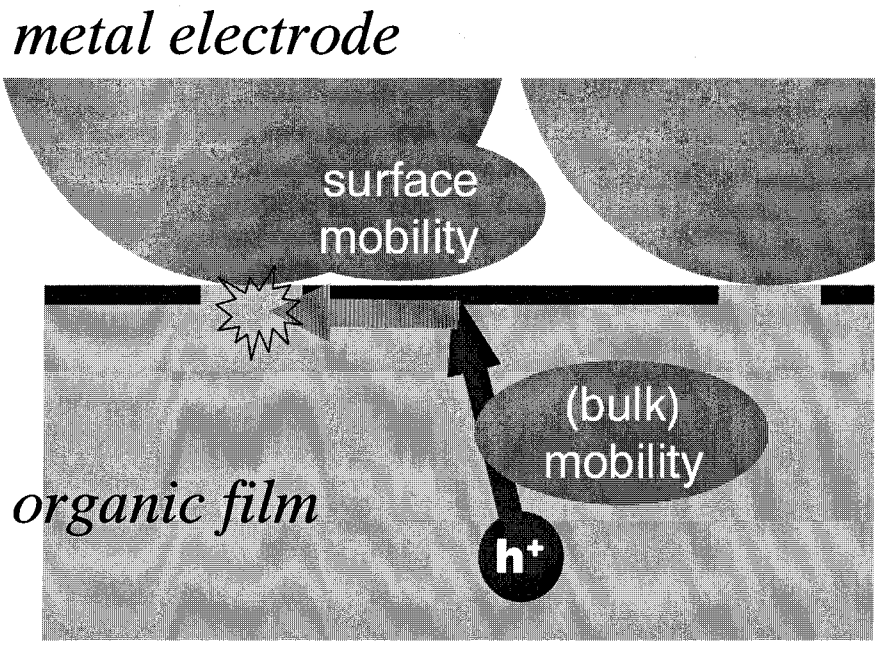

Fig.5-21 Schematic illustration of the surface mobility model at organic/metal interface.

the case of lower surface mobility, it can be seen that the injection field continues increasing for long time, while the injection field becomes saturated after photogerated carriers reach the interface in the case of surface mobility near unity. The amount of surface charges in the steady state increases with a decrease of surface mobility. These results are attributed to that the lower surface mobility extends the sojourn time of photogenerated carriers in the surface layer, resulting in charge accumulation and slow response. Consequently, the lower surface mobility brings about higher injection field in the steady state and slow response until current saturation.

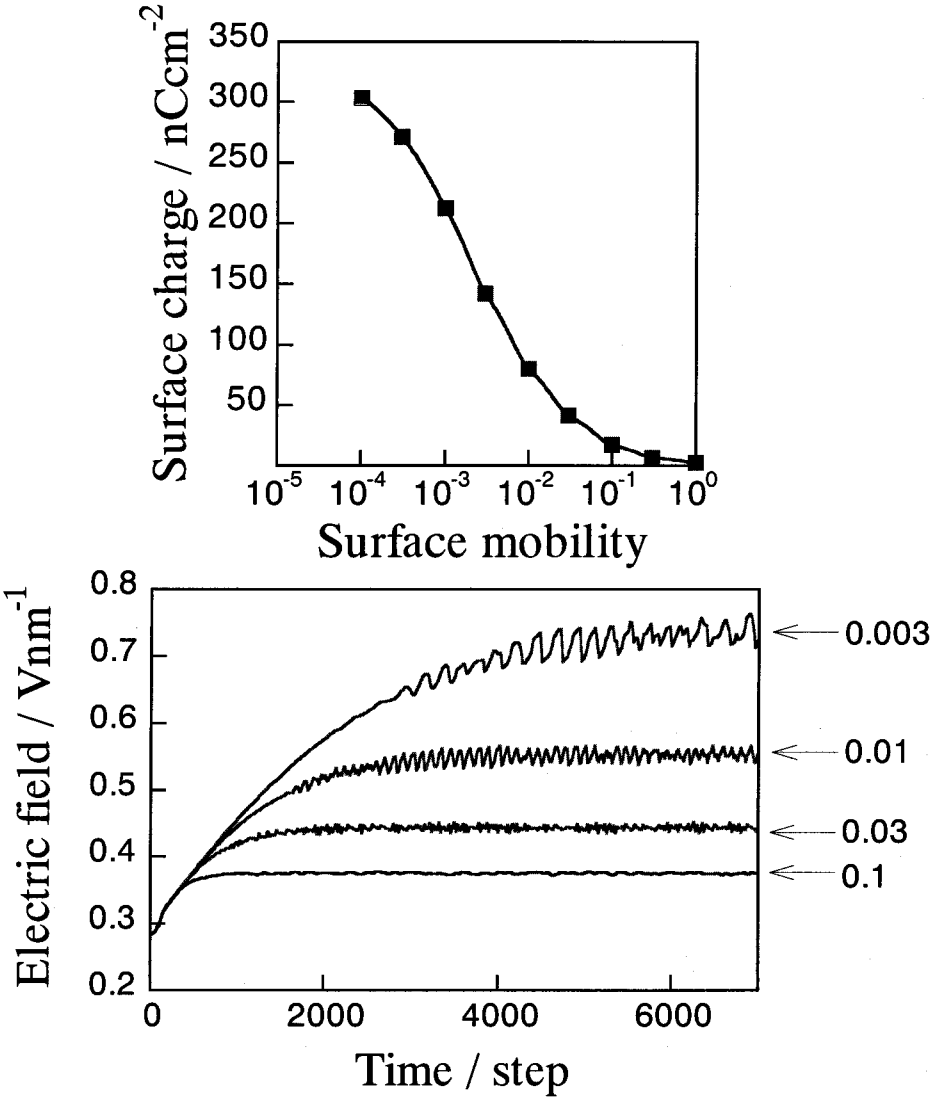

Fig.5-22 Dependence on the surface mobility. (a) Surface charge density in the steady state. (b) Transient electric field at contact point. The assumed surface mobility is shown for each transient curve in the figure (b).

Finally, we have tried to reproduce the transient response of the multiplied photocurrent by tracing the time development of injection current density. The electric field formed by the injected electrons is not taken into account. Figure 5-23(a) shows the typical transient photocurrent of the photocurrent multiplication device. As mentioned in Chapter 2, the transient photocurrent in multiplication device clearly shows the two-step. The first component is primary photocurrent originating from the photogenerated carriers. The second component rising after several tens milli-

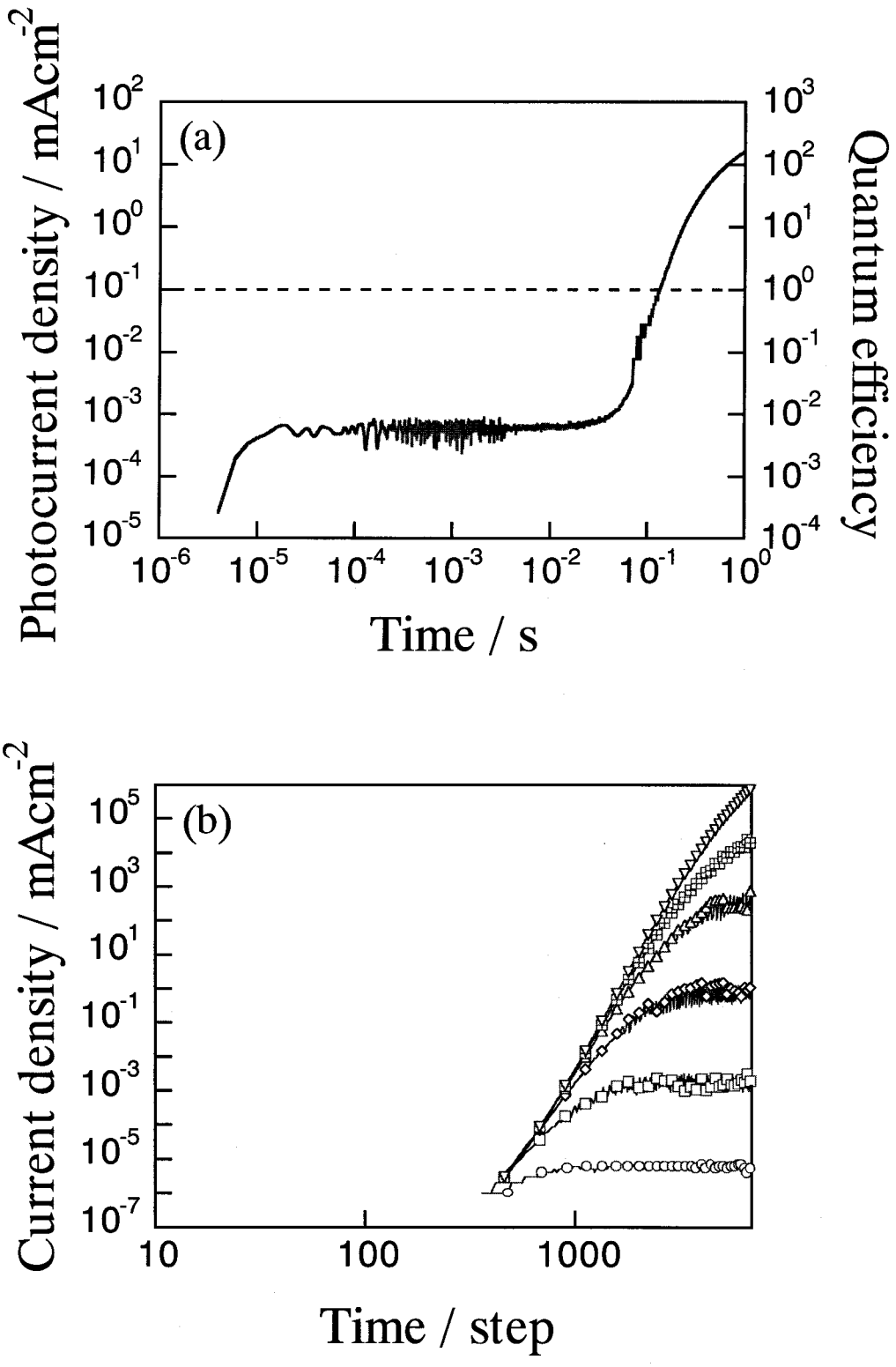

Fig.5-23 Transient response of the photocurrent observed in ITO/ perylene pigment/Au device experimentally (a). Simulated response of injected current density for various surface mobility (b).

seconds is the multiplied photocurrent due to the tunneling injection caused by charge accumulation. Figure 5-23(b) shows the calculated transient response of tunneling injection current with various surface mobilities. Some calculated curves reproduce the multiplied photocurrent observed experimentally, which show drastic increase up to several orders and slow response comparable to the time scale for charge moving in the organic film. An important point to emphasize is the fact that the calculated responses show good agreement by introducing lower surface mobility. This result suggests the large multiplication rate in real multiplication devices is attributed to the low surface mobility of organic film. The reason why such a large multiplication rate has been observed only in organic film is both factors of the low bulk mobility and the extremely lower surface mobility of organic film. Thus, the introducing the concept of low surface mobility successfully reproduces the transient response of multiplied photocurrent.

5-4. Conclusion

In conclusion, the electrostatic potential due to the trapped charges at the modeled organic/metal interface was calculated in order to elucidate the mechanism of the photocurrent multiplication phenomenon. It was proven that the trapped charges at in-between point can cause enough injection field at the contact point. The geometric pattern of trapped charges, sheet-like or mesh-like, was found to affect the injection field essentially. The shape of electrode particles also affects the electric field at the contact point. These results predict that the large multiplication would be possible in the devives by controlling electrode fabrication.

The charge accumulation process at the organic/metal interface having an imperfect contact was numerically simulated and the mechanism of the photocurrent

multiplication phenomenon was discussed. It was found that an imperfect contact of the organic/metal interface necessarily causes the charge accumulation in the steady state of charge flow when the photogenerated carriers are supplied continuously. The charge accumulation was related deeply to the sojourn time of photogenerated carriers at the surface layer. Furthermore, the introduction of lower surface mobility than the bulk mobility based on the concept for rough surface of the organic film, we succeeded in reproducing the charge accumulation process, and also the transient response of photocurrent multiplication phenomenon qualitatively.

Such imperfect contact of organic/metal interface may emerge not only in photocurrent multiplication devices but also in general organic film devices having metal electrodes, such as organic EL devices, organic solar cell. This result can be applied to these general devices and must be considered in electrical property.

Chapter 6

High-speed Photocurrent Multiplication Device Based on an Organic Double-layered Structure

6-1. Introduction

Photocurrent multiplication in organic films has a great sensitivity in photon-electron conversion reaching more than 10^5 of quantum efficiency. However, the observed multiplied photocurrent always exhibits a slow transient response of about several ten seconds. A high-speed response is desirable for practical applications.

In Chapter 2, the transient response of photocurrent multiplication was shown to have two components, which were identified as primary and subsequent multiplied photocurrents. The amount of photogenerated carriers until multiplication onset was also found to have a specific value. This means that the enhancement of the carrier generation efficiency of the primary photocurrent is expected to produce a high-speed response of the multiplied photocurrent. One way to accomplish this is to operate the device under a high electric field. Generally, however, many of the devices with a single organic thin film easily break down by applying high voltage, owing to the lack of uniformity in the films. A solution to this problem would enable the multiplication devices to operate under high fields, and consequently, enhance the carrier generation efficiency of the primary photocurrent.

In this chapter, we report on a high-speed response with a large multiplication rate in a new type of organic double-layered device that can be driven with a high voltage.

6-2. Experimental Section

A naphthalene derivative (naphthalenetetracarboxylic anhydride, NTCDA) and a phenethyl perylene pigment (N,N'-*bis*(phenylethyl)-perylene-3,4:9,10-*bis*(dicarboximide), PhEt-PTC) were purified twice by a train sublimation technique.[14] Figure 6-1(a) shows the cell structures of a conventional single-layered device of NTCDA, and Figure 6-1(b) shows the present double-layered device, consisting of NTCDA and PhEt-PTC. The film thickness of each layer is also shown in Figure 6-1. The thin films were prepared on an indium tin oxide (ITO) glass substrate by vacuum evaporation under 1×10^{-5} Torr. The deposition rates were 0.2 nm s^{-1} for the organic films and 0.05 nm s^{-1} for the Au electrode. The observation of microscopic structures of organic film surfaces was carried out with an atomic force microscope (AFM, SEIKO SPI-3800).

The cells were set in an optical cryostat (Janis Research Co. Inc., VPF-475)

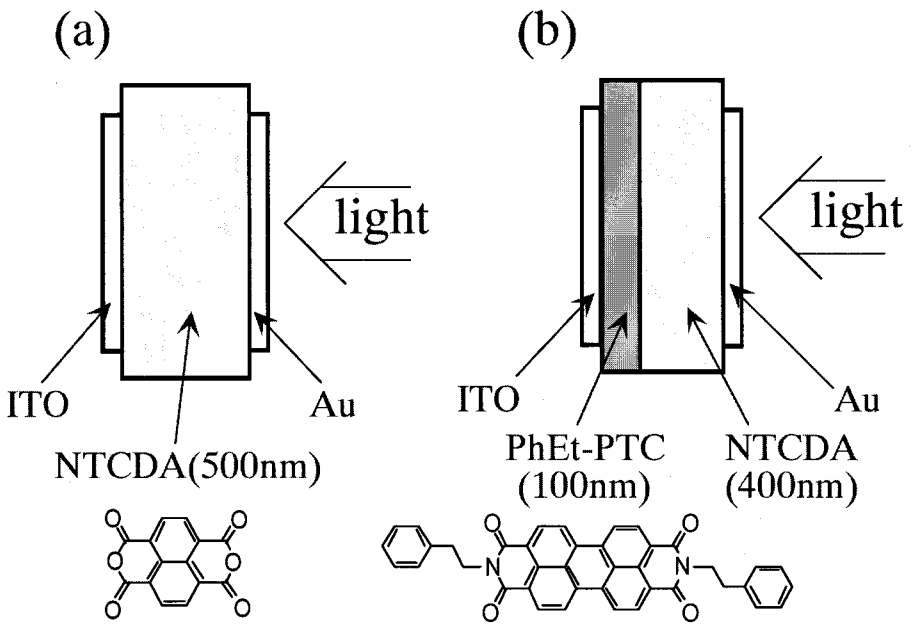

Fig. 6-1 The cell structures of (a) a single-layered device of NTCDA and (b) a double-layered device consisting of NTCDA and PhEt-PTC. The Au electrode was biased negatively with respect to the ITO electrode. Monochromatic light of 400 nm, which excites the NTCDA only, irradiated the Au electrode. Chemical structures of NTCDA and PhEt-PTC are also shown.

evacuated to 10^{-3} Torr. Monochromatic light of 400 nm from a Xe-lamp, filtered through a monochromator (Shimadzu, SPG-100ST), irradiated a semitransparent Au electrode biased negatively with respect to an ITO electrode. Light intensity was measured by a silicon photodiode (Hamamatsu, S1337-66BQ). Current–voltage characteristics were measured by a source-measure unit (Keithley Instruments Inc., model 238). The transient response of photocurrent was measured by a high-speed current amplifier (Keithley Instruments Inc., model 428) and a digital storage oscilloscope (Nicolet 3091). The photocurrent quantum efficiency (that is, the multiplication rate) was calculated as the ratio of the number of collected carriers that flowed across the sample to the number of photons absorbed by the organic thin film.

6-3. Results and Discussion

Figure 6-2 shows typical transient responses for a conventional single-layered

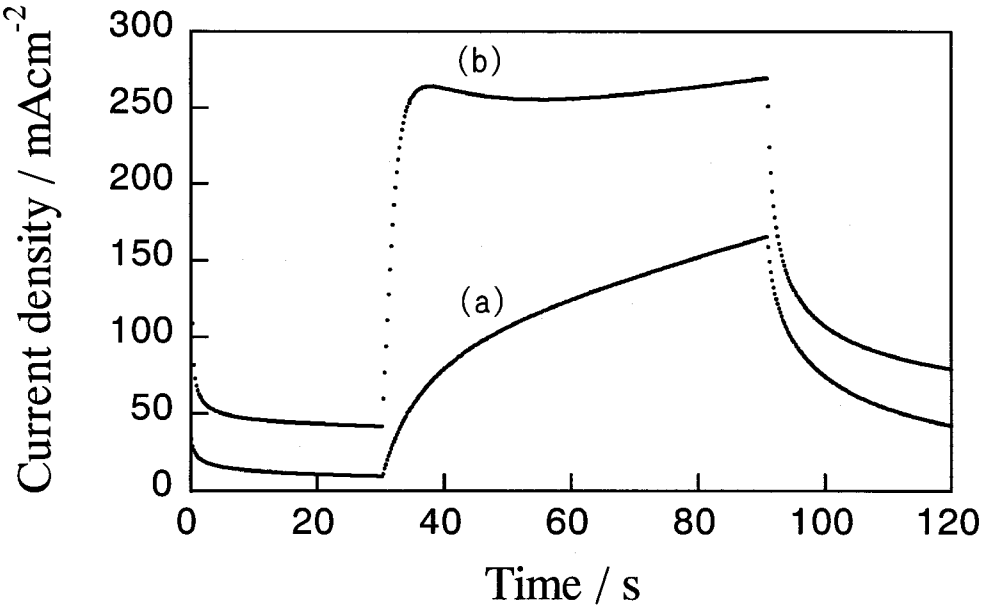

Fig. 6-2 Transient responses of the multiplied photocurrent in (a) a single-layered device and (b) a double-layered device. Applied voltages were 12 V (curve (a)) and 20 V (curve (b)). Measurements were performed at room temperature.

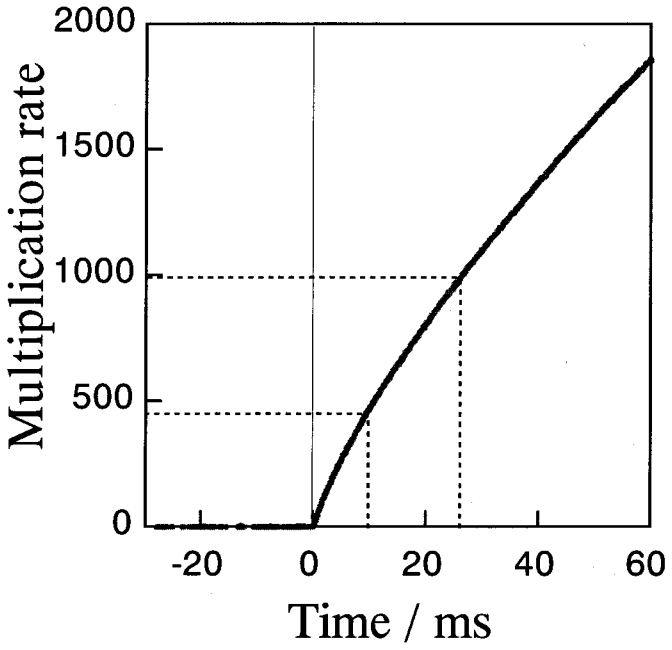

Fig. 6-3 Initial transient of photocurrent in double-layered multiplication device. Photocurrent is converted to multiplication rate. The light of 400nm was irradiated to the Au electrode which was biased negatively at 20 V.

cell (curve (a)) and for the present double-layered cell (curve (b)). In the single-layered cell, the multiplied photocurrent showed a very slow response, and saturation was hardly observed even after a prolonged irradiation for 60 s. On the other hand, in the double-layered cell, the multiplied photocurrent reached a constant value at a multiplication rate exceeding 1.5×10^5-fold only within 4 s (approximately) upon light irradiation. From the initial rise profile measured using an oscilloscope (Fig. 6-3), the multiplication rate was found to reach 470-fold after 10 ms of irradiation, and the time required to reach 1000-fold was only 26 ms. These values satisfy the required speed for a practical imaging device.

Figure 6-4 shows AFM images of NTCDA (a) and PhEt-PTC (b) films deposited on an ITO glass substrate. In the case of NTCDA films, many grains with a size of more than 100 nm were grown on an ITO glass substrate, and the film surface was very uneven. On the other hand, in the case of PhEt-PTC films, the grain size was

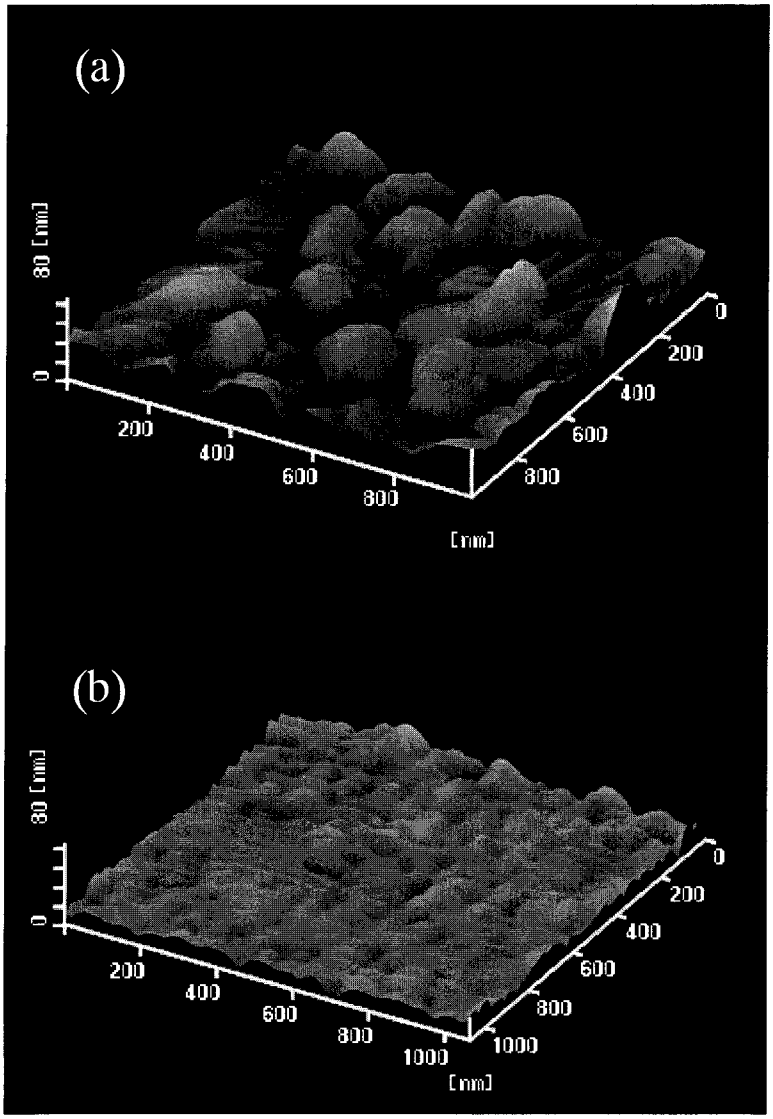

Fig. 6-4 The AFM images of organic films deposited on an ITO glass substrate. (a) NTCDA film (400 nm), (b) PhEt-PTC film (100 nm).

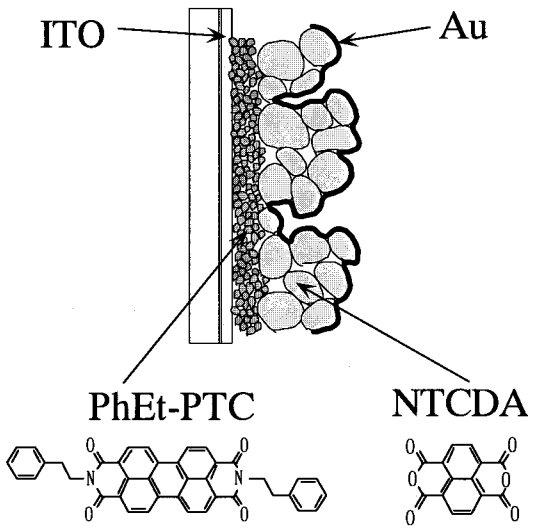

Fig. 6-5 Schematic illustration of device structure and chemical structure of pigments.

much smaller and the surface was relatively uniform. This difference is considered to be due to the type of substituents as discussed in Chapter 4. The NTCDA molecules, which have small substituents, tend to stack and form large grains. The PhEt-PTC molecules have bulky substituents and hardly form molecular stacking, resulting in small grains and an even surface. Indeed, from x-ray diffraction measurements, the PhEt-PTC films were shown to be amorphous-like with no diffraction peaks. The combination of these two pigments in a layered structure would result in a uniform film sample that is of better quality than a single NTCDA film as a whole (Figure 6-5).

The improvement of the film quality resulted in substantial effects on the dark current performance of the devices. In the NTCDA single-layered device, the dark current increased drastically with increasing applied voltage, and reached 2.6 mA cm^{-2} at 18 V (Fig. 6-6(a)). On the other hand, in the double-layered device, the dark

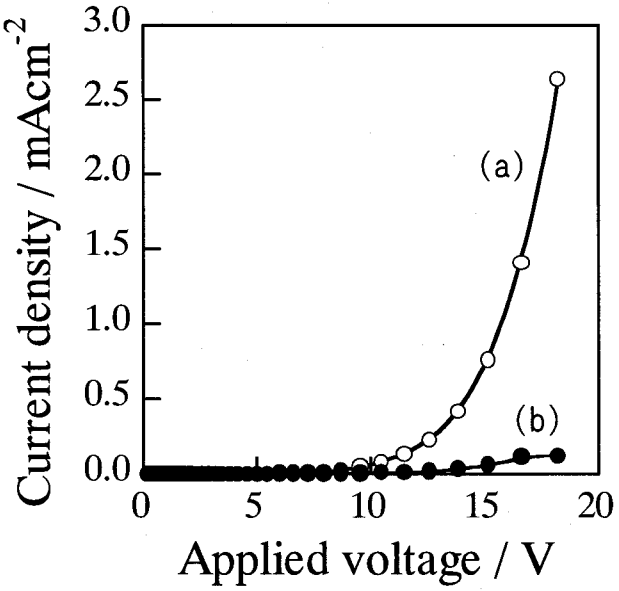

Fig. 6-6 Voltage dependence of the darkcurrent. (a) single-layered device composed of ITO/NTCDA(500nm)/Au. (b) double-layered device composed of ITO/PhEt-PTC(100nm)/NTCDA(400nm)/Au. The light of 400nm was irradiated onto Au electrode which was negatively biased with respect to ITO electrode.

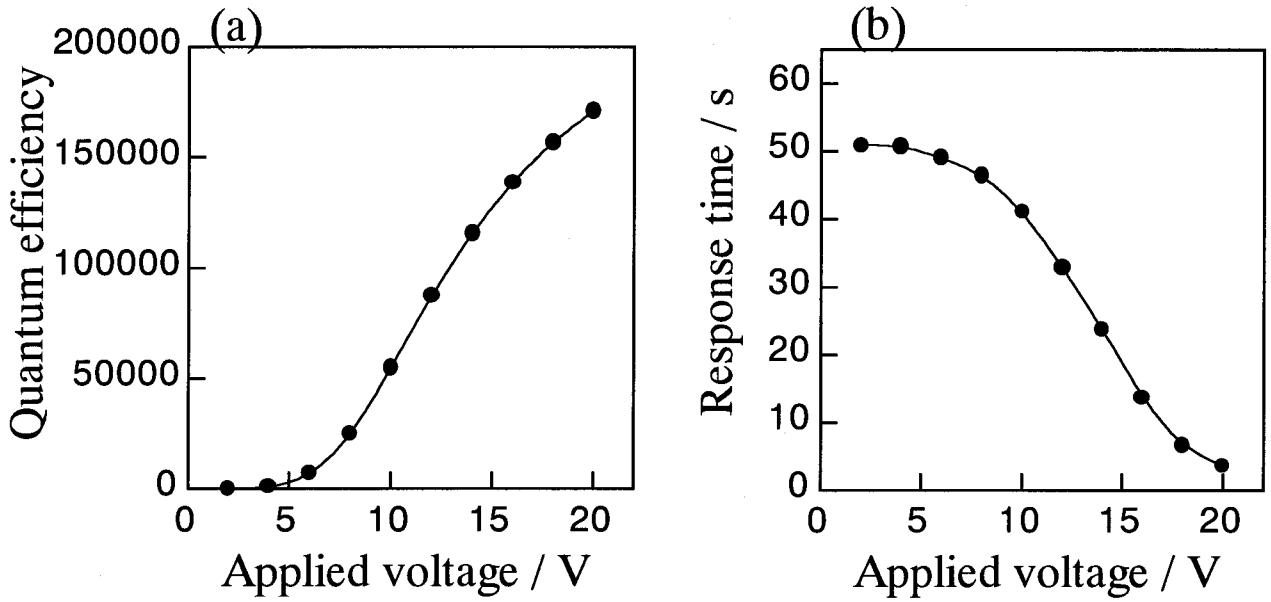

Fig. 6-7 The voltage dependence of (a) multiplication rate and (b) response time of the photocurrent in the double-layered device. The response time of the photocurrent multiplication is defined as the time to reach 90% of the magnitude of the multiplied photocurrent after light irradiation for 60 s. Measurements were performed at room temperature.

current was efficiently suppressed to 0.12 mA cm^{-2} at 18 V (Fig. 6-6(b)). In the latter case, the electric field applied to the device is distributed uniformly in the whole active area, and a pinpoint high electric field leading to breakdown (usually observed in the former case) was prevented by the improved film uniformity. Consequently, by the insertion of a PhEt-PTC layer, the dark current is suppressed and high voltage application to the device becomes possible.

Figure 6-7(a) shows the voltage-dependence of the multiplication rate in a double-layered device. As the multiplication rate reached a value of over 10^5-fold, which is as high as the single-layered device[6], the underlying PhEt-PTC layer did not perturb the multiplication at the NTCDA/Au interface. This is due to electrons injected from an Au electrode easily passing the PhEt-PTC layer and reaching the ITO electrode because the conduction band of PhEt-PTC is lower than that of NTCDA.

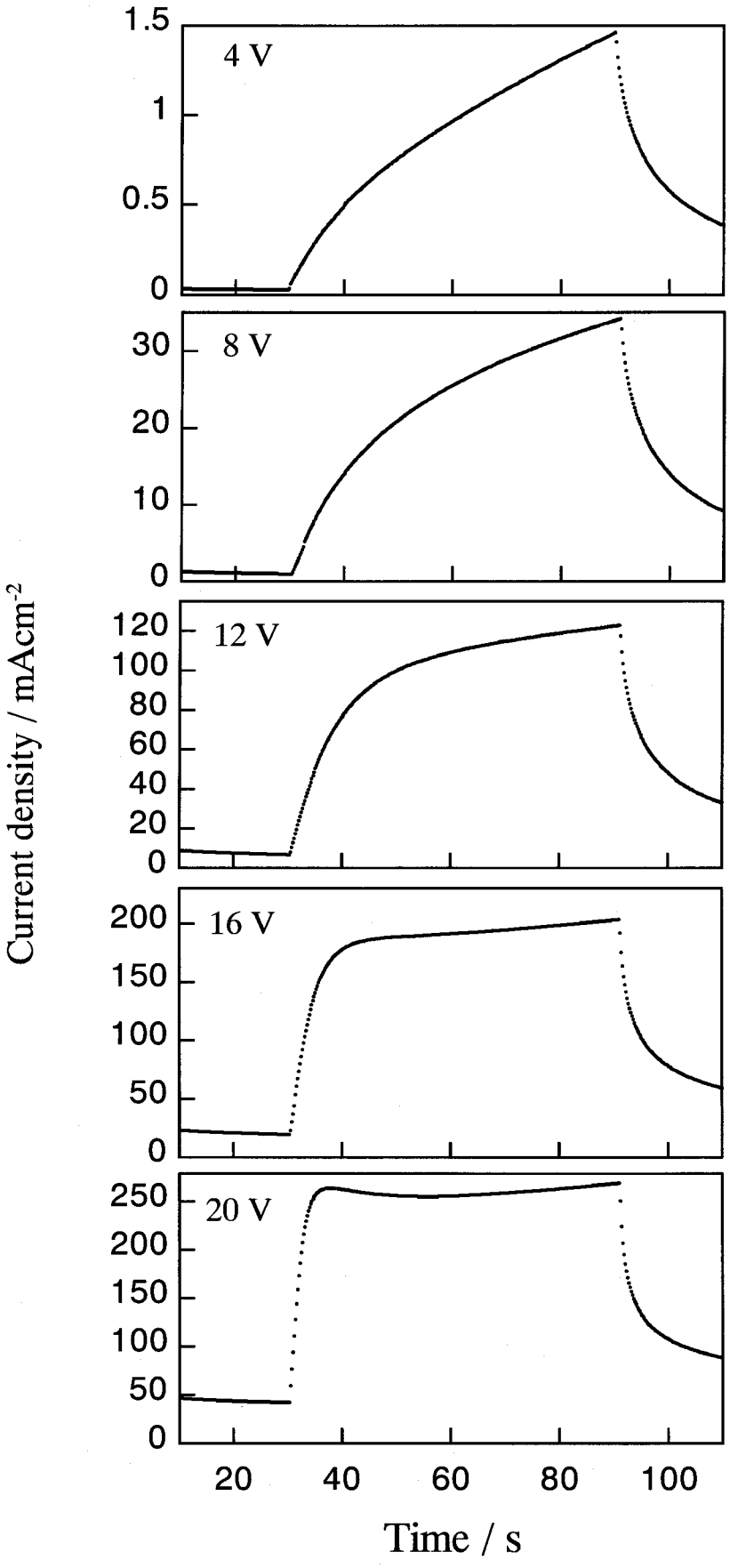

Fig. 6-8 The transient response of multiplied photocurrent in double-layered device for various applied voltage.

Figure 6-7(b) shows the response time of the multiplied photocurrent in the double-layered device. It is clear that the response time decreased with increasing applied voltage, reaching 3.7 s at 20 V. The transient response began to show saturation above 16 V (Fig. 6-8). Although the response time of the single-layered device showed a similar tendency, a voltage higher than 14 V could not be applied owing to breakdown. These results imply that high voltage operation in the double-layered device enables a high-speed response. Thus, by the insertion of a thin PhEt-PTC layer, we succeeded in achieving a quick response of 3.7 s with a large multiplication rate of 1.7×10^5-fold.

Finally, we discuss the reason for the high-speed response as a result of high voltage operation. According to our proposed model, the multiplication is caused by tunneling electrons injected from an Au electrode into the organic layer in a high electric field, which is built up by the photo-accumulated space charges of trapped holes near the organic/metal interface. When a higher voltage is applied, the photocarrier generation efficiency increases, and the number of photogenerated holes required for a multiplied photocurrent to occur is supplied to the NTCDA/Au interface and accumulates quickly at this interface. Thus, effective and quick charge supply to trapping sites at the organic/metal interface shortens the onset time of the multiplication. Actually, when the applied voltage increased, the primary photocurrent component of the transient photocurrent was observed to increase drastically, as is widely observed in organic photoconductors.

It should be pointed out that the magnitude of current saturation of the transient response in the high voltage region (Fig. 6-8) exhibited the ceiling of the multiplication rate (see Fig. 6-7(a)). Since the saturation of the multiplied photocurrent is dominated by the saturation of charge accumulation as discussed previously, the appearance of

current saturation means the trapping sites at the organic/metal interface are all occupied. In that case, excess photogenerated charges pass through the contact points of the organic/metal interface owing to Coulombic repulsion of trapped charges. This implies that there is limiting charge accumulation at the interface. From these considerations, we concluded that the high-speed response and current saturation is due to the rapid filling effect of the interfacial traps by a large number of carriers photogenerated by the application of a high voltage.

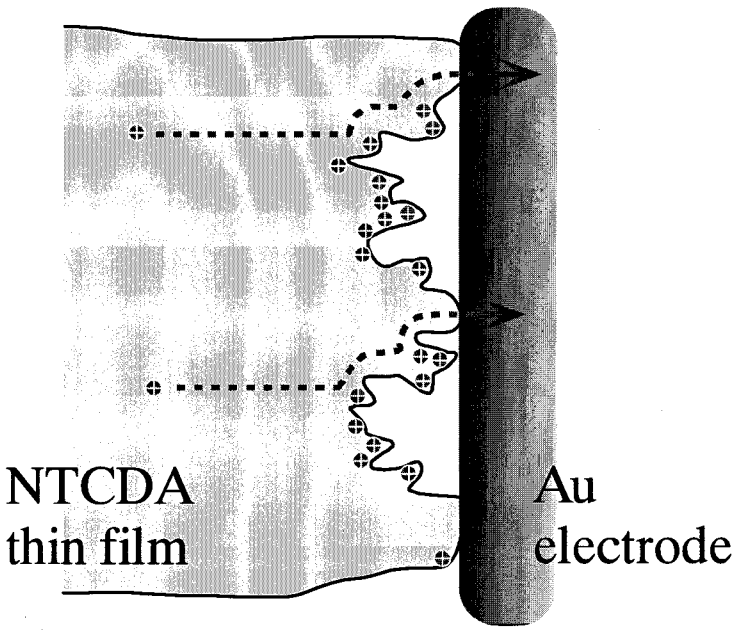

Fig. 6-9 Schematic illustration of interpretation for the photocurrent saturation by the structural trap model. Excess charges pass through the organic/metal interface by Coulombic repulsion.

6-4. Conclusion

In conclusion, we have succeeded in fabricating a double-layered device, composed of NTCDA and PhEt-PTC pigments, which shows a high-speed response of photocurrent multiplication. The double-layered device can be operated under high voltages because the uniformity of the PhEt-PTC layer prevents pinpoint breakdown caused by a high electric field. The response time of the multiplied photocurrent became shorter with higher applied voltages required for efficient carrier photogeneration. We have also succeeded in demonstrating a large multiplication rate of 1.7×10^5 with a short response time of 3.7 s at 20 V.

Chapter 7

Summary

In this study, the mechanism of photocurrent multiplication phenomena at organic/metal interface was investigated in detail.

In Chapter 2, the most important transient response of photocurent in multiplication devices was successfully observed. The response was revealed to have two components of the primary and the subsequent multiplied photocurrents. Namely, our previously proposed model that the electron tunneling injection is caused by the accumulation of photogenerated holes to the interfacial traps was directly traced and proved. The amount of charge required for multiplication onset was found to have a specific value. This result implys that an increase of the carrier generation efficiency of the primary photocurrent is expected to provide the guiding principle for achieving high speed multiplication.

In Chapter 3, the nature of interfacial traps taking the essential role for multiplication process was investigated by measurement of thermally stimulated current. The interfacial traps showed strange behaviors that the trap depth became deeper for higher applied field. It was also found that the density of the traps has a extremely high value of $10^{12}cm^{-1}$. To explain these properties of the interfacial traps, we proposed the field-activated structural trap model that photogenerated carriers accumulate to the structural blind alleys owing to the imperfect contacts between organic film and metal electrode.

In Chapter 4, the correlation between multiplication behaviors and the film struc-

ture at organic/metal interface was investigated in order to verify the field-activated structural trap model. As a result, crystalline organic films having microscopical roughness or granular electrodes prepared by slow-rate deposition tend to show large multiplication rate. On the other hand, amorphous-like organic films having flat surface or smooth electrodes show small multiplication rate. These results strongly support the existence of structural trap at organic/metal interface, and furthermore, show the first step toward the intentional control of multiplication characteristics by the design of the organic film morphology.

In Chapter 5, in order to clarify the more microscopical mechanism of photocurrent multiplication, the electric field distribution formed by the space charges near organic/metal interface was numerically calculated. We can obtain the result that the accumulated charges staying at the non-contact organic film interface can provide enough high field for tunneling charge injection leading to multiplication process, indicating the validity of structural trap model as well. The calculation was extended to simulating the charge accumulation process by tracing the dynamic flow of photogenerated carriers at the interface. It was found that high density of surface charges, namely, charge accumulation appears in the steady state when the photogenerated carriers are supplied continuously. By introducing lower surface mobility expressing surface roughness of orgainc film, the multiplied photocurrent response observed experimentally was well reproduced.

In Chapter 6, a high-speed photocurrent multiplication device based on an organic double-layered structure was fabricated. The improvement of the film uniformity by inserting an additional amorphous-like organic underlayer enabled high-electric-field operation of the device. Owing to efficient carrier photogeneration under the application of higher voltages, a large multiplication rate of 1.7×10^5-fold with a short

response time of 3.7 s was achieved.

The knowledge obtained in this study are applicable not only to photocurrent multiplication phenomena but also to charge injection process at general organic/ metal interface more widely because the most results are not dependent on the individual characteristics of materials. Thus, the important knowledge for the correlation between morphological structure of organic/metal interface and electric properties of charge injection process can be obtained through this study.

References

1) C. W. Tang, *Appl. Phys. Lett.* **48**, 183 (1986).

2) P. Borsenberger and D. Weiss, *Organic Photoreceptors for Imaging Systems* (Marcel Dekker, Inc., New York, 1993).

3) Y. Takasaki, K. Tsuji, T. Hirai, E. Maruyama, K. Tanioka, J. Yamazaki, K. Shidara, and K. Taketoshi, *Mater. Res. Symp. Proc.* **118**, 387 (1988)

4) M. Hiramoto, T. Imahigashi, and M. Yokoyama, *Appl. Phys. Lett.* **64**, 187 (1994).

5) M. Hiramoto, S. Kawase, and M. Yokoyama, *Jpn. J. Appl. Phys.* **35**, L349 (1996).

6) T. Katsume, M. Hiramoto, and M. Yokoyama, *Appl. Phys. Lett.* **69**, 3722 (1996).

7) T. Katsume, M. Hiramoto, and M. Yokoyama, *Appl. Phys. Lett.* **66**, 2992 (1995).

8) M. Hiramoto, T. Katsume, and M. Yokoyama, *Optical Review* **1**, 82 (1994).

9) T. Katsume, M. Hiramoto, and M. Yokoyama, *Appl. Phys. Lett.* **64**, 2546 (1994)

10) M. Hiramoto, H. Kumaoka, and M. Yokoyama, *Synthetic Metals* **91**, 77 (1997)

11) C. W. Tang and S. A. VanSlyke, *Appl. Phys. Lett.* **51**, 913 (1987).

12) S. Akita, H. Ueda, Y. Nakayama, *J. Appl. Phys.* **77**, 1120 (1995).

13) M. Yoshimi, T. Ishiko, K. Hattori, H. Okamoto, and Y. Hamakawa, *J. Appl. Phys.*, **72**, 3186 (1992).

14) H. J. Wagner, R. O. Loutfy, and C. Hsiao, *J. Mater. Sci.* **17**, 2781 (1982).

15) S. M. Sze, *Physics of Semiconductor Devices* (Wiley Interscience, a division of John Wiley & Sons, New York, 1981) p. 552.

16) H. Kirihata and M. Uda, *Rev. Sci. Instrum.* **52**, 68 (1981).

17) A. H. Booth, *Can. J. Chem.* **32**, 214 (1954).

18) B. A. Gregg, *J. Phys. Chem.* **100**, 852 (1996).

19) J. Mizuguchi, *J. Appl. Phys.* **84**, 4479 (1998).

List of Publication

[1] Field-activated structural traps at organic pigment/metal interfaces causing photocurrent multiplication phenomena,
M. Hiramoto, K. Nakayama, T. Katsume and M. Yokoyama,
Appl. Phys. Lett., **73**, 2627 (1998).

[2] Photocurrent multiplication at organic/metal interface and morphology of metal films,
M. Hiramoto, I. Sato, K. Nakayama and M. Yokoyama,
Jpn. J. Appl. Phys., **37**, L1184 (1998).

[3] Photocurrent multiplication phenomena at organic/metal and organic/organic interfaces,
M. Hiramoto, K. Nakayama, I. Sato, H. Kumaoka and M. Yokoyama,
Thin Solid Films, **331**, 71 (1998).

[4] Direct tracing of the photocurrent multiplication process in an organic pigment film,
K. Nakayama, M. Hiramoto, and M. Yokoyama,
J. Appl. Phys., **84**, 6154 (1998).

[5] High-speed photocurrent multiplication device having organic double-layered structure,
K. Nakayama, M. Hiramoto, and M. Yokoyama,
Appl. Phys. Lett., in press.

[6] Photocurrent multiplication at organic/metal interface and surface morphology of organic films,
K. Nakayama, M. Hiramoto, and M. Yokoyama,
J. Appl. Phys., in contribution.

[7] Numerical calculation of electric field distribution at organic/metal interface in photocurrent multiplication device,
K. Nakayama, M. Hiramoto, and M. Yokoyama,
in preparation.

[8] Numerical simulation of charge accumulation process at organic/metal interface in photocurrent multiplication device,
K. Nakayama, M. Hiramoto, and M. Yokoyama,
in preparation.

[9] Photocurrent multiplication phenomenon in C_{60} deposited film,
K. Nakayama, M. Hiramoto, and M. Yokoyama,
in preparation.

List of Supplementary Publication

[1] Transient Response of Multiplied Photocurrent Observed in Metal/Organic Pigment Film Interface,
K. Nakayama, M. Hiramoto, and M. Yokoyama,
Proceedings of IS&T's NIP14: International Conference on Digital Printing Technologies, p490-493 (1998)

[2] Numerical Simulations of Photocurrent Multiplication Phenomenon at Organic/Metal Interface,
K. Nakayama, M. Hiramoto, and M. Yokoyama,
Proceedings of IS&T's NIP15: International Conference on Digital Printing Technologies, p743-746 (1999)

[3] Direct Measurement of Internal Potential Distribution of Organic Electroluminescent Diodes under Operation,
M. Hiramoto, K. Keiji, K. Nakayama, and M. Yokoyama
Appl. Phys. Lett., in contribution.

Acknowledgment

The author would like to express his sincerest gratitude to Professor Masaaki Yokoyama, Osaka University for his hearty guidance and encouragement thoughout this work.

The author would like to thank Professor Shunichi Fukuzumi and Professor Yoshizo Takai for their helpful comments and suggestions.

The author wishes to express his sincere thanks to Associate Professor Masahiro Hiramoto for overall guidance and fruitful suggestions.

The author is grateful to Professor Keiichi Kimura, Wakayama University for his hearty encouragement and helpful comments.

The author would like to thank Mr. Ken-ichi Sano and Mr. Masanori Watanabe, Ion Engineering Research Institute Corporation for his fruitful discussions and comments.

The author would like to thank Mr. Ohki, Dainichiseika Color & Chemicals Manufacturing Co. Ltd. for providing the pigment sample.

The author also thanks Mr. Tadashi Katsume for his invaluable discussions and Mr. Ichiro Satoh, Mr. Shun-ichiro Kurihara, Mr. Hiroyuki Kumaoka, Miss Ryoko Mizutani, Mr. Ken Okamoto, and all other members of Yokoyama's Laboratory for their cooperation and friendship.

The author is grateful to his parents and sister for their encouragement and support.

Finally, on behalf of all entire members of Yokoyama Laboratory, the author would like to thank the Core Research for Evolutional Science and Technology (CREST), Japan Science and Technology Corporation (JST) for the finacial support to his work.